UNIVERSITY OF CALIFORNIA, SAN DIEGO

Contributions of Early Parallel Pathways to Extrastriate Visual Cortex in Macaque Monkey

A Dissertation submitted in partial satisfaction of the requirements for the degree

Doctor of Philosophy

in

Neurosciences

by

Jonathan J. Nassi

Committee in charge:

Professor Edward M. Callaway, Chair
Professor Harvey J. Karten, Co-Chair
Professor Thomas D. Albright
Professor Donald A. Macleod
Professor Pamela Reinagel

2007

The Dissertation of Jonathan J. Nassi is approved, and it is acceptable in quality and form for publication on microfilm:

_____

_____

_____

_____
Co-Chair

_____
Chair

University of California, San Diego

2007

DEDICATION

This dissertation is dedicated to my family (my mother Jean, my father Menahem, my brother Shaul) and to my fiancé Danielle. You have all helped make me the person who I am today and I thank you from the bottom of my heart for your love and support.

TABLE OF CONTENTS

LIST OF FIGURES

LIST OF TABLES

ACKNOWLEDGEMENTS

I would like to thank the members of my thesis committee: Drs. Harvey Karten, Thomas Albright, Donald Macleod, and Pamela Reinagel. Their guidance has been invaluable.

I would also like to thank the members of the Callaway lab, past and present. The friendly atmosphere they created both inside and outside of the lab has made my graduate studies more enjoyable than I ever could have imagined. Not only have they been wonderful colleagues, but many have become close friends.

Finally, I would like to thank my advisor, Dr. Edward Callaway. His passion and intellect for science is unmatched. He has been a mentor and a friend, and I can't thank him enough for his unflinching support over the years.

Chapter 2, in full, is a reprint of material as it appears in *Neuron* 2006; Nassi, JJ, Lyon, DC, and Callaway, EM; April 20, 50 (2): 319-327. The dissertation author was co-primary author on this paper. Secondary author was the thesis advisor.

Chapter 3, in full, is a reprint of material as it appears in *J Neurosci* 2006; Nassi, JJ, and Callaway, EM; December 6, 26 (49): 12789-12798. The dissertation author was primary author on this paper. Secondary author was the thesis advisor.

Chapter 4, in full, has been submitted for publication; Nassi, JJ, and Callaway, EM. The dissertation author was primary author on this paper. Secondary author was the thesis advisor.

VITA

1998-2002 University of California, Los Angeles
B.S. in Cognitive Science

2002-2007 University of California, San Diego
Ph.D. in Neurosciences

PUBLICATIONS

Nassi, J.J., Lyon, D.C., and Callaway, E.M. The parvocellular LGN provides a robust disynaptic input to the visual motion area MT. *Neuron*. 2006 Apr 20; 50 (2): 319-27.

Nassi, J.J. and Callaway, E.M. Multiple circuits relaying primate parallel visual pathways to the middle temporal area. *J Neurosci*. 2006 Dec 6; 26 (49): 12789-98.

Nassi, J.J. and Callaway, E.M. Specialized circuits from primary visual cortex to V2 and middle temporal area. *Submitted for publication*.

ABSTRACTS

Nassi, J.J. and Callaway, E.M. Contributions of magnocellular and parvocellular pathways to neurons in monkey primary visual cortex that provide direct versus indirect input to area MT. *Soc. Neurosci. Abs.* 2004, 135.1.

Lyon, D.C., Nassi, J.J., and Callaway, E.M. Disynaptic connections from the superior colliculus to cortical area MT revealed through transynaptic labeling with rabies virus. *Vis. Sci. Soc. Abs.* 2005, 353.5.

Nassi, J.J. and Callaway, E.M. Indirect parvocellular input to area MT of macaque monkey. *Soc. Neurosci. Abs.* 2005, 125.3.

Lyon, D.C., Nassi, J.J., and Callaway, E.M. Primate dorsal stream visual areas receive disynaptic inputs from the superior colliculus. *Soc. Neurosci. Abs.* 2005, 533.2.

Nassi, J.J. and Callaway, E.M. Specialized circuits relaying parallel visual pathways to area MT of macaque monkey. *Israel Soc. Neurosci. Abs.* 2006, 10.2.

ABSTRACT FOR DISSERTATION

Contributions of Early Parallel Pathways to

Extrastriate Visual Cortex in Macaque Monkey

by

Jonathan J. Nassi

Doctor of Philosophy in Neurosciences

University of California, San Diego, 2007

Professor Edward M. Callaway, Chair

Professor Harvey J. Karten, Co-Chair

Parallel Processing is a commonly used strategy in sensory systems of the mammalian brain. In the primate visual system, information is relayed from the retina to primary visual cortex (V1) along three parallel pathways: magnocellular (M), parvocellular (P), and koniocellular (K). These three pathways remain anatomically and physiologically distinct as they pass through M, P, and K layers of the lateral

geniculate nucleus (LGN) of the thalamus and into V1, with the M pathway terminating primarily in layer 4Cα, the P pathway in layer 4Cβ, and the K pathway in the cytochrome oxidase (CO) blobs of layer 2/3. Beyond V1, visual information is processed in relatively independent dorsal and ventral streams specialized for computations related to spatial vision and object recognition respectively. Understanding the relationship between early parallel pathways and dorsal and ventral cortical processing streams has proven difficult because of the substantial convergence of M, P, and K pathways outside of layer 4C of V1.

We used rabies virus as both a mono- and trans-synaptic retrograde tracer to determine the contributions of M and P pathways to dorsal stream cortical area MT in macaque monkey. MT is specialized for motion and depth processing and is thought to be dominated by the M pathway, with little or no contribution from the P or K pathways. We first injected rabies virus into MT with a 3 day survival time, allowing virus to cross one synapse and infect cells disynaptic to the injection site. We found large numbers of parvalbumin-positive, calbindin-negative neurons retrogradely labeled in the M and P layers of the LGN, providing evidence for a disynaptic M and P input to MT, likely mediated by layer 6 Meynert cells in V1.

We next analyzed V1 after the very same injections into MT and found disynaptic label in layer 4C to be confined almost exclusively to M-dominated layer 4Cα. This indicated that the most direct ascending input through layer 4C of V1 to MT is dominated by the M pathway. In order to determine if MT receives indirect P input through layer 4C of V1, we made injections into MT once again, this time with a 6 day survival time, allowing the virus to spread up to four synapses past the cells that

project directly to MT. In this case, we found transynaptic label throughout all layers of V1, including P-dominated layer 4Cβ, indicating that MT does receive indirect P inputs through layer 4C of V1. In order to determine the likely relay of this P input to MT, we made 3 day survival injections of virus into V3 and V2, areas that provide indirect inputs from layer 4B of V1 to MT. Only after certain injections into V2, but not V3, did we observe disynaptic label in both M and P sublayers of 4C. These results suggest that while the most direct ascending input through layer 4C of V1 to MT is dominated by the M pathway, within a few more synapses the P pathway contributes as well, likely through the CO thick stripes of V2.

In a final set of experiments, we used a modified rabies virus that expresses green fluorescent protein and doesn't cross synapses to compare the detailed morphology of neurons projecting directly from V1 to MT or V2. We found that cells projecting from layer 4B of V1 to MT were a majority spiny stellate and those projecting to V2 were overwhelmingly pyramidal. Additionally, MT-projecting cells had larger cell bodies, more total dendritic length, and were located deeper within layer 4B. Finally, pyramidal cells projecting to MT were located preferentially underneath CO blobs, where they could receive strong M inputs onto their apical dendrites. These results suggest that specialized and distinct cell populations in layer 4B of V1 mediate an M-dominated signal to MT and a mixed M and P signal to V2.

All together, these studies provide strong evidence for the existence of multiple circuits between LGN and MT. Each pathway receives a different combination of M and P inputs and is uniquely suited to convey visual information with varying degrees of spatial and temporal resolution, contrast sensitivity, and color selectivity. Distinct

cell types underlie many of these circuits, overcoming the lack of spatial compartmentalization of V1 outputs. Functional studies that can target these specialized cell types and circuits will be necessary to elucidate the contributions of each pathway to response properties in MT and, ultimately, to visual perception and behavior.

Chapter I

Introduction

Our richest life experiences and longest-lasting memories are formed through our interactions with the sensory world around us. The familiar smell of our childhood home or the soft touch of our first love becomes embedded in our minds and has a profound impact on our personality and sense of self. Each of these sensations is transmitted to our brains separately, through distinct biological machinery such as that found in the nose or under the skin. Yet, rather than perceive the world in a similarly disjoint collection of attributes, we most often experience a single unified percept. It is difficult to separate the fruity aroma, crisp texture, and spicy flavor of a favorite bottle of wine.

Parallel processing of sensory information is a commonly used strategy in the mammalian brain, not only between sensory modalities but across features of a single sense as well. Gasser and Erlanger (1929) first demonstrated that the sensations of pain and temperature were transmitted through axons of a different caliber than those transmitting touch. This work was shortly followed up by Bishop (1933) who proposed that three different classes of axons in the optic nerve process different sensory qualities related to vision. These early discoveries laid the foundation for our current understanding and interest in parallel processing strategies of the nervous system. In particular, parallel processing in the visual system has been an intensively studied area of research ever since.

The need for parallel processing in the visual system is immediately appreciated when one considers the multitude of qualities present in the visual environment and the physical limitations by which this information is initially encoded and signaled to the brain. Color, depth, shape, and motion are just a few of the many

dimensions by which we interpret our visual environment and generate appropriate behavior. Nevertheless, the complexity and intricate detail of our visual surroundings are encoded as a pattern of light on a two dimensional array of photoreceptors, with little direct resemblance to the original input or the ultimate percept. Additionally, the route by which this visual information leaves the eye and reaches the brain, the optic nerve, acts as an anatomical bottleneck, condensing the system into the minimum number of axons necessary to adequately represent the entirety of a visual scene. To overcome these constraints, incoming visual signals are processed by at least 80 anatomically and physiologically distinct neural cell populations (Sterling, 1998; Masland, 2001) and 20 separate circuits (Wassle and Boycott, 1991; Roska and Werblin, 2001; Rockhill et al., 2002) within the retina, ultimately packed into at least a dozen parallel pathways that connect to the brain for further processing (Dacey et al., 2003). It is then the job of visual cortex to extract the relevant information from this reduced signal and further elaborate and integrate this information into a unified and coherent perceptual experience.

A clear understanding of how parallel pathways within the visual system are decoded by cortex requires studies that can directly relate the structure and function of each pathway to the organization of visual cortex and related perception and behavior. For this very reason, much of our understanding of the human visual system and related parallel processing strategies has been obtained from over 50 years of research on the visual system of old world macaque monkey. Despite some clear differences resulting from millions of years of separate evolutionary history, striking similarities exist between the visual systems of humans and macaques. Not only do we share the

same cone photoreceptor types and postreceptoral circuitry within the retina (Dacey, 2004), but we also share remarkably similar anatomical organization and functional homology across both subcortical and cortical visual areas (Orban et al., 2004). Furthermore, macaque monkeys can be trained to perform complex visual tasks and report their perceptual experience. In no other species, therefore, have we been able to study the relationship between structure, function, and high level visual behavior in such detail. The goal of the work described in this dissertation is to elucidate how early parallel pathways in the primate visual system contribute to anatomically and functionally specialized areas and processing streams within visual cortex. This knowledge is critical to our understanding of the human visual system and, more generally, human sensory processing.

Background

Early Parallel Pathways from Retina to Cortex

The first steps in seeing begin in the retina, where a dense array of photoreceptors converts the incoming pattern of light into the electrochemical language of the brain. It is now well established that parallel visual pathways begin at the very next step, where an intricate web of bipolar, horizontal, and amacrine cells form specialized postreceptoral circuits and shape a diverse group of ganglion cells that exit the eye and connect to the brain. An early indication that visual signals leaving the retina are not homogeneous came from the anatomical work of Polyak (1941), in which he used Golgi stains to demonstrate the existence of at least two types of ganglion cells, now referred to as midget and parasol cells. It was not until

many years later, however, that Gouras (1968) recorded from ganglion cells in the eye and observed two types of visual responses, transient and sustained, confirming that retinal ganglion cells were functionally heterogeneous as well. A series of studies examining the visual responses of these retinal ganglion cells soon followed and provided evidence for at least two types of functional classes. The transient cells conducted rapidly, had large receptive fields, and lacked color selectivity, whereas the sustained cells conducted more slowly, had smaller receptive fields, and were color selective (De Valois, 1973; Gouras, 1981).

Around this same time, recordings from the lateral geniculate nucleus (LGN) of the thalamus, the major relay of retinal ganglion cells on their way to cortex, were providing mounting evidence for the existence of parallel pathways. The LGN is a six layered structure with the four most dorsal layers referred to as parvocellular (P) and the two most ventral layers as magnocellular (M) based on the presence of small and large sized cells respectively. Only later would the intercalated zones between each M and P layer as well as the extremely small cells found within be officially recognized as a separate population and referred to as koniocellular (K) (Kaas et al., 1978). Numerous differences were observed in the visual response properties of cells in the M or P layers of the LGN. M cells were found to have larger receptive fields, more transient response times, faster conduction velocities, and higher contrast sensitivity than P cells (DeMonasterio and Gouras, 1975; Dreher et al., 1976; Schiller and Malpeli, 1978; Shapley et al., 1981; Kaplan and Shapley, 1982). Most striking, was the presence of wavelength selective, color opponent cells in the P layers of the LGN and only broadband cells in the M layers (Wiesel and Hubel, 1966; Schiller and

Colby, 1983; Derrington et al., 1984). M cells were also shown to be responsive to higher temporal and lower spatial frequencies than P cells (Hicks et al., 1983; Derrington and Lennie, 1984), though considerable overlap existed between the two populations. Interestingly, similar response properties to those observed in M and P layers of the LGN were also found in the very sub lamina of primary visual cortex (V1) to which these layers were known to project (Blasdel and Fitzpatrick, 1984; Hawken and Parker, 1984; Hendrickson et al., 1978), providing evidence that the parallel pathways observed in the LGN remained separate and distinct up and into V1.

The numerous observations of physiological differences between M and P layers of the LGN, motivated studies to examine the relationship between these responses and the different ganglion cell types of the retina. A link was first established anatomically by placing retrograde tracers into either M or P layers of the LGN (Leventhal et al., 1981; Perry et al., 1984). These studies showed that parasol and midget ganglion cells of the retina, those first described by Polyak 40 years earlier, project to the M and P layers of the LGN respectively. Building upon these studies, Kaplan and Shapley (1986) simultaneously recorded retinal ganglion cell synaptic potentials (S potentials) and LGN relay cell action potentials in either M or P layers of the LGN. They showed that the high and low contrast sensitivities of M and P cells in the LGN were inherited from functionally distinct populations of retinal ganglion cells. Similar results were later extended to the broadband and color opponent responses of cells in M and P layers as well (Michael, 1988). Together, these studies provided the first direct links between anatomically and functionally

defined ganglion cell types in the retina and parallel pathways coursing through the LGN and into V1.

Just as the experiments above were being completed, a number of studies were carried out to confirm that the physiological differences observed between M and P pathways were both functionally and behaviorally significant. A series of studies tested for effects on behavior following lesions in either M or P layers of the LGN. It should be kept in mind, however, that at the time of these studies the K pathway was still not appreciated and was likely included in the lesions of either M or P pathways. The clearest impact of M lesions was a large decrease in luminance contrast sensitivity for stimuli of high temporal and low spatial frequencies (Merigan et al., 1991a). This result was consistent with the spatio-temporal sensitivities of cells in the M pathway. Additionally, M lesions had little effect on color contrast sensitivity (Merigan et al., 1991a,b), consistent with the absence of color opponent responses among cells in the M pathway. In striking contrast, P lesions caused an almost complete loss of color vision (Merigan, 1989; Schiller et al., 1990a; Merigan et al., 1991b). This result was consistent with the color opponent responses observed among cells in the P pathway. Complementary to M lesions, luminance contrast sensitivity was reduced for stimuli of higher spatial and lower temporal frequencies following P lesions (Merigan and Eskin, 1986; Merigan et al., 1991a,b). Interestingly, P lesions also resulted in a substantial decrease in visual acuity (Merigan et al., 1991b), likely due to the approximate 8:1 ratio of midget to parasol ganglion cells in the central retina (Perry et al., 1984; Silveira and Perry, 1991). All together, the above described data provided strong support for the existence of at least two parallel pathways that originate in the

retina, remain anatomically and physiologically separate through the LGN and into V1, and mediate distinct visual information important for perception and behavior.

It is now well understood that at least a dozen different retinal ganglion cell types project to the LGN (Dacey et al., 2003). Of these many cell types, three have been particularly well characterized and linked to parallel pathways (Dacey, 2000; Hendry and Reid, 2000). Each of these cell types tiles the retina, providing a complete representation across the entire visual field of the attributes it conveys to the brain. Midget ganglion cells are considered to be the origin of the P pathway and comprise approximately 70% of the total population of cells projecting to the LGN (Dacey, 2000). They have a relatively small dendritic field diameter with a dense branching pattern that is broadly monostratified in the inner plexiform layer. Within the central 10 degrees of visual angle, they receive almost all their excitatory input from a single midget bipolar cell, which in turn connects to a single cone photoreceptor (Calkins et al., 1994). This "private line" circuit is capable of preserving the limit on achromatic spatial resolution set by the peak density of cone photoreceptors in the fovea. Additionally, with inhibitory input from a different cone type, these cells are capable of mediating long (L) and middle (M) wavelength cone (red/green) opponent signals to the P layers of the LGN and on to layers 4A, 4Cβ, and 6 of V1 (Hendrickson et al., 1978; Blasdel and Lund, 1983; Michael, 1988; Dacey, 2000). Cells in this pathway are typically characterized as having small receptive fields, low contrast sensitivity, slow conduction velocities, and sensitivity to high spatial and low temporal frequencies.

Parasol ganglion cells are considered to be the origin of the M pathway and comprise approximately 10% of the total population of cells projecting to the LGN (Dacey, 2000). They have a relatively large dendritic field diameter with a compact, highly branched dendritic tree that is narrowly monostratified near the center of the inner plexiform layer. These cells receive input from several diffuse bipolar cells which in turn sample from several cones. Because their L and M cone input is additive and not opponent, these cells signal a broadband, achromatic signal to the M layers of the LGN and on to layers 4Cα and 6 of V1 (Hendrickson et al., 1978; Blasdel and Lund, 1983; Michael, 1988). Cells in this pathway are typically characterized as having large receptive fields, high contrast sensitivity, fast conduction velocities, and sensitivity to high temporal and low spatial frequencies.

Finally, small and large bistratified ganglion cells make up at least part of the K pathway and together comprise approximately 8% of the total population of cells projecting to the LGN (Dacey, 2000). They have dendritic field diameters that are as large or larger than parasol cells and a sparser dendritic branching pattern that is narrowly bistratified in the inner plexiform layer. These cells receive an excitatory input from small (S) wavelength cones and an inhibitory input from L and M cones, providing the basis for a blue-on/yellow-off color opponent signal (Dacey and Lee, 1994; Dacey et al., 2003). Small and large bistratified cells likely project to K layers 3 and 4 of the LGN, which in turn project to layer 1 and the cytochrome oxidase blobs of layer 2/3 in V1 (Livingstone and Hubel, 1982; Dacey and Lee, 1994; Hendry and Yoshioka, 1994; Hendry and Reid, 2000). K cells in the LGN are defined as cells that express αCAM kinase and/or calbindin (Hendry and Yoshioka, 1994) and are found

not only in the intercalated layers but also scattered throughout the M and P layers as well. It has, therefore, been difficult to characterize the full range of physiological response properties carried by the K pathway to V1.

While the existence of early parallel pathways in the primate visual system is well established and great headway has been made in assessing their functions, numerous questions remain unanswered. For instance, it is still unclear whether the color opponent responses of ganglion cells result from a specific or random sampling of the cone photoreceptor mosaic (Paulus and Kroger-Paulus, 1983; Martin et al., 2001). Also unclear, is the extent to which M and P pathways are homogeneous processing streams. The ganglion cells already characterized numerically dominate the retina, yet they only constitute a minority of the total number of cell types known to exist (Dacey et al., 2003). The less dense cell types of the retina likely confer heterogeneity to both M and P layers of the LGN, as well as the already heterogeneous K layers (Rodieck and Watanabe, 1993; Hendry and Reid, 2000). It is also likely that these cell types provide the substrates for additional parallel pathways that make important functional contributions to the visual system, such as the mono- and bi-stratified recursive retinal ganglion cells thought to be involved in the early stages of motion processing (Dacey, 2004). Finally, since the signals carried by the parallel pathways bear little resemblance to our perceptual experiences, the functional role of each pathway is still poorly understood. For instance, fundamental questions remain regarding the role of the M and P pathways in spatial vision, chromatic processes, and motion computations. Ultimately, the key to uncovering the functions of the early

parallel pathways may require a better understanding of the relationship between these pathways and processing streams within visual cortex.

Parallel Processing Streams in Visual Cortex

Once the condensed and parallel signals from the retina arrive in visual cortex, the original components of the visual scene must be extracted, elaborated upon, and integrated into a unified percept. Visual cortex uses both modular and hierarchical processing in order to accomplish these goals (Zeki and Shipp, 1988). While the basic tuning properties of cells do not differ substantially between retina and LGN, within the first cortical synapses new and more complex responses are formed such as orientation, direction, and color selectivity. Many of these responses are organized into overlapping functional maps, with a columnar organization for orientation tuning, ocular dominance, and visual space. As visual information passes through extrastriate cortex, the response properties found within each subsequent area tend to increase in complexity and selectivity. New computations are carried out along the way, eventually leading to highly specialized areas concerned with object recognition and sensorimotor integration. The functional organization of visual cortex is thought to be fundamental to our understanding of the visual system and the generation of behavior and perception.

Visual information related to color, form, and motion/depth were originally thought to be processed separately within V1. This tripartite theory was first proposed by Livingstone and Hubel (1988) and was motivated by the distinctive laminar organization of V1 and the discovery of alternating light and dark staining for the

mitochondrial enzyme cytochrome oxidase (CO) in the superficial layers. CO blobs (dark staining) in layer 2/3 were thought to subserve color processing, CO interblobs (light staining) form processing, and layer 4B motion and depth. The role of layer 4B in motion processing has proven to be least contentious, as numerous studies have reported the layer to contain a relatively high preponderance of cells with strong direction selectivity (Hawken et al., 1988; Gur et al., 2005). The role of blobs and interblobs, however, remains controversial. In support of the tripartite theory, CO blobs receive direct blue/yellow color opponent signals, likely from LGN K cells (Hendry and Yoshioka, 1994; Chatterjee and Callaway, 2003). Additionally, CO blobs have been shown to contain large numbers of unoriented, color opponent cells as compared to interblobs where orientation tuned color non-opponent cells are more common (Livingstone and Hubel, 1984; Ts'o and Gilbert, 1988; Yoshioka and Dow, 1996; Landisman and Ts'o, 2002; Tootell et al., 2004). Nevertheless, other studies have not seen such a clear relationship between the CO compartments and form or color processing (Edwards et al., 1995; Leventhal et al., 1995; O'Keefe et al., 1998). Furthermore, numerous studies have indicated that orientation and color tuning are commonly found in the same V1 cells and across almost all layers of V1 (Lennie et al., 1990; Leventhal et al., 1995; Johnson et al., 2001). It, therefore, remains controversial whether the CO blobs and interblobs truly act as substrates for separate color and form processing streams. Regardless of the true function of these various compartments, however, it does seem clear from the minimal crosstalk between blobs and interblobs (Yoshioka et al., 1996; Yabuta and Callaway, 1998a) that some form of parallel processing is being carried out.

Anatomical connections between V1 and functionally specialized compartments within V2 appear to maintain much of the proposed segregation of processing streams. CO blobs, interblobs, and layer 4B of V1 were originally thought to project specifically to the thin, pale, and thick CO stripes of V2 respectively (Livingstone and Hubel, 1983, 1987). Recordings from the three stripe compartments in V2 provided additional support for maintained segregation as responses were characterized as direction and depth tuned in the thick stripes, orientation tuned and end-stopped in the pale stripes, and color tuned in the thin stripes (DeYoe and Van Essen, 1985; Hubel and Livingstone, 1987; Roe and Ts'o, 1995; Shipp and Zeki, 2002). In fact, functional maps for color selectivity have been observed in the thin stripes of V2 providing evidence for highly specialized color processing in this V2 compartment (Xiao et al., 2003). However, recent evidence has also suggested that connections from V1 to V2 are not as cleanly segregated as first thought (Sincich and Horton, 2002; Xiao et al., 2003) and connections between stripes of different types are common within V2 (Levitt et al., 1994a). Furthermore, numerous studies have since recorded from the different V2 stripes and observed less correlation between response properties and stripe type than originally reported (Levitt et al., 1994b; Gegenfurtner et al., 1996). Part of the continued confusion regarding segregation in V2 may be due to the patchy and variable nature of the CO stripes which has made it difficult to isolate anatomical injections or physiological recordings to a particular stripe type. Despite these difficulties, substantial evidence exists in support of separate pathways through V2.

The outputs from V1 and V2 to areas V3, V4, and MT are the beginnings of a more pronounced anatomical segregation of processing streams. MT is an area specialized for processing motion and depth and V4 is an area specialized for processing color and form. The two areas, therefore, appear to be manifestations of earlier segregation in V1 and V2. Anatomical evidence supports this claim as numerous studies have shown that layer 4B of V1 and the thick stripes of V2 project to MT and V3, whereas the pale and thin stripes of V2 project to V4 (DeYoe and Van Essen, 1985; Shipp and Zeki, 1985; Burkhalter et al., 1986; Shipp and Zeki, 1989a; Felleman et al., 1997). Additionally, the pale and thin stripes of V2 may maintain segregation by connecting to separate compartments in V4 (DeYoe et al., 1994), although this remains somewhat unclear (Xiao et al., 1999). The relationship between V3 and these segregated pathways is less obvious. While its ascending input sources and complex motion responses have placed it firmly in a pathway leading to MT, strong connections with V4 and a large percentage of color selective cells have called this association into question (Burkhalter et al., 1986; Gegenfurtner et al., 1997; Beck and Kaas, 1999). Indeed, many of the same cells in V3 are selective for both color and direction of motion, making it intriguing to consider V3 a sight for integration of visual information important for further computations in both MT and V4. Additional crosstalk along these pathways likely exists in the feedback connections from MT and V4 which appear not to respect the borders of V2 stripes (Shipp and Zeki, 1989b; Zeki and Shipp, 1989).

Finally, extrastriate cortical areas MT and V4 appear to act as gateways to further processing in relatively separate and independent dorsal and ventral stream

cortical areas. First proposed by Ungerleider and Mishkin (1982), the existence of separate pathways for the visual recognition of objects (ventral) and the spatial relationships among objects and visual guidance toward them (dorsal) now has extensive anatomical and functional support. MT connects dorsally within posterior parietal cortex to other areas in the superior temporal sulcus (STS) including medial superior temporal (MST) area and the fundus of the superior temporal (FST) area (Maunsell and Van Essen, 1983; Ungerleider and Desimone, 1986) which both project to superior temporal polysensory (STP) area (Boussaoud et al., 1990). MT also projects to ventral intraparietal (VIP) area (Ungerleider and Desimone, 1986) which projects to area 7a and lateral intraparietal (LIP) area (Blatt et al., 1990; Boussaoud et al., 1990). Meanwhile, V4 projects ventrally to areas temporal occipital (TEO) and temporal (TE), which together comprise inferior temporal (IT) cortex (Distler et al., 1993; Nakamura et al., 1993). While these anatomical connections are surprisingly immune from crosstalk, there is evidence for interconnections between MT/MST and V4 (Maunsell and Van Essen, 1983; Ungerleider and Desimone, 1986) as well as input from both dorsal and ventral streams into STP (Boussaoud et al., 1990).

Strong functional evidence also exists in support of separate dorsal and ventral processing streams. Neuronal responses along the ventral stream are best characterized by the selectivity to color and contours in V4 (Desimone et al., 1985) and more complex combinations of colors, patterns and/or shapes in TEO and TE (Desimone et al., 1984; Komatsu and Ideura, 1993), including a high concentration of face selective cells in TE (Perrett et al., 1982). Neuronal responses along the dorsal stream are best characterized by the selectivity to direction of motion and depth in MT

(Albright, 1984; DeAngelis and Newsome, 1998), more complex motion analysis in MST and area 7a such as that related to optic flow (Lappe et al., 1996; Siegel and Read, 1997), and sensorimotor transformations in preparation for action in LIP (Gnadt and Andersen, 1988). It is important to note, however, that very few studies have directly compared the neuronal response properties in areas beyond MT and V4 in the dorsal and ventral streams. Therefore, the degree of specialization along the two processing streams is not fully understood.

Lesion studies have further corroborated the observed physiological differences along the two processing streams. Dorsal stream lesions have been shown to affect motion and spatial perception, including the effect of MT/MST lesions on smooth pursuit eye movements, speed processing, and complex motion perception (Newsome and Pare, 1988; Pasternak and Merigan, 1994; Orban et al., 1995) and LIP/area 7a lesions on accurate encoding of visual space (Latto, 1986; Quintana and Fuster, 1993). Ventral stream lesions, on the other hand, have been shown to affect form related perception, including the effect of V4 and IT lesions on orientation and complex shape discriminations, perceptual invariance, and attention (Merigan, 1996; Vogels et al., 1997; De Weerd et al., 1999). Surprisingly, only modest effects on color discriminations have been reported following lesions of V4 (Heywood and Cowey, 1987; Walsh et al., 1993). Overall, few studies have attempted a double dissociation of the effects of dorsal and ventral stream lesions, leaving the extent of segregation between the two processing streams unclear.

Despite some evidence of intermixing and remaining questions regarding their function, parallel pathways are a well established feature of visual cortex. They

originate in the output layers of V1 and V2 and form specialized dorsal and ventral processing streams that extend to the farthest reaches of extrastriate cortex. Still a great mystery, however, are the cortical strategies used to eventually integrate distinct visual information into a unified and coherent percept. Studies that probe the detailed functional organization of these cortical pathways promise to uncover the neural mechanisms responsible for this critical step. Equally important, are the remaining mysteries surrounding how separate dorsal and ventral processing streams are formed in the first place. Early parallel pathways that originate in the retina are thought to play an integral role in this process, yet major questions remain regarding the degree to which they converge or maintain segregation in visual cortex.

Relating Early Parallel Pathways to Cortical Processing

The relationship between the M, P, and K pathways of the retina and LGN and the dorsal and ventral streams of visual cortex is not well understood and continues to be an active area of research. Early studies suggested that dorsal and ventral streams are the continuations of the M and P pathways. The conclusions drawn from these studies relied on the belief that the compartments within V1 were mechanisms for strict segregation of early parallel pathways. It is now clear, however, that the M and P pathways intermix significantly within V1, and outputs from V1 to extrastriate cortex are less compartmentalized than originally proposed. Also, the existence of the K pathway was not fully appreciated until recently and further complicates earlier interpretations. In light of these new findings, the relationship between M, P, and K pathways and dorsal and ventral stream cortical processing must be reassessed.

In order to understand the relationship between early parallel pathways and dorsal and ventral cortical streams, the contributions of the M, P, and K pathways to the compartments of V1 must first be addressed. Anatomically, these contributions have been determined through the use of local tracer injections and intracellular fills to visualize the connections between LGN-recipient layers or compartments and the output layers of V1. Layer 4B receives its strongest input from M-recipient layer 4Cα (Fitzpatrick et al., 1985; Yoshioka et al., 1994; Callaway and Wiser, 1996). Cells in layer 4Cα have dense axonal branches in layer 4B, whereas those from P-recipient 4Cβ pass through layer 4B without branching. Likewise, pyramidal cells in the K-recipient layer 2/3 blobs have only sparse axonal branches in layer 4B (Anderson et al., 1993; Callaway and Wiser, 1996). Importantly, though, layer 4B contains two types of morphologically distinct projection neurons: spiny stellates and pyramids. While the dendrites of spiny stellates are almost entirely confined to layers 4B and 4Cα, pyramids have an apical dendrite that extends through layer 2/3 and to the top of layer 1. Photostimulation studies in monkey V1 slices have confirmed that while spiny stellates receive input only from layer 4Cα, pyramids receive substantial, though less dominant input from 4Cβ as well (Yabuta et al., 2001). As this study analyzed input only from deeper layers, it remains unclear whether layer 4B pyramids also receive input from K-recipient layer 1 or the blobs of layer 2/3.

The connections from layer 4C to the CO blobs and interblobs of layer 2/3 provide even more opportunity for mixing of early parallel pathways. In particular, the blobs of layer 2/3 appear to receive convergent input from M, P, and K pathways.

Several studies have shown that cells in layer 4Cα specifically target the blobs, providing strong input from the M pathway (Lachica et al., 1992; Yabuta and Callaway, 1998b). A subpopulation of cells at the bottom of layer 4Cα, however, projects to both and interblobs and may be in a position to receive mixed M and P inputs from the LGN. Layer 4B cells also target the blobs, providing indirect input from the M pathway (Lachica et al., 1992; Yoshioka et al., 1994; Callaway and Wiser, 1996). P input from layer 4Cβ projects rather uniformly to both blobs and interblobs (Lachica et al., 1992; Callaway and Wiser, 1996). Finally, the blobs receive direct input from K layers of the LGN (Hendry and Yoshioka, 1994). Both CO blobs and interblobs, therefore, receive convergent input from M and P pathways, with the blobs receiving additional strong input from the K pathway as well. Photostimulation studies later confirmed that single neurons within layer 3 receive convergent input from the M and P pathways (Sawatari and Callaway, 2000). Interestingly, this convergent input may require an additional synapse before exiting V1 as layer 3 projection neurons were shown to receive direct input only from layer 4Cα.

Functionally, the relationship between early parallel pathways and V1 compartments has been assessed by comparing neuronal responses recorded in V1 output layers with those recorded in LGN input layers and layers of the LGN. The most striking property of cells in layer 4B is their strong direction selectivity (Hawken et al., 1988; Gur et al., 2005). The transient responses of M pathway neurons and their sensitivity to high temporal frequencies have often been cited as support for their role in motion processing. The connection between these M pathway responses and direction selectivity, however, remains ill-defined and inactivation of M layers in the

LGN does not abolish direction selectivity in most V1 neurons (Malpeli et al., 1981). Nevertheless, layer 4B neurons are also characterized by their high contrast sensitivity, low spatial frequency selectivity, and lack of color opponency (Hawken et al., 1988) which relate them much more clearly to neurons in the M pathway. It should be noted, however, that high contrast sensitivity could be conferred upon layer 4B neurons via summed input from the P pathway and, likewise, a lack of color opponent responses doesn't preclude the possibility of color non-opponent input from the P pathway. Indeed, inactivation of M layers of the LGN can have strong or small effects on the responsiveness of individual layer 4B cells (Nealey and Maunsell, 1994).

Functional evidence relating the early parallel pathways to layer 2/3 blobs and interblobs is rather inconclusive due to disagreement regarding the extent to which blobs and interblobs differ physiologically (Leventhal et al., 1995). The high contrast sensitivity and low spatial frequency selectivity of CO blobs are consistent with strong M inputs (Tootell et al., 1988; Silverman et al., 1989; Hubel and Livingstone, 1990), yet K cells in the LGN have been shown to have similar response properties (Hendry and Reid, 2000). Likewise, the supposedly high prevalence of unoriented, color opponent cells in the blobs (Livingstone and Hubel, 1984) could be mediated by direct K input rather than indirect P input. Nevertheless, red/green color opponency has been observed in the blobs and is likely conveyed via the P pathway (Ts'o and Gilbert, 1988). The CO interblobs, on the other hand, were originally thought to consist mainly of cells that are strongly orientation tuned but not color opponent (Livingstone and Hubel, 1984). Even if this was the case, it would be difficult to surmise the clear presence or absence of a certain pathway contribution based on these response

properties. Surprisingly, lesion studies have given no indication that the blobs or interblobs differ substantially in their dependence on the M or P pathways (Malpeli et al., 1981; Nealey and Maunsell, 1994).

Attempts to relate early parallel pathways to extrastriate dorsal and ventral streams have largely relied on the supposedly clean segregation and compartmentalization of the M, P, and K pathways in V1. Indirect anatomical evidence regarding M, P, and K contributions to extrastriate cortex could then be obtained by injecting retrograde tracer into a specific cortical area and observing which V1 compartments were labeled. Convergence of early parallel pathways onto the compartments of V1, however, has made such an approach rather limited.

Retrograde tracer studies have shown that MT, V3, and the CO thick stripes of V2 all receive input primarily from separate populations of cells in layer 4B of V1 (Burkhalter et al., 1986; Livingstone and Hubel, 1987; Shipp and Zeki, 1989a; Sincich and Horton, 2003). Because V3 and the thick stripes of V2 have been shown to provide indirect inputs from V1 to MT (Maunsell and Van Essen, 1983), layer 4B of V1 was identified as the primary conduit of visual information to MT and dorsal stream cortical areas. Layer 4B of V1 was originally thought to receive M only signals from layer 4Cα, which led to the simple conclusion that the dorsal stream was fed by M only input. Yet, the existence of convergent M and P input onto layer 4B pyramidal cells and M only input onto spiny stellate cells has created a more complex reality (Yabuta et al., 2001). In order to determine the M and P contributions to MT, V3, or the thick stripes of V2, the proportion of cell type in layer 4B of V1 must be ascertained. An attempt has been made to do just that, with the resultant claim that

spiny stellates make up the majority cell type projecting directly to MT (Shipp and Zeki, 1989a). This would be consistent with an M only input to MT. Nevertheless, these studies were unable to obtain detailed morphology of their labeled cells in layer 4B of V1 and their conclusions, therefore, remain in question. Additionally, the proportion of cell types projecting from layer 4B of V1 to V3 and the CO thick stripes of V2 has never been determined. The mere fact that pyramidal cells make up the majority cell type in layer 4B of V1, however, makes it quite likely that MT receives some P input, either directly from V1 or indirectly through V2 or V3. Furthermore, recent data suggests that the CO thick stripes of V2 receive input from layer 2/3 interblobs as well (Sincich and Horton, 2002), yet another potential source for indirect P input to MT and the dorsal stream. Finally, a direct input from K cells in the LGN to MT has recently been confirmed (Sincich et al., 2004) and indicates that the dorsal stream may actually receive signals from all three early parallel pathways, albeit with different relative strengths.

The thin and pale stripes of V2 were originally shown to receive input from the layer 2/3 blobs and interblobs of V1 respectively (Livingstone and Hubel, 1983). Because the thin and pale stripes of V2 project on to V4, layer 2/3 of V1 was considered that primary relay of visual information to V4 and ventral stream cortical areas. Layer 2/3 of V1 was originally thought to receive P only inputs, which led to the simple conclusion that the ventral stream was fed by the P pathway. It is now clear, however, that both blobs and interblobs receive inputs from M and P pathways, with additional K input provided at least to the blobs. Additionally, photostimulation data suggests that projection neurons in layer 3 receive input only from layer 4Cα and

only local pyramidal neurons in layer 3 receive input from layer 4Cβ as well (Yabuta et al., 2001). It may, therefore, require an additional synapse for any P input to reach V2 at all. Even the original tripartite segregation of connections between V1 and V2 has now been called into question by showing strong connections from interblobs of V1 to the thin stripes of V2 (Xiao and Felleman, 2004) and that all projection layers underneath interblobs, not just layer 2/3, project to either pale or thick stripes (Sincich and Horton, 2002). This lack of compartmentalization in the outputs from V1 to V2 makes it even less clear how the early parallel pathways contribute to the ventral processing stream.

Attempts to understand the functional contributions of early parallel pathways to dorsal and ventral stream processing have relied on comparing neuronal responses and visual behavior following M/P lesions and dorsal/ventral lesions. It is important to note that one limitation of this approach is that lesions of M or P layers inevitably include partial lesions of the K layers as well, which can complicate the interpretation of any observed effects. Lesions of the M layers of the LGN have been shown to have pronounced effects on the responsiveness of cells in MT, a dorsal stream cortical area specialized for motion processing. Nevertheless, responses are often not completely abolished and P layer lesions produce small but significant effects as well. It is, therefore, possible that the P or K pathways underlie the preserved ability to make motion direction and speed discriminations following M lesions (Merigan et al., 1991a). Rather than affect motion perception, per se, M lesions appear to decrease contrast sensitivity for stimuli of high temporal and low spatial frequencies. These effects are not consistent with lesions of dorsal stream areas which show no clear

effects on contrast sensitivity (Newsome and Pare, 1988; Merigan et al, 1991a). Lesions of MT itself results in disruption of some aspects of motion perception and eye movements, and lesions farther along in parietal cortex can result in spatial disorientation (Lynch, 1980). Together, these data suggest that the dorsal stream relies heavily on visual information provided by the M pathway, yet it does not depend on the M pathway alone for its role in motion perception and other functions.

Lesions of either M or P layers of the LGN have been shown to strongly diminish the responsiveness of cells in V4 (Ferrera et al., 1991), supporting an important role for both pathways in processing within V4 and ventral stream cortical areas. Nevertheless, the disruptions of color vision, acuity, and contrast sensitivity for stimuli of low temporal and high spatial frequencies following P lesions is rather inconsistent with only modest disruption of color discriminations following V4 lesions (Heywood and Cowey, 1987) and little, if any, effect on thresholds for acuity following IT lesions (Gross, 1973). The most pronounced effects of ventral stream lesions are disruptions of shape discrimination after V4 and IT lesions (Heywood and Cowey, 1987) and effects on visual memory after lesions of area TE (Phillips et al., 1988). Nevertheless, P lesions result in no obvious impairments related to shape discriminations (Schiller et al., 1990a,b) and no study has examined effects of P lesions on memory. Together, these data demonstrate a lack of clear correspondence between the P pathway and ventral stream processing related to shape discriminations and other functions. All three early parallel pathways likely play an important role in processing of visual information along the ventral stream.

A final way in which contributions of early parallel pathways have been assessed relative to dorsal and ventral stream processing is through the use of stimuli that are designed to isolate one or the other system. Stimuli constructed to isolate the P pathway have typically been defined by isoluminant chromatic contrast or high spatial frequencies that only minimally stimulate the M pathway or high contrasts which like saturate M pathways responses (Livingstone and Hubel, 1988; Cavanagh and Mathers, 1989; Saito et al., 1989; Croner and Albright, 1999). Unfortunately, the conclusions that can be made using such stimuli are very limited due to the fact that any effects observed can be attributed either to the small responses that typically remain in the M pathway or the unintended yet inevitable diminishment of responses in the P pathway. Indeed, direction selective responses to isoluminant chromatic stimuli in MT have been attributed to unbalanced cone inputs in M pathway neurons (Dobkins and Albright, 1994). Stimuli constructed to isolate the M pathway have typically been defined by low contrasts and high temporal frequencies that only minimally drive responses in the P pathway. The use of these stimuli, however, suffers from the same limitations as described above.

Despite intense efforts, the contributions of early parallel pathways to dorsal and ventral stream cortical processing remain poorly understood. While earlier models possessed an attractive simplicity, the complex reality of cortical circuitry demands new approaches and updated theories. In the remaining chapters of this dissertation, we describe studies that aim to elucidate the relationship between early parallel pathways and extrastriate cortical processing, with a particular emphasis on M and P pathways and the dorsal stream. To address these questions, we utilized rabies

virus as a mono- and trans-synaptic retrograde tracer of neural circuits in the primate visual system. We provide evidence for multiple pathways from the LGN to dorsal stream cortical areas, mediated by specific cell types and circuits in V1. Each of these pathways receives a different combination of M and P inputs and likely provides the dorsal stream with specialized visual information uniquely suited for specific visual tasks and computations.

References

Albright, T.D. (1984). Direction and orientation selectivity of neurons in visual area MT of the macaque. J. Neurophysiol. 52, 1106-1130.

Anderson, J.C., Martin, K.A.C., and Whitteridge, D. (1993). Form, function, and intracortical projections of neurons in the striate cortex of the monkey Macacus nemestrinus. Cereb. Cortex 3, 412-420.

Beck, P.D., and Kaas, J.H. (1999). Cortical connections of the dorsomedial visual area in old world macaque monkeys. J. Comp. Neurol. 406, 487-502.

Bishop, G.H. (1933). Fiber groups in the optic nerves. Am. J. Physiol. 106, 460-470.

Blasdel, G.G., and Fitzpatrick, D. (1984). Physiological organization of layer 4 in macaque striate cortex. J. Neurosci. 4, 880-895.

Blasdel, G.G., and Lund, J.S. (1983). Termination of afferent axons in macaque striate cortex. J. Neurosci. 3, 1389-1413.

Blatt, G.J.R., Andersen, A., and Stoner, G.R. (1990). Visual receptive field organization and cortico-cortical connections of the lateral intraparietal area (area LIP) in the macaque. J. Comp. Neurol. 299, 421-445.

Boussaoud, D., Ungerleider, L.G., and Desimone, R. (1990). Pathways for motion analysis: cortical connections of the medial superior temporal and fundus of the superior temporal visual areas in the macaque. J. Comp. Neurol. 296, 462-495.

Burkhalter, A., Felleman, D.J., Newsome, W.T., and Van Essen, D.C. (1986).

Anatomical and physiological asymmetries related to visual areas V3 and VP in macaque extrastriate cortex. Vision Res. 26, 63-80.

Calkins, D.J., Schein, S.J., Tsukamoto, Y., Sterling, P. (1994). M and L cones in macaque fovea connect to midget ganglion cells by different numbers of excitatory synapses. Nature 371, 70-72.

Callaway, E.M., and Wiser, K. (1996). Contributions of individual layer 2-5 spiny neurons to local circuits in macaque primary visual cortex. Vis. Neurosci. 13, 907-922.

Cavanagh, P., and Mather, G. (1989). Motion: the long and short of it. Spatial Vis. 4, 103-129.

Chatterjee, S., and Callaway, E.M. (2003). Parallel colour-opponent pathways to primary visual cortex. Nature 426, 668-671.

Croner, L.J., and Albright, T.D. (1999). Segmentation by color influences responses of motion-sensitive neurons in the cortical middle temporal visual area. J. Neurosci. 19, 3935-3951.

Dacey, D.M. (2000). Parallel pathways for spectral coding in primate retina. Annu. Rev. Neurosci. 23, 743-775.

Dacey, D.M. (2004). Origins of perception: retinal ganglion cell diversity and the creation of parallel visual pathways. In: The Cognitive Neurosciences, M.S. Gazzaniga, ed. (Cambridge: MIT Press), pp. 281-301.

Dacey, D.M., and Lee, B.B (1994). The 'blue on' opponent pathway in primate retina originates from a distinct bistratified ganglion cell type. Nature 367, 731-735.

Dacey, D.M., Peterson, B.B., Robinson, F.R., and Gamlin, P.D. (2003). Fireworks in the primate retina: in vitro photodynamics reveals diverse LGN-projecting ganglion cell types. Neuron 37, 15-27.

De Valois, R.L. (1973). Central mechanisms of color vision. In: Handbook of Sensory Physiology, Central Processing of Visual Information, Vol. 7, R. Jung, ed. (Berlin: Springer), pp. 209-253.

De Weerd, P., Peralta, M.R., Desimone, R., and Ungerleider, L.G. (1999). Loss of attentional stimulus selection after extrastriate cortical lesions in macaques. Nat. Neurosci. 2, 753-758.

DeAngelis, G.C., Cumming, B.B., and Newsome, W.T. (1998). Cortical area MT and the perception of stereoscopic depth. Nature 394, 677-680.

DeMonasterio, F.M., and Gouras, P. (1975). Functional properties of ganglion cells of the rhesus monkey retina. J. Physiol. 251, 167-195.

Derrington, A.M., Krauskopf, J., and Lennie, P. (1984). Chromatic mechanisms in the lateral geniculate nucleus of macaque. J. Physiol. 357, 241-265.

Derrington, A.M. and Lennie, P. (1984). Spatial and temporal contrast sensitivities of neurons in lateral geniculate nucleus of macaque. J. Physiol. 357, 219-240.

Desimone, R., Albright, T.D., Gross, C.G., and Bruce, C. (1984). Stimulus-selective properties of inferior temporal neurons in the macaque. J. Neurosci. 4, 2051-2062.

Desimone, R., Schein, S.J., Moran, J., Ungerleider, L.G. (1985). Contour, color and shape analysis beyond the striate cortex. Vision Res. 25, 441-452.

DeYoe, E.A., Felleman, D.J., Van Essen, D.C., and McClendon, E. (1994). Multiple processing streams in occipito-temporal visual cortex. Nature 371, 151-154.

DeYoe, E.G., and Van Essen, D.C. (1985). Segregation of efferent connections and receptive field properties in visual area V2 of the macaque monkey. 317, 58-61.

Distler, C., Boussaoud, D., Desimone, R., and Ungerleider, L.G. (1993). Cortical connections of inferior temporal area TEO in macaque monkeys. J. Comp. Neurol. 334, 125-150.

Dobkins, K.R., and Albright, T.D. (1994). What happens if it changes color when it moves?: the nature of chromatic input to macaque visual area MT. J. Neurosci. 14, 4854-4870.

Dreher, B., Fukada, Y., and Rodieck, R.W. (1976). Identification, classification and anatomical segregation of cells with X-like and Y-like properties in the lateral geniculate nucleus of old-world primates. J. Physiol. 258, 433-452.

Edwards, D.P., Purpura, K.P., and Kaplan, E. (1995). Contrast sensitivity and spatial frequency response of primate cortical neurons in and around the cytochrome oxidase blobs. Vision Res. 35, 1501-1523.

Felleman, D.J., Burkhalter, A., and Van Essen, D.C. (1997). Cortical connections of areas V3 and VP of macaque monkey extrastriate visual cortex. J. Comp. Neurol. 379, 21-47.

Ferrera, V.P., Nealey, T.A., and Maunsell, J.H.R. (1991). Magnocellular and

parvocellular contributions to macaque area V4. Invest. Ophthalmol. Vis. Sci. 32, 1117.

Fitzpatrick, D., Lund, J.S., Blasdel, G.G. (1985). Intrinsic connections of macaque striate cortex: afferent and efferent connections of lamina 4C. J. Neurosci. 5, 3329-3349.

Gasser, H.S., and Erlanger, J. (1929). The role of fiber size in the establishment of a nerve block by pressure or cocaine. Am. J. Physiol. 88, 581-591.

Gegenfurtner, K.R., Kiper, D.C., and Fenstemaker, S.B. (1996). Processing of color, form, and motion in macaque area V2. Vis. Neurosci. 13, 161-172.

Gegenfurtner, K.R., Kiper, D.C., and Levitt, J.B. (1997). Functional properties of neurons in macaque area V3. J. Neurophysiol. 77, 1906-1923.

Gnadt, J.W., and Andersen, R.A. (1988). Memory related motion planning activity in posterior parietal cortex of macaque. Exp. Brain Res. 70, 216-220.

Gouras, P. (1968). Identification of cone mechanisms in monkey ganglion cells. J. Physiol. 199, 533-547.

Gouras, P. (1981). Visual system IV: Color vision. In: Principles of Neuroscience, E. Kandel and J. Schwartz, eds. (Amsterdam: Elsevier), pp. 249-257.

Gross, C.G. (1973). Inferotemporal cortex and vision. In: Progress in Physiological Psychology, E. Stellar and J.M. Sprague, eds. (New York: Academic), pp. 77-124.

Gur, M., Kagan, I., and Snodderly, D.M. (2005). Orientation and direction selectivity of neurons in V1 of alert monkeys: functional relationships and laminar distributions. Cereb. Cortex 15, 1207-1221.

Hawken, M.J., and Parker, A.J. (1984). Contrast sensitivity and orientation selectivity in lamina IV of the striate cortex of old world monkeys. Exp. Brain Res. 54, 367-372.

Hawken, M.J., Parker, A.J., and Lund, J.S. (1988). Laminar organization and contrast sensitivity of direction-selective cells in the striate cortex of the old world monkey. J. Neurosci. 8, 3541-48.

Hendrickson, A.E., Wilson, J.R., and Ogren, M.P. (1978). The neuroanatomical organization of pathways between the dorsal lateral geniculate nucleus and visual cortex in old world and new world primates. J. Comp. Neurol. 182, 123-136.

Hendry, S.H., and Reid, R.C. (2000). The koniocellular pathway in primate vision. Annu. Rev. Neurosci. 23, 127-153.

Hendry, S.H., and Yoshioka, T. (1994). A neurochemically distinct third channel in the macaque dorsal lateral geniculate nucleus. Science 264, 575-577.

Heywood, C.A., and Cowey, A. (1987). On the role of cortical area V4 in the discrimination of hue and pattern in macaque monkeys. J. Neurosci. 7, 2601-2617.

Hicks, T.P., Lee, B.B., and Vidyasagar, T.R. (1983). The responses of cells in the macaque lateral geniculate nucleus to sinusoidal gratings. J. Physiol. 337, 183-200.

Hubel, D.H., and Livingstone, M.S. (1987). Segregation of form, color, and stereopsis in primate 18. J. Neurosci. 7, 3378-3415.

Hubel, D.H., and Livingstone, M.S. (1990). Color and contrast sensitivity in the lateral geniculate body and primary visual cortex of the macaque monkey. J. Neurosci. 10, 2223-2237.

Johnson, E.N., Hawken, M.J., and Shapley, R. (2001). The spatial transformation of color in the primary visual cortex of the macaque monkey. Nat. Neurosci. 4, 409-416.

Kaas, J.H., Huerta, M.F., Weber, J.T., Harting, J.K. (1978). Patterns of retinal terminations and laminar organization of the lateral geniculate nucleus of primates. J. Comp. Neurol. 182, 517-553.

Kaplan, E., and Shapley, R.M. (1982). X and Y cells in the lateral geniculate nucleus of macaque monkeys. J. Physiol. 330, 125-143.

Kaplan, E., and Shapley, R.M. (1986). The primate retina contains two types of ganglion cells, with high and low contrast sensitivity. Proc. Natl. Acad. Sci. U.S.A. 83, 2755-2757.

Komatsu, H., and Ideura, Y. (1993). Relationships between color, shape, and pattern selectivities of neurons in the inferior temporal cortex of the monkey. J. Neurophysiol. 70, 677-694.

Lachica, E.A., Beck, P.D., and Casagrande, V.A. (1992). Parallel pathways in macaque monkey striate cortex: anatomically defined columns in layer III. Proc. Natl. Acad. Sci. U.S.A. 89, 3566-3570.

Landisman, C.F., and Ts'o, D.Y. (2002). Color processing in macaque striate cortex:

relationships to ocular dominance, cytochrome oxidase, and orientation. J. Neurophysiol. 87, 3126-3137.

Lappe, M., Bremmer, F., Pekel, M., Thiele, A., and Hoffmann, K.P. (1996). Optic flow processing in monkey STS: a theoretical and experimental approach. J. Neurosci. 16, 6265-6285.

Latto, R. (1986). The role of inferior parietal cortex and the frontal eye-fields in visuospatial discriminations in the macaque monkey. Behav. Brain Res. 22, 41-52.

Lennie, P., Krauskopf, J., and Sclar, G. (1990). Chromatic mechanisms in striate cortex of macaque. J. Neurosci. 10, 649-669.

Leventhal, A.G., Rodieck, R.W., Dreher, B. (1981). Retinal ganglion cell classes in the old world monkey: morphology and central projections. Science 213, 1139-1142.

Leventhal, A.G., Thompson, K.G., Liu, D., Zhou, Y., and Ault, S. (1995). Concomitant sensitivity to orientation, direction, and color of cells in layers 2, 3, and 4 of monkey striate cortex. J. Neurosci. 15, 1808-1818.

Levitt, J.B., Yoshioka, T., and Lund, J.S. (1994a). Intrinsic cortical connections in macaque visual area V2: evidence for interactions between different functional streams. J. Comp. Neurol. 342, 551-570.

Levitt, J.B., Kiper, D.C., and Movshon, J.A. (1994b). Receptive fields and functional architecture of macaque V2. J. Neurophysiol. 71, 2517-2542.

Livingstone, M.S., and Hubel, D.H. (1982). Thalamic inputs to cytochrome oxidase-rich regions in monkey visual cortex. Proc. Natl. Acad. Sci. U.S.A. 79, 6098-6101.

Livingstone, M.S., and Hubel, D.H. (1983). Specificity of cortico-cortical connections in monkey visual system. Nature 304, 531-534.

Livingstone, M.S., and Hubel, D.H. (1984). Anatomy and physiology of a color system in the primate visual cortex. J. Neurosci. 4, 309-356.

Livingstone, M.S., and Hubel, D.H. (1987). Connections between layer 4B of area 17 and the thick cytochrome oxidase stripes of area 18 in the squirrel monkey. J. Neurosci. 7, 3371-3377.

Livingstone, M., and Hubel, D. (1988). Segregation of form, color, movement, and depth: anatomy, physiology, and perception. Science 240, 740-749.

Lynch, J.C. (1980). The functional organization of posterior parietal association cortex. Behav. Brain Sci. 3, 485-534.

Malpeli, J.G., Schiller, P.H., and Colby, C.L. (1981). Response properties of single cells in monkey striate cortex during reversible inactivation of individual lateral geniculate laminae. J. Neurophysiol. 46, 1102-1119.

Martin, P.R., Lee, B.B., White, A.J., Solomon, S.G., and Ruttiger, L. (2001). Chromatic sensitivity of ganglion cells in the peripheral primate retina. Nature 410, 933-936.

Masland, R.H. (2001). Neuronal diversity in the retina. Curr. Opin. Neurobiol. 11, 431-436.

Maunsell, J.H., and Van Essen, D.C. (1983). The connections of the middle temporal visual area (MT) and their relationship to a cortical hierarchy in the macaque monkey. J. Neurosci. 3, 2563-2586.

Merigan, W.H. (1989). Chromatic and achromatic vision of macaques: role of the P pathways. J. Neurosci. 9, 776-783.

Merigan, W.H. (1996). Basic visual capacities and shape discrimination after lesions of extrastriate area V4 in macaques. Vis. Neurosci. 13, 51-60.

Merigan, W.H., Byrne, C., and Maunsell, J.H.R. (1991a). Does primate motion perception depend on the magnocellular pathway? J. Neurosci. 11, 3422-3429.

Merigan, W.H., and Eskin, T.A. (1986). Spatio-temporal vision of macaques with sever loss of P beta retinal ganglion cells. Vision Res. 26, 1751-1761.

Merigan, W.H., Katz, L.M., and Maunsell, J.H.R. (1991b). The effects of parvocellular lateral geniculate lesions on the acuity and contrast sensitivity of macaque monkeys. J. Neurosci. 11, 994-1101.

Michael, C.R. (1988). Retinal afferent arborization patterns, dendritic field orientations, and the segregation of function in the lateral geniculate nucleus of the monkey. Proc. Natl. Acad. Sci. U.S.A. 85, 4914-4918.

Nakamura, H., Gattas, R., Desimone, R., and Ungerleider, L.G. (1993). The modular organization of projections from areas V1 and V2 to areas V4 and TEO in macaques. J. Neurosci. 13, 3681-3691.

Nealey, T.A., and Maunsell, J.H.R. (1994). Magnocellular and parvocellular contributions to the responses of neurons in macaque striate cortex. J. Neurosci. 14, 2069-2079.

Newsome, W.T., and Pare, E.B. (1988). A selective impairment of motion perception following lesions of the middle temporal visual area (MT). J. Neurosci. 8, 2201-2211.

O'Keefe, L.P., Levitt, J.B., Kiper, D.C., Shapley, R.M., and Movshon, J.A. (1998). Functional organization of owl monkey lateral geniculate nucleus and visual cortex. J. Neurophysiol. 80, 594-609.

Orban, G.A., Saunders, R.C., Vandenbussche, E. (1995). Lesions of the superior temporal cortical motion areas impair speed discrimination in the macaque monkey. Eur. J. Neurosci. 7, 2261-2276.

Orban, G.A., Van Essen, D.C., and Vanduffel, W. (2004). Comparative mapping of higher visual areas in monkeys and humans. Trends Cogn. Sci. 8, 315-324.

Pasternak, T., and Merigan, W.H. (1994). Motion perception following lesions of the superior temporal sulcus in the monkey. Cereb. Cortex 4, 247-259.

Paulus, W., and Kroger-Paulus, A. (1983). A new concept of retinal colour coding. Vision Res. 23, 529-540.

Perrett, D.I., Rolls, E.T., Caan, W. (1982). Visual neurons responsive to faces in the monkey temporal cortex. Exp. Brain Res. 47, 329-342.

Perry, V.H., Oehler, R., and Cowey, A. (1984). Retinal ganglion cells that project to the dorsal lateral geniculate nucleus in the macaque monkey. Neuroscience 12, 1101-1123.

Phillips, R.R., Malamut, B.L., Bachevalier, J., and Mishkin, M. (1988). Dissociation of the effects of inferior temporal and limbic lesions on object discrimination learning with 24-h intertrial intervals. Behav. Brain Res. 27, 99-107.

Polyak, S.L. (1941). The Retina. University of Chicago Press, Chicago.

Quintana, J., and Fuster, J.M. (1993). Spatial and temporal factors in the role of prefrontal and parietal cortex in visuomotor integration. Cereb. Cortex 3, 122-132.

Rockhill, R.L., Daly, F.J., MacNeil, M.A., Brown, S.P., and Masland, R.H. (2002). The diversity of ganglion cells in a mammalian retina. J. Neurosci. 22, 3831-3843.

Rodieck, R.W., and Watanabe, M. (1993). Survey of the morphology of macaque

retinal ganglion cells that project to the pretectum, superior colliculus, and parvocellular laminae of the lateral geniculate nucleus. J. Comp. Neurol. 338, 289-303.

Roe, A.W., and Ts'o, D.Y. (1995). Visual topography in primate V2: multiple representations across functional stripes. J. Neurosci. 15, 3689-3715.

Roska, B., and Werblin, F. (2001). Vertical interactions across ten parallel, stacked representations in the mammalian retina. Nature 410, 583-587.

Saito, H., Tanaka, K., Isono, H., Yasuda, M., and Mikami, A. (1989). Directionally selective responses of cells in the middle temporal area (MT) of the macaque monkey to the movement of equiluminous opponent color stimuli. Exp. Brain Res. 75, 1-14.

Sawatari, A., and Callaway, E.M. (2000). Diversity and cell type specificity of local excitatory connections to neurons in layer 3B of monkey primary visual cortex. Neuron 25, 459-471.

Schiller, P.H., and Colby, C.L. (1983). The responses of single cells in the lateral geniculate nucleus of the rhesus monkey to color and luminance contrast. Vision Res. 23, 1631-1641.

Schiller, P.H., Logothetis, N.K., and Charles, E.R. (1990a). Role of the color-opponent and broad-band channels in vision. Vis. Neurosci. 5, 321-346.

Schiller, P.H., Logothetis, N.K., and Charles, E.R. (1990b). Functions of the colour-opponent and broad-band channels of the visual system. Nature 343, 68-70.

Schiller, P.H., and Malpeli, J.G. (1978). Functional specificity of lateral geniculate nucleus laminae of the rhesus monkey. J. Neurophysiol. 41, 788-797.

Shapley, R., Kaplan, E., and Soodak, R. (1981). Spatial summation and contrast sensitivity of X and Y cells in the lateral geniculate nucleus of the macaque. Nature 292, 543-545.

Shipp, S., and Zeki, S. (1985). Segregation of pathways leading from area V2 to areas V4 and V5 of macaque monkey visual cortex. Nature 315, 322-325.

Shipp, S., and Zeki, S. (1989a). The organization of connections between areas V5 and V1 in macaque monkey visual cortex. Eur. J. Neurosci. 1, 309-332.

Shipp, S., and Zeki, S., (1989b). The organization of connections between areas V5 and V2 in macaque monkey visual cortex. Eur. J. Neurosci. 1, 333-354.

Shipp, S., and Zeki, S. (2002). The functional organization of area V2, I: specialization across stripes and layers. Vis. Neurosci. 19, 211-231.

Siegel, R.M., and Read, H.L. (1997). Analysis of optic flow in the monkey parietal area 7a. Cereb. Cortex 7, 327-346.

Silveira, L.C.L., and Perry, V.H. (1991). The topography of magnocellular projecting ganglion cells (M ganglion cells) in the primate retina. Neuroscience 40, 217-237.

Silverman, M.S., Grosof, D.H., De Valois, R.L., and Elfar, S.D. (1989). Spatial-frequency organization in primate striate cortex. Proc. Natl. Acad. Sci. U.S.A. 86, 711-715.

Sincich, L.C., and Horton, J.C. (2002). Divided by cytochrome oxidase: a map of the projections from V1 to V2 in macaques. Science 295, 1734-1737.

Sincich, L.C., and Horton, J.C. (2003). Independent projection streams from macaque striate cortex to the second visual area and middle temporal area. J. Neurosci. 23, 5684-5692.

Sincich, L.C., Park, K.F., Wohlgemuth, M.J., and Horton, J.C. (2004). Bypassing V1: a direct geniculate input to area MT. Nat. Neurosci. 7, 1123-1128.

Sterling, P. (1988). Retina. In: The Synaptic Organization of the Brain, 4th ed., G.M. Shepherd, ed. (New York: Oxford University Press), pp. 205-253.

Tootell, R.B.H., Hamilton, S.L., and Switkes, E. (1988). Functional anatomy of macaque striate cortex: IV. Contrast and magno-parvo streams. J. Neurosci. 8, 1594-1609.

Tootell, R.B., Nelissen, K., Vanduffel, W., and Orban, G.A. (2004). Search for color 'center(s)' in macaque visual cortex. Cereb. Cortex 14, 353-363.

Ts'o, D.Y., and Gilbert, C.D. (1988). The organization of chromatic and spatial interactions in the primate striate cortex. J. Neurosci. 8, 1712-1727.

Ungerleider, L.G., and Desimone, R. (1986). Cortical connections of visual area MT in the macaque. J. Comp. Neurol. 248, 190-222.

Ungerleider, L.G., and Mishkin, M. (1982). Two cortical visual systems. In: The Analysis of Visual Behavior, D.J. Ingle, R.J.W. Mansfield, and M.S. Goodale, eds. (Cambridge: MIT Press), pp. 549-586.

Vogels, R., Saunders, R.C., and Orban, G.A. (1997). Effects of inferior temporal

lesions on two types of orientation discrimination in the macaque monkey. Eur. J. Neurosci. 9, 229-245.

Walsh, V., Carden, D., Butler, S.R., and Kulikowski, J.J. (1993). The effects of V4 lesions on the visual abilities of macaques: hue discrimination and colour constancy. Behav. Brain Res. 53, 51-62.

Wassle, H., and Boycott, B.B. (1991). Functional architecture of the mammalian retina. Physiol. Rev. 71, 447-480.

Wiesel, T.N., and Hubel, D.H. (1966). Spatial and chromatic interactions in the lateral geniculate body of the rhesus monkey. J. Neurophysiol. 29, 1115-1156.

Xiao, Y., and Felleman, D.J. (2004). Projections from primary visual cortex to cytochrome oxidase thin stripes and interstripes of macaque visual area 2. Proc. Natl. Acad. Sci. U.S.A. 101, 7147-7151.

Xiao, Y., Wang, Y., and Felleman, D.J. (2003). A spatially organized representation of colour in macaque cortical area V2. Nature 421, 535-539.

Xiao, Y., Zych, A., and Felleman, D.J. (1999). Segregation and convergence of functionally defined V2 thin stripes and interstripe compartment projections to area V4 of macaques. Cereb. Cortex 9, 792-804.

Yabuta, N.H., and Callaway, E.M. (1998a). Cytochrome-oxidase blobs and intrinsic horizontal connections of layer 2/3 pyramidal neurons in primate V1. Vis. Neurosci. 15, 1007-1027.

Yabuta, N.H., and Callaway, E.M. (1998b). Functional streams and local connections of layer 4C neurons in primary visual cortex of the macaque monkey. J. Neurosci. 18, 9489-9499.

Yabuta, N.H., Sawatari, A., and Callaway, E.M. (2001). Two functional channels from primary visual cortex to dorsal visual cortical areas. Science 292, 297-300.

Yoshioka, T., and Dow, B.M. (1996). Color, orientation and cytochrome oxidase reactivity in areas V1, V2 and V4 of macaque monkey visual cortex. Behav. Brain Res. 76, 71-88.

Yoshioka, T., Blasdel, G.G., Levitt, J.B., and Lund, J.S. (1996). Relation between patterns of intrinsic lateral connectivity, ocular dominance, and cytochrome oxidase-reactive regions in macaque monkey striate cortex. Cereb. Cortex 6, 297–310.

Yoshioka, T., Levitt, J.B., and Lund, J.S. (1994). Independence and merger of

thalamocortical channels within macaque monkey primary visual cortex: anatomy of interlaminar projections. Vis. Neurosci. 11, 467-489.

Zeki, S., and Shipp, S. (1988). The functional logic of cortical connections. Nature 335, 311-317.

Zeki, S., and Ship, S. (1989). Modular connections between areas V2 and V4 of macaque monkey visual cortex. Eur. J. Neurosci. 1, 494-506.

Chapter II

The parvocellular LGN provides a robust disynaptic input to the visual motion area MT

Summary

Dorsal visual cortical areas are thought to be dominated by input from the magnocellular (M) visual pathway, with little or no parvocellular (P) contribution. These relationships are supported by a close correlation between the functional properties of these areas and the M pathway and by a lack of anatomical evidence for P input. Here we use rabies virus as a retrograde transynaptic tracer to show that the dorsal area MT receives strong input, via a single relay, from both M and P cells of the lateral geniculate nucleus. This surprising P input, likely relayed via layer 6 Meynert cells in primary visual cortex, can provide MT with sensitivity to a more complete range of spatial, temporal, and chromatic cues than the M pathway alone. These observations provide definitive evidence for P pathway input to MT and show that convergence of parallel visual pathways occurs in the dorsal stream.

Introduction

Parallel processing is a common feature of sensory systems in the mammalian brain. A fundamental problem, therefore, is the integration of information across parallel systems to create a unified percept. Do subcortical pathways remain segregated as they contribute to activity in the cerebral cortex and ultimately to perception? The primate visual cortex is composed of multiple areas that can be divided into relatively independent dorsal and ventral streams (DeYoe and Van Essen, 1988; Zeki and Shipp, 1988; Merigan and Maunsell, 1993; Livingstone and Hubel, 1988). The dorsal stream is specialized for analyses of motion and spatial relationships, whereas the ventral stream is specialized for analyses of object attributes

like shape and color. Dorsal visual areas are thought to be dominated by input from the magnocellular (M) visual pathway, which is highly sensitive to low-contrast, quickly moving stimuli but is insensitive to high spatial frequencies and chromatic opponency, which are instead carried by the parvocellular (P) pathway. The dorsal stream cortical area MT is specialized for motion processing (Allman and Kaas, 1971; Zeki, 1974; Albright et al., 1984; Born and Bradley, 2005) and is traditionally viewed as having anatomical input and physiological properties dominated by the M visual pathway (Livingstone and Hubel, 1988; Merigan and Maunsell, 1993; Born and Bradley, 2005). Additional contributions from the P pathway to MT could, in theory, extend the range of temporal, spatial, and chromatic cues that can be used to extract motion information. However, there is no definitive anatomical, physiological, or behavioral evidence that such a contribution exists (Merigan and Maunsell, 1993).

Previous anatomical and physiological studies have provided important insight into the likely contributions of M and P pathways to MT. These pathways are segregated into layers in the lateral geniculate nucleus (LGN) and in their terminations within layer 4C of primary visual cortex (V1), allowing functional inferences to be made from anatomical investigation (Casagrande and Kaas, 1994; Callaway, 1998; Sincich and Horton, 2005). MT receives its main ascending cortical input directly (Shipp and Zeki, 1989a; Sincich and Horton, 2003) and indirectly (Burkhalter et al., 1986; Shipp and Zeki, 1989b) from layer 4B of V1, a layer that has been shown to receive the bulk of its input from M layers of the LGN via layer 4Cα of V1 (Hendrickson et al., 1978; Fitzpatrick et al., 1985; Yabuta et al., 2001). Response

properties in MT are typically described as direction, speed, and disparity tuned with high-contrast sensitivity and lacking chromatic opponency (Livingstone and Hubel, 1988; Merigan and Maunsell, 1993; Born and Bradley, 2005). These response properties share much in common with the response properties of cells in M layers of the LGN and layer 4B of V1. In addition, studies have shown that lesions of the M layers drastically reduce responses in MT (Maunsell et al., 1990) and negatively impact behavioral performance on motion-related tasks (Schiller et al., 1990).

While MT receives its main ascending input from layer 4B of V1, there exists an even shorter and often overlooked MT-projecting pathway that arises from specialized Meynert cells in layer 6 of V1 (Fries et al., 1985; Shipp and Zeki, 1989a). These neurons have a large soma size and wide dendritic spread in layer 6, a layer which receives direct input from the LGN (Hendrickson et al., 1978; Winfield et al., 1983). These observations implicate Meynert cells in relaying a fast, motion-related signal to MT and have suggested a model for the formation of direction selectivity in V1 (Movshon and Newsome, 1996; Livingstone, 1998). Traditionally, Meynert cells are characterized as carrying an M signal to MT, yet both M and P layers of the LGN send axon collaterals to layer 6 (Hendrickson et al., 1978), making both streams of information potential sources of input to the Meynert cells.

We used rabies virus as a transynaptic retrograde tracer to study disynaptic connections to area MT of macaque monkey. Studies in both rodents and primates have shown that rabies virus spreads retrogradely across synapses in a time dependent manner (Ugolini, 1995; Kelly and Strick, 2000, 2003). Rabies virus transport occurs only at synaptic connections and not along axons of passage. Leaving cells intact is a

hallmark of the rabies virus, preventing unspecific spillage of the virus into the surrounding neuropil. Moreover, the time dependent transynaptic spread of rabies virus has been carefully worked out in well-defined systems. After 3 days postinjection, the particular strain and preparation of rabies virus that was used in our experiments (see Experimental Procedures; Kelly and Strick, 2003) has time to transport across one synapse and infect neurons disynaptic to the injection site. This was confirmed by our own control experiments replicating previous studies conducted in the primate motor system (see Experimental Procedures; Kelly and Strick, 2003) and using precisely the same batch of rabies virus used for the studies described here. We, therefore, chose a 3 day survival time for our studies in order to make it quite unlikely that virus would spread past neurons disynaptic to our injection site. Although we are confident that a 3 day survival time did not result in trisynaptic labeling, it does leave open the possibility that some weak disynaptic connections remained unlabeled.

We find that 3 days after injections of rabies virus into MT, there is extensive labeling in both the M and P layers of the LGN. The majority of these cells stain positive for the M and P marker parvalbumin and negative for the koniocellular (K) marker calbindin. The P pathway, therefore, provides a strong and surprisingly direct input to MT. These observations suggest that future studies should re-evaluate the functional contributions of the P pathway to visual responses in MT and to the perception of motion.

Results

Injections of the CVS-11 strain of rabies virus (see Experimental Procedures) were targeted to cortical area MT of two macaque monkeys using stereotaxic coordinates of the posterior bank of the superior temporal sulcus (STS) obtained through structural MRI images. Following a survival period of 3 days, animals were perfused and the brains were sectioned and stained with an antibody against the rabies nucleocapsid protein (see Experimental Procedures). The locations of the unilateral injections were confirmed histologically to be confined to MT (Figure 2.1D) (see Experimental Procedures). The syringe penetration can be seen within the densely myelinated region along the posterior bank of the STS, and in an adjacent rabies-stained section, the densest label is found in this same region (Figure 2.1D). On examination of the histological sections, we were surprised to find a large number of rabies-labeled cells in the LGN (Figure 2.1A). Most striking was the observation that labeled cells were present with high density in both M and P layers (Figures 2.1A–C), in addition to the expected (Stepniewska et al., 1999; Sincich et al., 2004) scattered label in K layers (Figures 2.2B and 2.2D).

We counted the numbers of rabies-labeled neurons in sections through the LGN. For one case (JNM10; Figures 2.2A and 2.2B), a systematic series of one out of every sixth section was stained for both rabies and cytochrome oxidase (CO), while in the other case (JNM1; Figures 2.2C and 2.2D), a smaller number of irregularly spaced sections was available. In the more systematically studied case, rabies was detected in the LGN across a series of more than 30 coronal sections, spanning more than 1.2 mm along the anterior-posterior axis. There were more than 700 rabies-labeled cells in six,

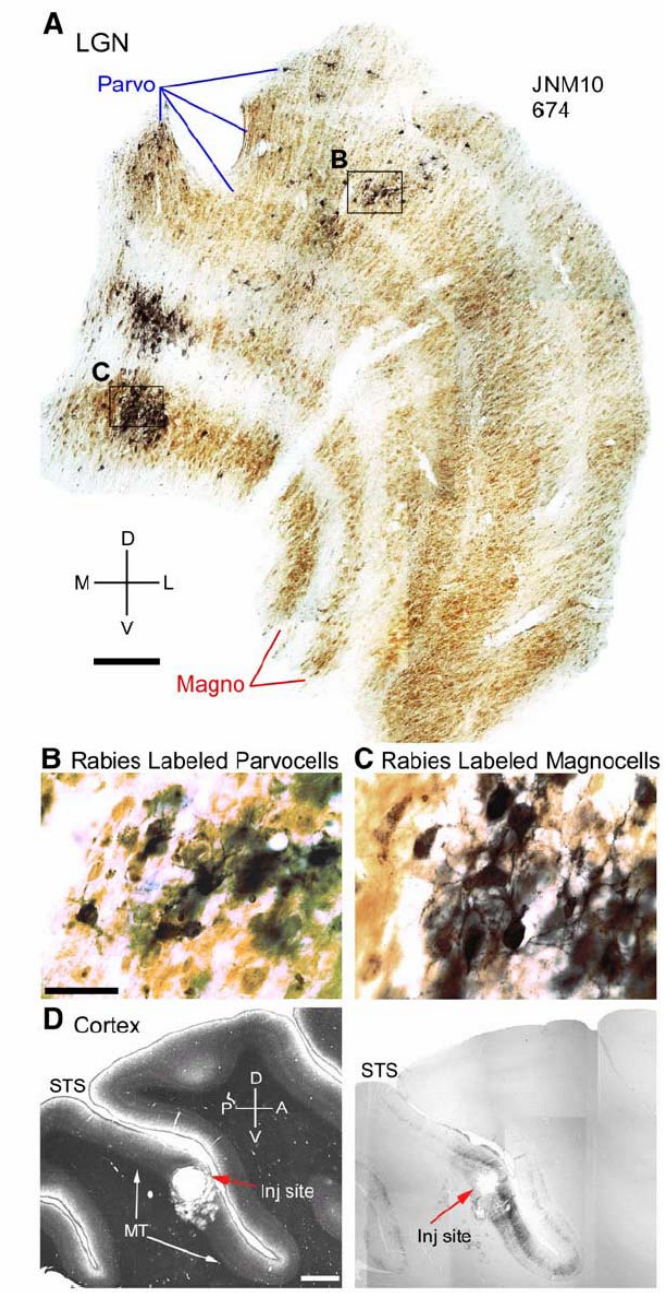

Figure 2.1: Retrogradely labeled neurons in the LGN following injections of rabies virus in cortical area MT.
(**A**) A montage of digitally photographed images of a single section of the LGN stained for the nucleocapsid protein of the rabies virus (black) and for cytochrome oxidase (CO; brown) is shown. Blue and red lines indicate P (Parvo) and M (Magno) layers. Scale bar, 500 μm. Rectangles in (**A**) indicate the locations of higher-magnification images of P cells (**B**) and M cells (**C**) labeled with rabies virus. Scale bar in (**B**) also applies to (**C**) and equals 50 μm. (**D**) The location of the rabies-injected region (red arrow) is shown on a parasagittally cut cortical section stained for myelin (left) and an adjacent section stained for the rabies nucleocapsid protein (right). MT is distinguishable as the densely myelinated region (white arrows) on the posterior bank of the superior temporal sulcus (STS). Scale bar in (**D**), 2 mm. Medial (M), lateral (L), dorsal (D), ventral (V), anterior (A), and posterior (P).

40 μm thick sections studied within this span. Interpolating, the total number of neurons would have been more than 4000 if all sections were counted. The great majority of the rabies-labeled neurons was found in the P layers of the LGN (74%), with a substantial proportion in the M layers (21%) and a small minority in the intercalated zones, or K layers (5%). In the second case, in which fewer sections were available for staining with the rabies antibody, the overall numbers of labeled cells were comparable, with nearly 100 cells in each section. The labeled neurons in this case were more evenly distributed between M and P layers, with 53% in M layers, 44% in P layers, and only 3% in K layers. The large numbers of cells in M and P layers in these cases (Figure 2.2) were more than ten times that of the sparse pattern described in previous studies of LGN cells monosynaptic to MT (Stepniewska et al., 1999; Sincich et al., 2004).

While substantial label was unexpectedly found in both M and P layers of the LGN, it remained feasible that the majority of these cells might be displaced K cells and simply monosynaptic to MT. Sincich et al. (2004) reported that LGN cells monosynaptic to MT were present in all layers of the LGN and that the majority were positive for the α subunit of type II Ca^{2+}/calmodulin-dependent protein kinase, a marker for K cells. In order to confirm that our results consisted primarily of M and P cells disynaptic to MT, we analyzed the proportion of rabies-labeled LGN cells that expressed parvalbumin, a marker for M and P cells (Jones and Hendry, 1989). In contrast, to determine the proportion of K cells mono- and disynaptically labeled with rabies, we tested for double labeling with the K cell marker calbindin (Jones and Hendry,1989).

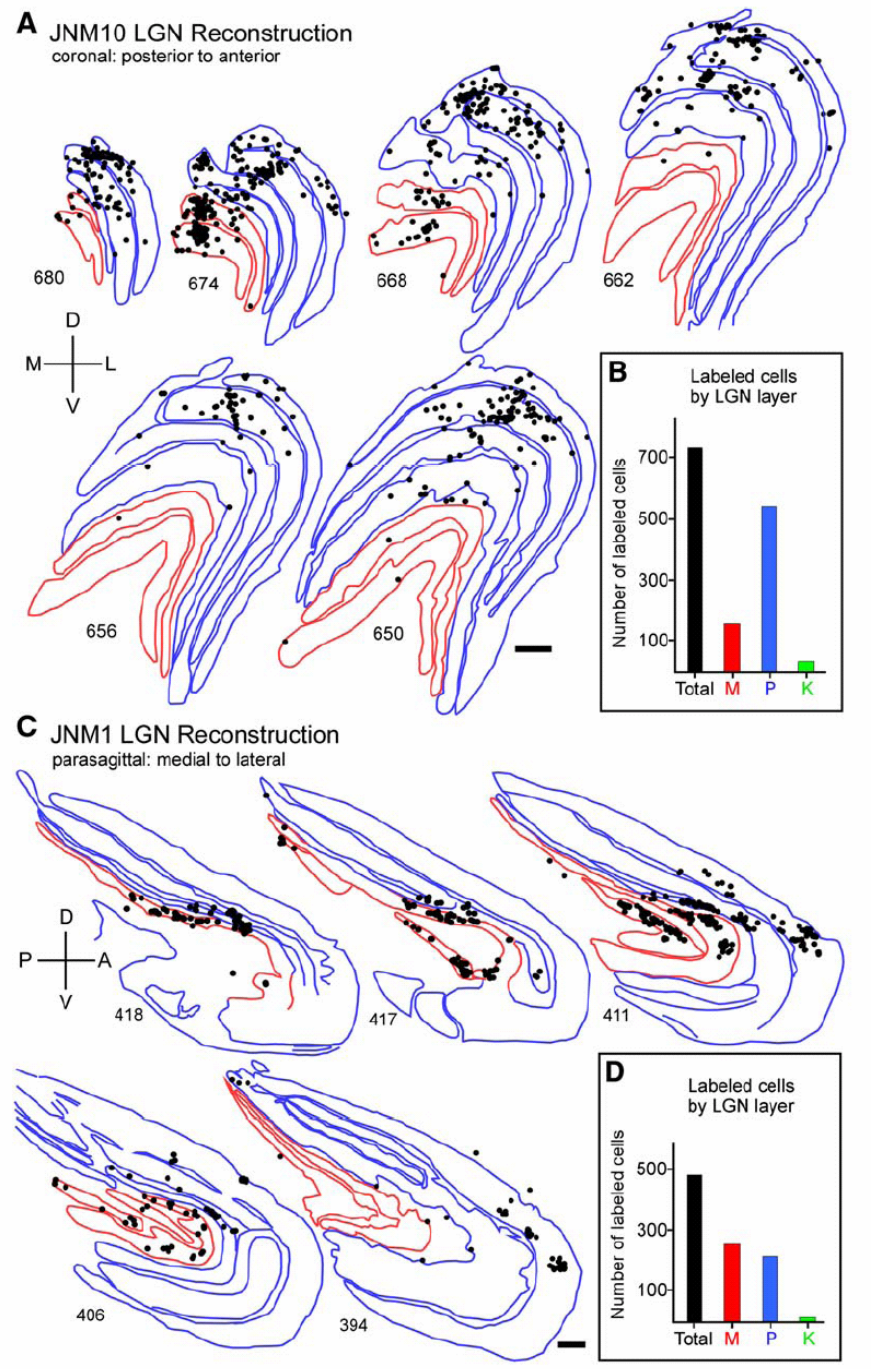

Figure 2.2: Retrogradely labeled neurons in M, P, and K layers of LGN. Reconstructions of the distribution of rabies-labeled cells (black dots) in several coronal (**A**) and parasagittal (**C**) sections of the LGN from two cases (JNM10 and JNM1). P and M layers are outlined in blue and red. Sections in (**A**) are from the same case as in Figure 2.1A, which also shows section 674. Scale bars, 500 µm. (**B** and **D**) Bar graphs show the numbers of rabies-labeled cells for each series of sections. The numbers of cells found in M, P, and the intercalated, or koniocellular (K), layers are shown in red, blue, and green. Medial (M), lateral (L), dorsal (D), ventral (V), anterior (A), and posterior (P).

Every sixth LGN section from one of our cases (JNM10) was stained for both rabies virus and parvalbumin in order to assess the proportion of double-labeled neurons in M and P layers of the LGN (Figure 2.3A) (see Experimental Procedures). We found many double-labeled cells in M and P layers, with far fewer cells labeled only for rabies (Figure 2.3B). In all, 69% of the cells were positive for parvalbumin, with 74% and 69% in M and P layers, respectively (Figure 2.3D). We also stained another series of LGN sections for both rabies virus and the K cell marker calbindin (Jones and Hendry, 1989). We found few double-labeled cells in M and P layers; most cells were labeled only for rabies (85%) (Figure 2.3C). Only 15% of rabies-labeled cells were positive for calbindin and could be considered K cells, with 13% and 10% in M and P layers, respectively (Figure 2.3D).

The results presented thus far provide strong evidence for a robust disynaptic connection from both M and P layers of LGN to MT. This interpretation is further strengthened by observations of rabies labeling in layers 4B and 6 of V1 (Figure 2.4), layers that provide monosynaptic projections to MT (Shipp and Zeki, 1989a; Sincich and Horton, 2003) and could, thus, serve as a relay for disynaptic label in the LGN. As expected from the transport of rabies virus from MT to LGN via these intermediate relays in V1, the distribution of rabies-labeled cells in the LGN and V1 was in close retinotopic correspondence in both monkeys (Figure 2.5) (see Experimental Procedures). The laminar distribution of rabies-labeled cells in V1 was determined for both cases. Of the nearly 7100 rabies-labeled cells identified in V1, large numbers were found in layers 4B (23%), 4Cα (44%), and 6 (17%), with fewer found in layers 2/3 (11%) and 5 (2.6%). Negligible numbers were found in layers 4A (1.5%) and 4Cβ

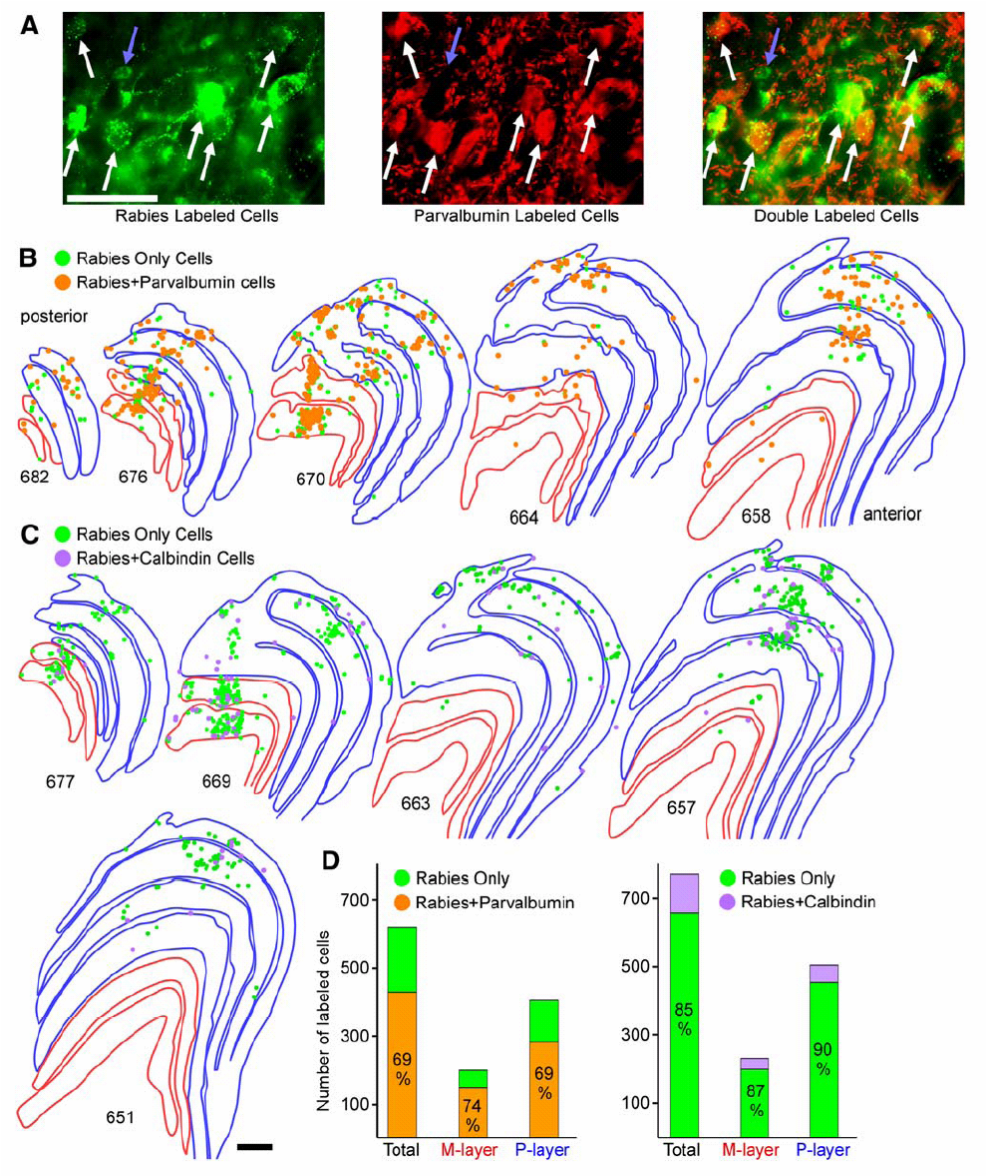

Figure 2.3: Retrogradely labeled M, P, or K cells double labeled for rabies and either parvalbumin or calbindin.
(**A**) Fluorescent images of cells in a P layer stained for rabies virus (left; green) and parvalbumin (center; red) used to identify double-labeled cells (right) taken from section 676 in (**B**). White arrows indicate some of the cells that are double labeled, whereas the blue arrow indicates a cell that is positively labeled only for the rabies virus. Scale bar, 50 μm. (**B** and **C**) Reconstructions of the distribution of cells retrogradely labeled for the rabies virus only (green dots) and double labeled with rabies and parvalbumin ([**B**]; orange dots) or rabies and calbindin ([**C**]; purple dots) in several LGN sections from case JNM10. Blue and red lines outline the P and M layers. Scale bar in (**C**) also applies to (**B**) and equals 500 μm. (**D**) The numbers of cells labeled with rabies virus only or double labeled are indicated in histograms. The bars labeled ‘‘Total’’ refer to all cells found in the M, P, and K layers. Subsets of these cells found in the M or P layers are indicated by separate histograms labeled ‘‘M-Layer’’ or ‘‘P-Layer.’’ Histograms to the left are based on sections plotted in (**B**) and those to the right are based on sections in (**C**). Percentages of cells that can be considered as M or P, based on double labeling, are indicated.

(1.4%) (Figure 2.4C). The relative absence of rabies-labeled cells in layers 4A and 4Cβ provided strong evidence against trisynaptic labeling of P geniculate cells through these divisions of layer 4.

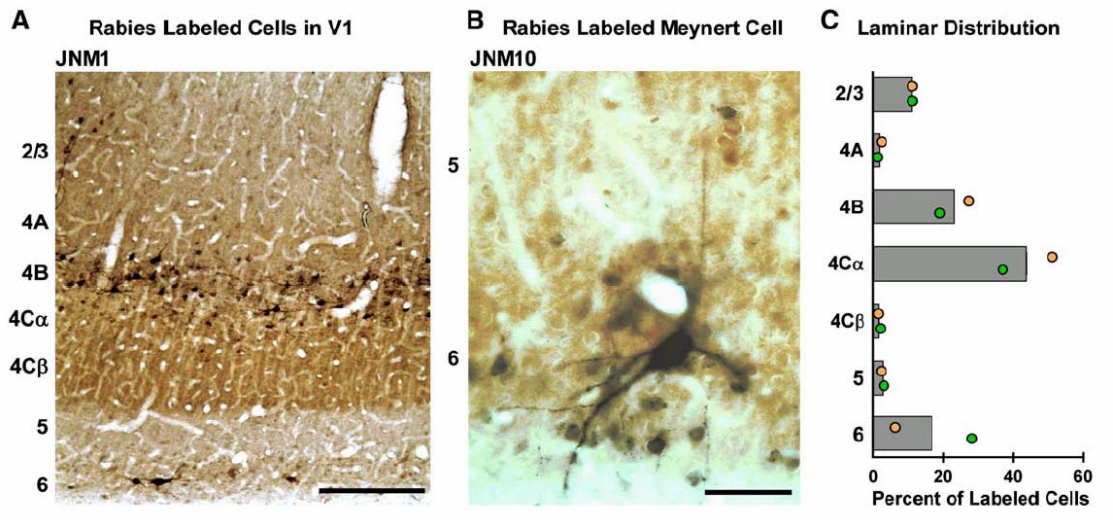

Figure 2.4: Laminar distribution of rabies-labeled cells in V1.
Parasagittal sections of V1 from cases JNM1 in the calcarine sulcus (**A**) and JNM10 on the opercular surface (**B**), stained for CO and the rabies nucleocapsid protein. Rabies-labeled cells were found primarily in layers 4B, 4Cα, and 6, with low levels in layer 2/3 and 5. Negligible label was found in layers 4A and 4Cβ. Several of the neurons labeled in layer 6 were large Meynert cells. (**C**) The percentages of rabies-labeled cells in each layer of V1 for JNM1 (orange dots) and JNM10 (green dots) are indicated. The averaged values across both cases (gray bars) were derived from a total of 7076 labeled cells. Scale bar, 250 μm (**A**) and 50 μm (**B**). Medial (M), lateral (L), dorsal (D), ventral (V), anterior (A), and posterior (P).

Discussion

Our observations demonstrate a surprisingly robust disynaptic connection from the LGN to MT. This projection arises predominantly from parvalbumin-positive, calbindin-negative neurons in the M and P layers. Interestingly, the numbers of neurons in the P layers are nearly equal to or greater than those in the M layers. These M and P neurons are far more numerous than expected from monosynaptic projections to MT (Stepniewska et al., 1999; Sincich et al., 2004), which are sparse and dominated

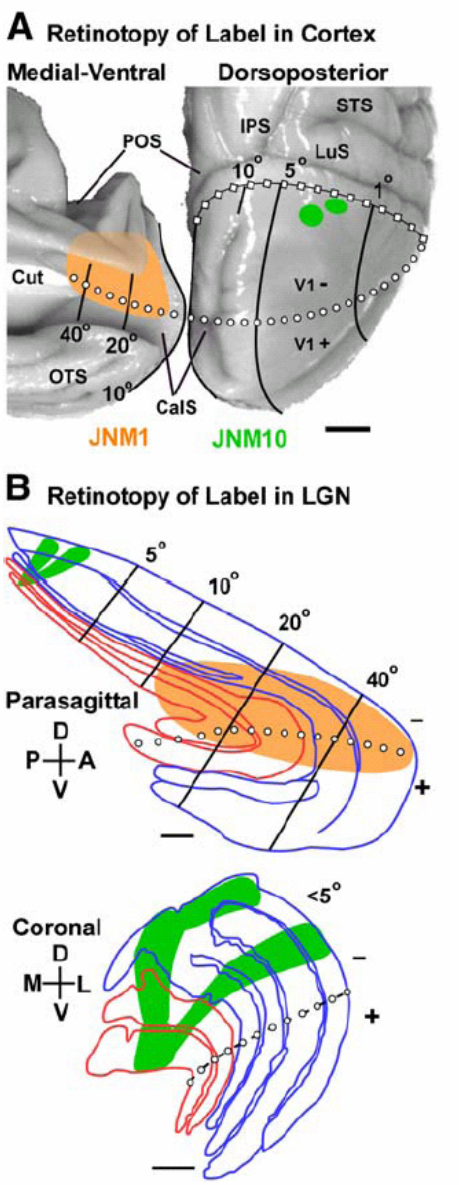

Figure 2.5: Retinotopic distributions of rabies-labeled cells in LGN and V1.
(**A**) Retinotopic locations of cells mono- and disynaptically labeled with rabies virus in V1 from cases JNM1 (orange) and JNM10 (green). The images, from a representative brain, show a medial view of the calcarine sulcus that is partially unfolded (left) and a dorsal view of the posterior end of the cortex (right). The vertical (squares) and horizontal (circles) meridians are marked. Azimuths 1º, 5º, 10º, 20º, and 40º are shown, along with iso-azimuth contours (black lines). Lower (-) and upper (+) visual fields are noted. The retinotopic summary has been adapted from Lyon and Kaas (2002) and is based on retinotopic maps from Weller and Kaas (1983) and Van Essen et al. (1984). V1 (primary visual cortex), IPS (intraparietal sulcus), STS (superior temporal sulcus), LuS (lunate sulcus), CalS (calcarine sulcus), POS (parietal occipital sulcus), OTS (occipital temporal sulcus). Scale bar, 5 mm. (**B**) Retinotopic locations of rabies-labeled cells in the LGN from cases JNM1 (orange) and JNM10 (green) are shown in representative parasagittal (top) and coronal (bottom) sections. The LGN retinotopy is based on Malpeli and Baker (1975), Kaas and Huerta (1988), and Erwin et al. (1999). M layers (red) and P layers (blue). Scale bar, 500 µm.

by K cells. Our experimental procedures ensured that LGN cells were not labeled trisynaptically. Furthermore, the large numbers of rabies labeled cells in layers 4B and 6 of V1, but not layer 4Cβ, provide additional evidence that M and P neurons in the LGN were labeled disynaptically via layers 4B and/or 6 of V1 and not trisynaptically through layer 4C.

Although previous anatomical studies suggest at least two possible neural substrates for this disynaptic pathway, the most likely is a connection via the layer 6 Meynert cells in V1. The nature of our experimental results indicates that neurons mediating this disynaptic pathway must receive a direct connection from both M and P LGN cells and also project directly to MT. Only neurons in V1 meet these criteria, because input from LGN to other cortical areas appears to arise predominantly from K cells rather than M or P cells (Bullier and Kennedy, 1983; Lysakowski et al., 1988; Stepniewska et al., 1999; Sincich et al., 2004). Within V1, MT-projecting cells are found only in layers 4B and 6 (Shipp and Zeki, 1989a; Sincich and Horton, 2003), leaving two potential routes by which cells in the LGN might connect disynaptically with MT (Figure 2.6). Neurons in both of these V1 layers were labeled in our study, as required for M and P neurons of the LGN to be labeled via this pathway (Figure 2.4). It is possible that LGN axons could form synapses onto the dendrites of layer 4B cells that extend into layers 4Cα and 4A, which are V1 layers that receive input from M and P layers of the LGN, respectively (Hendrickson et al., 1978). However, the majority of the dendrites from layer 4B neurons are not found in these LGN recipient zones, making them poor candidates. Layer 6 Meynert cells, in contrast, are ideally situated. Both M and P layers of the LGN are known to project to layer 6 of V1

(Hendrickson et al., 1978), and the expansive, laterally extending dendritic fields of Meynert cells (Winfield et al., 1983) make them a prime candidate for receiving convergent input from the M and P pathways. In addition, Meynert cells could receive direct thalamic input onto apical dendrites in M recipient layer 4Cα and P recipient layers 4Cβ and 4A. As expected, we found numerous large layer 6 cells in V1 with

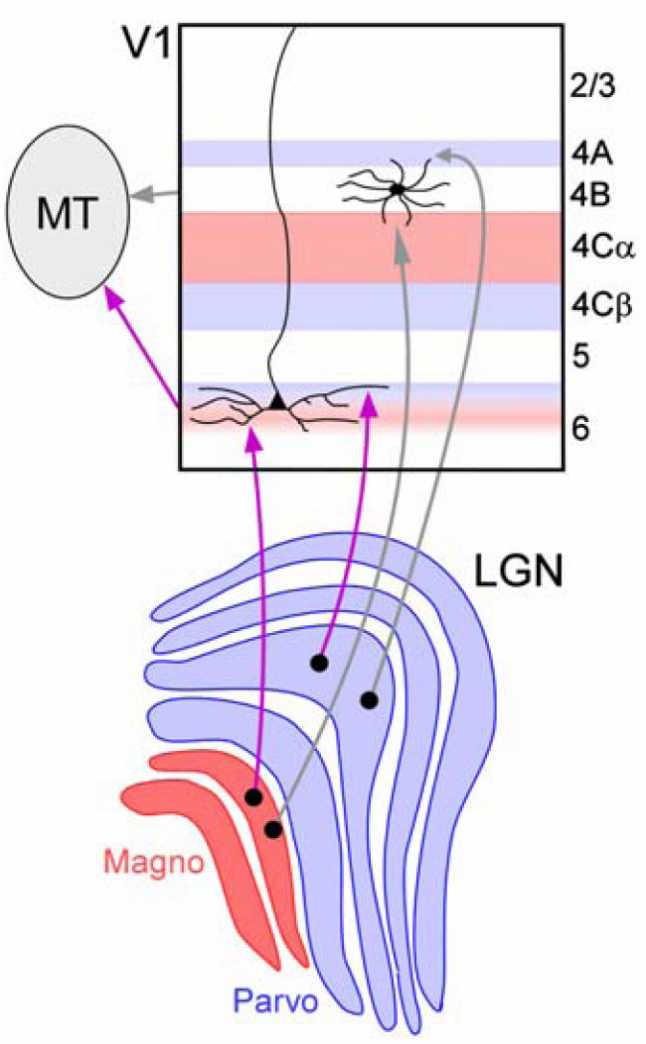

Figure 2.6: Potential substrates for disynaptic connections from the LGN to MT.
Our current data demonstrate that a robust disynaptic pathway to MT originates in M and P cells of the LGN. M and P cell terminations onto the expansive dendritic fields of layer 6 Meynert cells of V1 represent the most likely disynaptic pathway to MT (purple arrows, see text). Although less likely, a second pathway could arise from M cell projections to layer 4Cα and P cell projections to layer 4A of V1, where they may occasionally overlap with dendrites from layer 4B cells that project to MT (gray arrows).

characteristic Meynert cell morphology (Figures 2.4A and 2.4B). Large numbers of layer 6 non-Meynert cells were also found in V1 of both cases, as expected from disynaptic transfer to other neurons that provide input to Meynert cells. Our observations, therefore, suggest that layer 6 neurons, which are known to be direction selective and project to MT (Movshon and Newsome, 1996), receive both M and P input from the LGN.

A disynaptic P input to MT is an unexpected result. To date, the strongest functional evidence for P input to MT comes from lesions of the LGN P layers, which produced only small, but significant response reductions in MT (Maunsell et al., 1990); in contrast, lesions of the M layers of the LGN drastically reduced visual responses in MT (Maunsell et al., 1990). Direction selectivity in V1 cells is resilient to lesions of either M or P layers alone (Malpeli et al., 1981); only lesions of both M and P layers could eliminate direction selectivity in V1, a condition that also eliminates responses in MT (Malpeli et al., 1981; Maunsell et al., 1990). A P pathway contribution to MT is also suggested by studies showing that MT neurons have direction-selective responses to chromatically defined isoluminant gratings (Dobkins and Albright, 1994; Gegenfurtner et al., 1994). These responses, however, have been explained by weak activation of M cells (Dobkins and Albright, 1994; Gegenfurtner et al., 1994), leaving it unclear whether they are mediated by the M or P pathway, or both.

Other evidence for P input to MT is based on behavioral observations that implicate the P pathway in motion perception, but that may not depend on MT per se.

In particular, Merigan et al. (1991) showed that lesions of the M layers of the LGN reduced the visibility of low spatial and high temporal frequencies, but had little direct effect on discrimination of direction and speed. Thus, motion perception does not require the M pathway. It is not clear, however, whether MT was involved in the residual motion discrimination that was presumably mediated by the P pathway. Various models have assigned an integral role to the P visual pathway in motion processing in both monkeys and humans. De Valois et al. (2000) proposed that M and P pathways may need to be combined to create direction selectivity in V1 neurons. Differences in the temporal and spatial phase of M and P cells, when combined, accounted for the direction-selective receptive field properties of V1 neurons, a finding confirmed more recently (Saul et al., 2005). The P pathway has also been implicated in human motion processing because the sampling density of P ganglion cells limits veridical motion acuity in peripheral vision, even for high velocities (Anderson et al., 1995).

Previous studies have suggested less direct anatomical substrates by which the P pathway could potentially reach MT (Merigan and Maunsell, 1993; Yabuta et al., 2001; Born and Bradley, 2005). A recent study revealed that in V1, layer 4B pyramidal neurons, but not spiny stellates, receive convergent M and P input via layer 4C (Yabuta et al., 2001). Since layer 4B neurons contribute to the dorsal stream, this suggested a possible source of P input to MT. However, the direct projection from layer 4B to MT arises predominantly from spiny stellates (Shipp and Zeki, 1989a). Thus, neurons projecting directly from layer 4B to MT likely do not receive P input via layer 4Cβ of V1. If there is a P input to MT relayed by layer 4B pyramids, it likely

connects indirectly through V2 or V3 (Born and Bradley, 2005). Any indirect P input relayed by this pathway would involve at least four synapses from LGN to MT, and the continuity of this potential pathway has not been demonstrated. While the disynaptic pathway from LGN to MT via layer 6 Meynert cells in V1 is likely less prominent than the trisynaptic pathway from LGN to MT through layers 4C and 4B of V1, it is nevertheless a robust connection. Notably, it is unique in that it provides MT with convergent input from both M and P visual pathways. The early mixing of M and P inputs along this route may be particularly useful in providing MT with a quick signal that covers a more complete range of spatial, temporal, luminance, and chromatic contrasts. Although some of the physiological properties of MT-projecting layer 6 cells have been described (Movshon and Newsome, 1996), more studies will be necessary to elucidate the details of this unique input to MT and to fully reveal the functional relevance of the contributions from the P pathway to visual motion processing.

Experimental Procedures

Surgical Procedures

Two adult male macaque monkeys (JNM1 and JNM10) were used, following procedures approved by the Salk Institute Animal Care and Use Committee. In addition, all procedures using rabies virus were conducted using biosafety level 2 precautions as described elsewhere (Kelly and Strick, 2000).

A 1.5 Tesla Siemens Symphony MR scanner (UCSD Hillcrest Medical Center/Tenet Magnetic Resonance Institute) was used to obtain a full coronal series of

1 mm thick images for each monkey. Resulting structural images were used to calculate stereotaxic coordinates for our injections along the posterior bank of the superior temporal sulcus (STS).

In monkey JNM1, MT was targeted with three Hamilton syringe penetrations aimed at the posterior bank of the STS. Approximately 0.4 μl of the CVS-11 strain of rabies virus (see ‘‘Rabies Virus Strain and Speed of Transport’’ below) was injected at each of four depths spaced 0.5 mm apart. In addition, one of the injection sites included 10% rhodamine dextran (10,000 MW; Molecular Probes, Carlsbad, CA) in the solution of rabies virus. In monkey JNM10, two penetrations were made into the posterior STS, and 0.4 μl of virus was injected at five different depths.

Rabies Virus Strain and Speed of Transport

To trace disynaptic connections to area MT, we injected the CVS-11 strain of rabies virus and allowed a survival time of 3 days. It is important to note that different preparations of rabies virus, including those of the same strain, can spread through the nervous system at different rates, largely dependent on the passage history of the virus (Morimoto et al., 1998; Kelly and Strick, 2000). The particular preparation of the CVS-11 rabies virus that we used was obtained from Dr. Donald Lodmell, Rocky Mountain Laboratory, and was passaged four times in mouse brain followed by five times in cultured chicken embryo-related cells.

Based on the similarity in strain and passage history between the virus we used and the CVS-11 rabies virus used by Kelly and Strick (2003), we expected our virus to spread only disynaptically in 3 days. To explicitly test the rate of spread of our virus,

we repeated the experiments of Kelly and Strick (2003), injecting virus into motor cortex (M1) of the macaque monkey. Following a survival period of 3 days (three animals tested), rabies was detected only in neurons that project directly to M1 (VL of thalamus) or disynaptically to M1 (thalamic reticular nucleus, deep cerebellar nuclei and internal segment of the globus pallidus). Importantly, in none of the three animals tested was there any label detected in trisynaptically connected cerebellar Purkinje cells. Only following a 4 day survival period (one animal) was any label detected in cerebellar Purkinje cells. These results are indistinguishable from those reported previously by Kelly and Strick (2003) and confirmed that the virus we injected into MT would only travel disynaptically within the 3 day survival time.

Histology

After 3 days survival time, the animals were sacrificed, perfused with fixative, and their brains removed. Sections including the STS and LGN were cut at 40 μm on a freezing microtome parasagittally (JNM1) or coronally (JNM10). Sections of V1 were cut parasagittally for both cases. Separate series of every 12th section were processed for Nissl substance for both cases. Series of cortical sections that included the STS were processed for either rabies nucleocapsid protein, myelin, cytochrome oxidase (CO), or Nissl substance. Anatomical features of MT (Van Essen et al., 1981; Tootell et al., 1985), such as heavy myelination, dark and patchy CO staining, greater cortical thickness, and relative position on the posterior bank of the STS, were used to verify that injections were confined to MT (see Figure 2.1D).

In both monkeys, our syringe penetrations entered the white matter directly underneath MT. We are confident, however, that label in the LGN did not result from our injections involving the white matter or optic radiations directly beneath MT. Previous studies have shown that rabies virus uptake along cut peripheral axons is inefficient compared to uptake at axon terminals (Ugolini, 1995; Kelly and Strick, 2000) and rabies uptake along cut central axons has not been demonstrated. In addition, we have made multiple MT injections of a glycoprotein-deleted rabies virus, which does not transport transynaptically, that have involved white matter in a similar way to the injections in this study. We found no evidence of white matter uptake in these cases, with very few, sparsely distributed cells found in the LGN. Retrograde label in the LGN looked nothing like the disynaptic results we report in the present study and were more characteristic of monosynaptic connections to MT reported in previous studies (Stepniewska et al., 1999; Sincich et al., 2004). Most convincingly, rabies-labeled cells in the LGN were in retinotopically confined locations that matched closely with the retinotopic locations of rabies-labeled cells in V1 (see Figure 2.5) (see ‘‘Retinotopic Correspondence’’ below). This provided strong evidence that our injections were confined to MT and did not significantly involve the underlying white matter or optic radiations. In a separate experiment we made similar injections of the same CVS-11 strain of rabies virus used in the present study directly into cortical area V4 and found no retrograde label in the LGN. This argues against the possibility that our LGN label in the present study could have come from spread of our virus into adjacent cortical areas on or near the STS.

Immunohistochemistry for the rabies nucleocapsid protein was carried out using the anti-nucleocapsid mouse monoclonal antibody (gift from Dr. Lodmell), the biotinylated horse anti-mouse secondary antibody (Vector Labs, Burlingame, CA) and revealed through a Diaminobenzidine (DAB) reaction. Immunofluorescent double labeling of sections (see Figure 2.3) utilized the anti nucleocapsid mouse monoclonal antibody and either anti-parvalbumin or anti calbindin rabbit polyclonal antibody (Swant, San Diego, CA). Labeled cells were revealed using the fluorescent secondary Cy3 anti-mouse and Cy2 anti-rabbit antibodies (Swant, San Diego, CA). For case JNM10, nonfluorescent sections were also stained for CO prior to rabies immunohistochemistry. For case JNM1, sections 411 and 417 were processed for Nissl substance following rabies immunohistochemistry. Three sections from JNM1 and three sections from JNM10, used to determine the laminar distribution of label in V1 (see Figure 2.4), were stained for CO prior to rabies immunohistochemistry. These same sections were later processed for Nissl substance once cell plot reconstructions were completed.

Retinotopic Correspondence

The retrograde label in the present study was found in confined retinotopic locations in the LGN that closely matched the retinotopic locations of mono- and disynaptic label in V1 (see Figure 2.5). If the label in the LGN was the result of uptake by optic radiations, we would not expect to find a match in retinotopy between label in the LGN and V1. In case JNM1, label in V1 was confined to locations in the calcarine sulcus, which represent visual fields along the horizontal meridian (near zero

elevation, but biased toward lower visual fields), and at azimuths of approximately 10–40 degrees into the periphery (Figure 2.5A, orange shading). Label in the LGN from this same case was found at the corresponding retinotopic representations (Figure 2.5B, orange shading). In case JNM10, label in V1 was found primarily on the opercular surface approximately 1–2 mm posterior to the V1/V2 border and approximately 15 mm lateral from the midline. These locations correspond to lower visual field representations at less than 5 degrees elevation and near the vertical meridian (Figure 2.5A, green shading). Label in the LGN from this same case was again found at the corresponding retinotopic representations (Figure 2.5B, green shading). The close match in retinotopy between rabies-labeled cells in V1 and LGN provides strong evidence that our injections were confined to MT and did not significantly involve the underlying white matter, or, in particular, the underlying optic radiations. The retinotopic maps of V1 are adapted from Lyon and Kaas (2002) and are based on summaries from Weller and Kaas (1983) and Van Essen et al. (1984). The LGN retinotopy is based on summaries from Malpeli and Baker (1975), Kaas and Huerta (1988), and Erwin et al. (1999).

Laminar Distribution of Rabies Label in V1

The locations of rabies-labeled cells were plotted in relation to the laminar boundaries within V1. For each case, a single region within V1 was reconstructed at 403 magnification where disynaptic label was at its densest. Three sections were reconstructed for each region and a total of 7076 rabies-labeled cells were plotted. Percentages of rabies-labeled cells were calculated separately for JNM1 (Figure 2.4C,

orange dots) and JNM10 (Figure 2.4C, green dots) and averaged across both cases (Figure 2.4C, gray bars).

Data Analysis

Positions of LGN and V1 neuronal cell bodies labeled with rabies virus were plotted using Neurolucida software (MicroBrightField, Williston, VT). For the fluorescent sections of case JNM10 (see Figure 2.3), green (rabies) and red (parvalbumin or calbindin) fluorescent images of LGN sections were overlaid and viewed within Canvas X software (ACD Systems, Victoria, British Columbia, Canada). Reconstructions of the laminar boundaries of the LGN from JNM10 were aided by CO staining of the same sections that were stained for rabies virus with DAB (see Figure 2.1A for an example of a section processed for rabies and CO). Reconstructions of the laminar boundaries of the LGN from JNM1 (see Figure 2.2C) were aided by counterstaining for Nissl in sections 411 and 417; the light background staining from DAB and Nissl staining of adjacent sections was used for sections 394, 406, and 418.

For the sections of V1, the distribution of rabies-labeled cells was assigned to the correct laminar locations based on boundaries determined through CO staining and subsequent Nissl staining in the same sections. A Matlab (The Math Works, Inc., Natick, MA) algorithm was used to calculate the numbers and percentages of cells in each layer.

Acknowledgements

We are grateful for support from the National Institutes of Health. We thank Dr. Roberta Kelly for crucial advice in the design and interpretation of these experiments and for participating in the execution and analysis of control experiments testing the rate of spread of rabies virus in the primate motor system. We thank Dr. Donald Lodmell for providing the CVS-11 strain of rabies virus and antibodies to the rabies nucleocapsid; Cecelia Kemper for technical assistance with structural MRIs; Mauricio De La Parra for assistance with animal care and surgical procedures; Ian Wickersham for technical advice and helpful discussions; and Drs. Karen Dobkins and Ralph Siegel for comments on the manuscript.

This chapter, in full, is a reprint of material as it appears in *Neuron* 2006; Nassi, JJ, Lyon, DC, and Callaway, EM; April 20, 50 (2): 319-327. The dissertation author was co-primary author on this paper. Secondary author was the thesis advisor.

References

Albright, T.D., Desimone, R., and Gross, C.G. (1984). Columnar organization of directionally selective cells in visual area MT of the macaque. J. Neurophysiol. 51, 16–31.

Allman, J.M., and Kaas, J.H. (1971). A representation of the visual field in the caudal third of the middle tempral gyrus of the owl monkey (Aotus trivirgatus). Brain Res. 31, 85–105.

Anderson, S.J., Drasdo, N., and Thompson, C.M. (1995). Parvocellular neurons limit motion acuity in human peripheral vision. Proc. Biol. Sci. 261, 129–138.

Born, R.T., and Bradley, D.C. (2005). Structure and function of visual area MT. Annu. Rev. Neurosci. 28, 157–189.

Bullier, J., and Kennedy, H. (1983). Projection of the lateral geniculate nucleus onto

cortical area V2 in the macaque monkey. Exp. Brain Res. 53, 168–172.

Burkhalter, A., Felleman, D.J., Newsome, W.T., and Van Essen, D.C. (1986). Anatomical and physiological asymmetries related to visual areas V3 and VP in macaque extrastriate cortex. Vision Res. 26, 63–80.

Callaway, E.M. (1998). Local circuits in primary visual cortex of the macaque monkey. Annu. Rev. Neurosci. 21, 47–74.

Casagrande, V.A., and Kaas, J.H. (1994). The afferent, intrinsic, and efferent connections of primary visual cortex in primates. In: Cerebral Cortex, A. Peters and K.S. Rockland, eds. (New York: Plenum Publishing Co.), pp. 201–259.

De Valois, R.L., Cottaris, N.P., Mahon, L.E., Elfar, S.D., and Wilson, J.A. (2000). Spatial and temporal receptive fields of geniculate and cortical cells and directional selectivity. Vision Res. 40, 3685–3702.

DeYoe, E.A., and Van Essen, D.C. (1988). Concurrent processing streams in monkey visual cortex. Trends Neurosci. 11, 219–226.

Dobkins, K.R., and Albright, T.D. (1994). What happens if it changes color when it moves?: the nature of chromatic input to macaque visual area MT. J. Neurosci. 14, 4854–4870.

Erwin, E., Baker, F.H., Busen, W.F., and Malpeli, J.G. (1999). Relationship between laminar topology and retinotopy in the rhesus lateral geniculate nucleus: results from a functional atlas. J. Comp. Neurol. 407, 92–102.

Fitzpatrick, D., Lund, J.S., and Blasdel, G.G. (1985). Intrinsic connections of macaque striate cortex: afferent and efferent connections of lamina 4C. J. Neurosci. 5, 3329–3349.

Fries, W., Keizer, K., and Kuypers, H.G. (1985). Large layer VI cells in macaque striate cortex (Meynert cells) project to both superior colliculus and prestriate visual area V5. Exp. Brain Res. 58, 613–616.

Gegenfurtner, K.R., Kiper, D.C., Beusmans, J.M., Carandini, M., Zaidi,Q., and Movshon, J.A. (1994). Chromatic properties of neurons in macaque MT. Vis. Neurosci. 11, 455–466.

Hendrickson, A.E., Wilson, J.R., and Ogren, M.P. (1978). The neuroanatomical organization of pathways between the dorsal lateral geniculate nucleus and visual cortex in Old World and New World primates. J. Comp. Neurol. 182, 123–136.

Jones, E.G., and Hendry, S.H. (1989). Differential calcium binding protein immunoreactivity distinguishes classes of relay neurons in monkey thalamic nuclei. Eur. J. Neurosci. 1, 222–246.

Kaas, J.H., and Huerta,M.F. (1988). Subcortical visual system of primates. In: Comparative Primate Biology, H.P. Steklis, ed. (New York: Liss), pp. 327–391.

Kelly, R.M., and Strick, P.L. (2000). Rabies as a transneuronal tracer of circuits in the central nervous system. J. Neurosci. Methods 103, 63–71.

Kelly, R.M., and Strick, P.L. (2003). Cerebellar loops with motor cortex and prefrontal cortex of a nonhuman primate. J. Neurosci. 23, 8432–8444.

Livingstone, M.S. (1998). Mechanisms of direction selectivity in macaque V1. Neuron 20, 509–526.

Livingstone, M., and Hubel, D. (1988). Segregation of form, color, movement, and depth: anatomy, physiology, and perception. Science 240, 740–749.

Lyon, D.C., and Kaas, J.H. (2002). Evidence for a modified V3 with dorsal and ventral halves in macaque monkeys. Neuron 33, 453–461.

Lysakowski, A., Standage, G.P., and Benevento, L.A. (1988). An investigation of collateral projections of the dorsal lateral geniculate nucleus and other subcortical structures to cortical areas V1 and V4 in the macaque monkey: a double label retrograde tracer study. Exp. Brain Res. 69, 651–661.

Malpeli, J.G., and Baker, F.H. (1975). The representation of the visual field in the lateral geniculate nucleus of Macaca mulatta. J. Comp. Neurol. 161, 569–594.

Malpeli, J.G., Schiller, P.H., and Colby, C.L. (1981). Response properties of single cells in monkey striate cortex during reversible inactivation of individual lateral geniculate laminae. J. Neurophysiol. 46, 1102–1119.

Maunsell, J.H., Nealey, T.A., and DePriest, D.D. (1990). Magnocellular and parvocellular contributions to responses in the middle temporal visual area (MT) of the macaque monkey. J. Neurosci. 10, 3323–3334.

Merigan, W.H., and Maunsell, J.H. (1993). How parallel are the primate visual pathways? Annu. Rev. Neurosci. 16, 369–402.

Merigan, W.H., Byrne, C.E., and Maunsell, J.H. (1991). Does primate motion perception depend on the magnocellular pathway? J. Neurosci. 11, 3422–3429.

Morimoto, K., Hooper, D.C., Carbaugh, H., Fu, Z.F., Koprowski, H., and Dietzschold, B. (1998). Rabies virus quasispecies: implications for pathogenesis. Proc. Natl. Acad. Sci. USA 95, 3152–3156.

Movshon, J.A., and Newsome, W.T. (1996). Visual response properties of striate cortical neurons projecting to area MT in macaque monkeys. J. Neurosci. 16, 7733–7741.

Saul, A.B., Carras, P.L., and Humphrey, A.L. (2005). Temporal properties of inputs to direction-selective neurons in monkey V1. J. Neurophysiol. 94, 282–294.

Schiller, P.H., Logothetis, N.K., and Charles, E.R. (1990). Functions of the colour opponent and broad-band channels of the visual system. Nature 343, 68–70.

Shipp, S., and Zeki, S. (1989a). The organization of connections between areas V5 and V1 in macaque monkey visual cortex. Eur. J. Neurosci. 1, 309–332.

Shipp, S., and Zeki, S. (1989b). The organization of connections between areas V5 and V2 in macaque monkey visual cortex. Eur. J. Neurosci. 1, 333–354.

Sincich, L.C., and Horton, J.C. (2003). Independent projection streams from macaque striate cortex to the second visual area and middle temporal area. J. Neurosci. 23, 5684–5692.

Sincich, L.C., and Horton, J.C. (2005). The circuitry of V1 and V2: integration of color, form, and motion. Annu. Rev. Neurosci. 28, 303–326.

Sincich, L.C., Park, K.F., Wohlgemuth, M.J., and Horton, J.C. (2004). Bypassing V1: a direct geniculate input to area MT. Nat. Neurosci. 7, 1123–1128.

Stepniewska, I., Qi, H.X., and Kaas, J.H. (1999). Do superior colliculus projection zones in the inferior pulvinar project to MT in primates? Eur. J. Neurosci. 11, 469–480.

Tootell, R.B., Hamilton, S.L., and Silverman, M.S. (1985). Topography of cytochrome oxidase activity in owl monkey cortex. J. Neurosci. 5, 2786–2800.

Ugolini, G. (1995). Specificity of rabies virus as a transneuronal tracer of motor networks: transfer from hypoglossal motoneurons to connected second-order and higher order central nervous system cell groups. J. Comp. Neurol. 356, 457–480.

Van Essen, D.C., Maunsell, J.H., and Bixby, J.L. (1981). The middle temporal visual area in the macaque: myeloarchitecture, connections, functional properties and

topographic organization. J. Comp. Neurol. 199, 293–326.

Van Essen, D.C., Newsome, W.T., and Maunsell, J.H. (1984). The visual field representation in striate cortex of the macaque monkey: asymmetries, anisotropies, and individual variability. Vision Res. 24, 429–448.

Weller, R.E., and Kaas, J.H. (1983). Retinotopic patterns of connections of area 17 with visual areas V–II and MT in macaque monkeys. J. Comp. Neurol. 220, 253–279.

Winfield, D.A., Neal, J.W., and Powell, T.P. (1983). The basal dendrites of Meynert cells in the striate cortex of the monkey. Proc. R. Soc. Lond. B. Biol. Sci. 217, 129–139.

Yabuta, N.H., Sawatari, A., and Callaway, E.M. (2001). Two functional channels from primary visual cortex to dorsal visual cortical areas. Science 292, 297–300.

Zeki, S.M. (1974). Functional organization of a visual area in the posterior bank of the superior temporal sulcus of the rhesus monkey. J. Physiol. 236, 549–573.

Zeki, S., and Shipp, S. (1988). The functional logic of cortical connections. Nature 335, 311–317.

Chapter III

Multiple circuits relaying primate parallel visual pathways to the middle temporal area

Summary

Parallel pathways in the primate visual system parse the sensory signal into magnocellular (M), parvocellular (P), and koniocellular (K) streams. These pathways remain anatomically separate and distinct from their origination in different retinal ganglion cell types, through distinct layers of the lateral geniculate nucleus, and into primary visual cortex (V1), with the M pathway terminating primarily in layer 4Cα, the P pathway in layer 4Cβ, and the K pathway in the cytochrome oxidase blobs of layer 2/3. Recent studies indicate that outputs from V1 are less compartmental than previously thought, making it difficult to assess the contributions of M and P pathways to areas beyond V1 in the dorsal and ventral streams. Here we use rabies virus as a retrograde transsynaptic tracer to study the contributions of M and P pathways to areas middle temporal (MT), V3, and V2 of macaque monkey. We find that, although disynaptic inputs through layer 4C of V1 to dorsal stream area MT are dominated by the M pathway, within an additional three synapses MT receives a substantial P input. This P input is unlikely to reach MT via V3, which we show also receives disynaptic inputs dominated by the M pathway. We find that disynaptic inputs to V2, however, can be more balanced and may carry convergent M and P input to MT. Our observations provide evidence for multiple pathways from V1 to MT, with varying degrees of M and P convergence. Each pathway likely provides functionally specialized information to MT and dorsal stream visual processing.

Introduction

The primate visual cortex is divided into multiple areas and relatively independent dorsal and ventral streams (DeYoe and Van Essen, 1988; Livingstone and Hubel, 1988; Zeki and Shipp, 1988; Merigan and Maunsell, 1993). Dorsal stream cortical areas are specialized for analyses of motion and spatial relationships, whereas ventral stream cortical areas are specialized for processing of fine form and color information. It long has been attractive to link the magnocellular (M) pathway to the dorsal stream and the parvocellular (P) pathway to the ventral stream, mainly based on similarities in their respective visual response profiles, yet other theoretical considerations suggest that both M and P pathways can provide useful information for computations conducted in both dorsal and ventral visual areas (Merigan and Maunsell, 1993; Van Essen and Deyoe, 1994). Furthermore, anatomical and functional studies have indicated that the early parallel visual pathways converge significantly via the local circuitry within V1 and onto both dorsal and ventral stream cortical areas (Merigan and Maunsell, 1993; Callaway, 2005; Sincich and Horton, 2005).

Identifying the circuits that mediate the complex interactions between M and P pathways and understanding how they contribute to perception are critical to our understanding of the primate visual system. For example, it is unclear how and to what extent the M and P pathways contribute to the dorsal stream motion processing area middle temporal (MT). MT receives its main ascending input via layer 4C and, subsequently, layer 4B of V1 (Shipp and Zeki, 1989a). Cells projecting directly from layer 4B of V1 to MT are thought to receive input predominantly from M-recipient

layer 4Cα, yet layer 4B cells can receive input either from layer 4Cα alone or from both layer 4Cα and P-recipient layer 4Cβ (Yabuta et al., 2001). Furthermore, MT projecting cells in layer 4B of V1 are intermixed spatially with separate populations of cells in layer 4B of V1 that project to V3 and the cytochrome oxidase (CO) thick stripes of V2 (Maunsell and van Essen, 1983; Burkhalter et al., 1986; Shipp and Zeki,1989b; Sincich and Horton, 2003). These populations may, in turn, provide indirect projections to MT, yet the absence of clear compartmentalization in V1 (Sincich and Horton, 2002; Xiao and Felleman, 2004) as well as heterogeneity within compartments has made it difficult to determine the contributions of M and P pathways to each of these specialized cortical circuits.

Transsynaptic retrograde labeling with rabies virus, however, provides a means of identifying directly the cells in M-recipient layer 4Cα and P-recipient layer 4Cβ presynaptic to extrastriate projecting neurons in V1. We made multiple injections of rabies virus into MT, V3, and V2 to assess the contributions of M and P pathways to MT. We find that, although the most direct input through layer 4C of V1 to MT is dominated by the M pathway, less direct input can be more balanced, carrying a substantial P input to MT.

Materials and Methods

Surgical Procedures

Six adult macaque monkeys were used, following procedures approved by the Salk Institute Animal Care and Use Committee. In addition, all procedures using

rabies virus were conducted by using biosafety level 2 precautions as described previously (Kelly and Strick, 2000).

A 1.5 tesla Siemens (Erlangen, Germany) Symphony magnetic resonance scanner (University of California, San Diego Hillcrest Medical Center/Tenet Magnetic Resonance Institute, San Diego, CA) was used to obtain a full coronal (JNM1, JNM10, and JNM11) or parasagittal (JNM3 and JNM4) series of 1-mm-thick images for each monkey used for injections into MT or V3. Resulting structural images were used to calculate stereotaxic coordinates for our injections either along the posterior bank of the superior temporal sulcus (STS) for MT injections or the annectent gyrus for V3 injections. This was not necessary for our V2 injections, because we simply targeted the opercular surface just posterior to the lip of the lunate sulcus.

MT was targeted in three monkeys, JNM1, JNM10R (right hemisphere of JNM10), and JNM11. MT injections were made by using Hamilton syringes with a 30 gauge needle. In monkey JNM1 three penetrations were aimed at the posterior bank of the STS. Approximately 0.4 μl of the challenge virus strain-11 (CVS-11) strain of rabies virus (see below, Rabies virus strain and speed of transport) was injected at each of four depths spaced 0.5 mm apart. In addition, one of the injection sites included 10% rhodamine dextran (10,000 MW; Molecular Probes, Carlsbad, CA) in the solution of rabies virus. In monkey JNM10R two penetrations were made into the posterior STS, and 0.4 μl of virus was injected at five different depths. In monkey JNM11 the injections were made similarly as in JNM10R.

V3 was targeted in two monkeys, JNM3 and JNM4. V3 injections were made by using Hamilton syringes with a 30 gauge needle. In monkey JNM3 two

penetrations were aimed at the annectent gyrus, spaced ~1 mm apart mediolaterally. Approximately 0.3 μl of virus, including 10% rhodamine dextran, was injected at each of three depths spaced 0.5 mm apart. In monkey JNM4 the injections were made similarly as in JNM3.

V2 was targeted in two monkeys, JNM10L (left hemisphere of JNM10) and JNM13. V2 injections were made by using glass micropipettes (tip diameter, ~30 μm), and pressure was applied by a Picospritzer. In monkey JNM10L seven penetrations were made along the opercular surface, perpendicular to the cortical surface, just posterior to the lip of the lunate sulcus. Penetrations were separated by ~5 mm mediolaterally. Approximately 0.3 μl of virus was injected at each of three depths spaced 0.5 mm apart (0.4, 0.8, and 1.2 mm deep). In monkey JNM13 10 injections were made similarly as in JNM10L, except with mediolateral separation between penetrations of ~2 mm.

Rabies Virus Strain and Speed of Transport

To trace disynaptic connections to areas MT, V3, and V2, we injected the CVS-11 strain of rabies virus and allowed a survival time of 3 d. It is important to note that different preparations of rabies virus, including those of the same strain, can spread through the nervous system at different rates, mainly dependent on the passage history of the virus (Morimoto et al., 1998; Kelly and Strick, 2000). The particular preparation of the CVS-11 rabies virus that we used was obtained from Dr. Donald Lodmell, Rocky Mountain Laboratory (Hamilton, MT), and was passaged four times in mouse brain, followed by five times in cultured chicken embryo-related cells.

On the basis of the similarity in strain and passage history between the virus we used and the CVS-11 rabies virus used by Kelly and Strick (2003), we expected our virus to spread only disynaptically in 3 d and up to five synapses in 6 d. To test the rate of spread of our virus explicitly, we repeated the experiments of Kelly and Strick (2003), injecting virus into motor cortex (M1) of the macaque monkey, as described previously (Nassi et al., 2006). These control experiments confirmed that the virus we injected into MT, V3, and V2 would travel only disynaptically within the 3 d survival time and up to five synapses within the 6 d survival time.

Histology

After 3 d survival time (6 d survival in the case of JNM11) the animals were killed and perfused with 4% paraformaldehyde, and their brains were removed. Sections were cut at 40 μm on a freezing microtome parasagittally (JNM1, JNM3, JNM4, JNM10, JNM11) or coronally (JNM13). First a series of every 12th section was processed for both CO and rabies immunohistochemistry. We used this initially processed series to determine the extent of label in V1 and to select specific regions for more extensive processing. Each section was stained first for CO, followed by rabies immunostaining. Immunohistochemistry for the rabies nucleocapsid was performed by using the anti-nucleocapsid mouse monoclonal antibody (gift from Dr. Lodmell), the biotinylated horse anti-mouse secondary antibody (Vector Laboratories, Burlingame, CA), and an ABC avidin–peroxidase kit (Vector Laboratories) and was revealed via a diaminobenzidine (DAB) reaction enhanced with nickel and cobalt

(black reaction product). After cell count reconstructions the same sections then were stained for Nissl substance to determine the border between layers 4Cα and 4Cβ.

For cases JNM1, JNM10R, and JNM11 a series of cortical sections that included the STS was processed for myelin, CO, or Nissl substance. Anatomical features of MT (Van Essen et al., 1981; Tootell et al., 1985), such as heavy and uniform myelination (particularly in deeper layers), dark and patchy CO staining, greater cortical thickness, and relative position on the posterior bank of the STS, were used to verify that injections were confined to area MT (see Figs. 3.1*A*,*B*, 3.2*A*). For cases JNM3 and JNM4 a series of cortical sections that included the annectent gyrus was processed for myelin, CO, or Nissl substance. Anatomical features of V3 (Van Essen et al., 1986), such as heavy and uniform myelination (particularly in deeper layers) and distance from the V1/V2 border, were used to verify that injections were confined to V3 (see Fig. 3.4*A*,*B*). For cases JNM10L and JNM13 a series of cortical sections was processed for CO to visualize the V1/V2 border and to verify that injections were confined to V2 (see Fig. 3.5*A*).

In the MT and V3 injections our needle penetrations entered the white matter directly underneath cortex. Previous studies have shown that rabies virus uptake along cut peripheral axons is inefficient compared with uptake at axon terminals (Ugolini, 1995; Kelly and Strick, 2000), and rabies uptake along cut central axons has not been demonstrated. In addition, we have made multiple MT injections of a glycoprotein deleted rabies virus, which does not transport transsynaptically, that have involved white matter in a similar way to the injections in this study. We found no evidence of white matter uptake in these cases, with retrogradely labeled cells localized to layers

4B and 6 in V1, exactly what we would expect from an injection in cortical MT (Shipp and Zeki, 1989a). Furthermore, we have shown in previously published work a close retinotopic correspondence between our label in V1 and lateral geniculate nucleus (LGN) after injections into MT (Nassi et al., 2006). These data show convincing evidence that our injections were localized to cortical MT and not the underlying white matter or optic radiations. In both V3 cases all of our retrograde label was confined to the dorsal one-half of the calcarine sulcus and showed a strikingly different pattern from what we observed after injections into V2, making us confident that our injections were confined to V3 and did not involve white matter uptake or spread of virus to nearby cortical visual areas.

Data Analysis

Positions of neuronal cell bodies labeled with rabies virus were plotted with Neurolucida software (MicroBrightField, Williston, VT). Only cell bodies with a visible nucleus were counted. For cases with 3 d survival only regions of V1 in which disynaptic label was densest were reconstructed. We defined these regions as those that had maximum label in layer 4C, because this was the only layer affording certain identification of disynaptic labeling. Once a boundary contour was drawn around a region of densest disynaptic label, the cells were visualized and plotted with a 40x objective, using automatic motorized scanning of the defined region. Reconstructions of the laminar boundaries of V1 were aided by CO staining of the same sections that were stained for rabies virus with DAB (for an example of a section processed for rabies and CO, see Fig. 3.1*C*). Reconstructions of the laminar boundary between

layers 4Cα and 4Cβ were aided by Nissl staining of these same sections after cell count reconstructions. LGN afferents have been shown to terminate in a pattern that corresponds well with the border visualized with a Nissl stain, with magnocellular axons occupying more than one-half of layer 4C (Blasdel and Lund, 1983).

Quantification of the laminar distribution of labeled cells was performed in MatLab (MathWorks, Natick, MA). Three nonadjacent reconstructions were analyzed from each region of V1 label. The numbers of labeled cells were summed across the three reconstructions within a region, and the resultant laminar proportions from each region were averaged across regions within the same animal and then across animals with the same cortical injection target.

Results

We used rabies virus as a transsynaptic retrograde tracer to study disynaptic connections from V1 to areas MT, V3, and V2 of macaque monkey. In particular, we were interested in delineating the contributions of M and P pathways by looking at the proportion of disynaptic label in layers 4Cα and 4Cβ of V1 after injections of rabies virus into either MT itself or into V3 or V2, which can provide MT with less direct V1 input (Maunsell and van Essen, 1983; Shipp and Zeki, 1989b). Physiological recordings have confirmed that cells within layers 4Cα and 4Cβ have visual response properties dominated by the M and P layers of the LGN from which they receive their feedforward, ascending input (Blasdel and Fitzpatrick, 1984). Therefore, contributions from the M and P pathways to extrastriate cortex could be assessed

directly, based on the proportion of disynaptic label in M-dominated layer 4Cα and P-dominated layer 4Cβ.

Studies in both rodents and primates have shown that rabies virus spreads retrogradely across synapses in a time-dependent manner (Ugolini, 1995; Kelly and Strick, 2000). At 3 d after injection the particular strain and preparation of rabies virus that was used in our experiments (see Materials and Methods) (Kelly and Strick, 2003) has time to transport across one synapse and infect neurons disynaptic to the injection site. The virus has time to transport across up to one additional synapse with each subsequent day of survival. Although the rabies virus shows no apparent preference for any particular cell type or size, the rate of transport does depend on strength of connections, leaving open the possibility that with a 3 d survival time some weak disynaptic connections remained unlabeled (Ugolini, 1995). We therefore chose a 3 d survival time for most of our experiments to make it quite unlikely that virus would spread past neurons disynaptic to our injection site. Additionally, in a single experiment we chose a 6 d survival time to allow virus to spread up to five synapses retrograde to the injection site.

We assessed disynaptic inputs to areas MT, V3, and V2 by making injections of the CVS-11 strain of rabies virus (3 d survival) into MT of two monkeys, V3 of two monkeys, and V2 of two monkeys. Additionally, in one monkey we made injections into MT with a 6 d survival time to assess inputs to MT up to five synapses away. We begin by describing detailed results for injections of rabies virus into MT, followed by V3 and then V2. Injections of rabies virus were targeted to cortical area MT of two macaque monkeys by using stereotaxic coordinates of the posterior bank of the STS

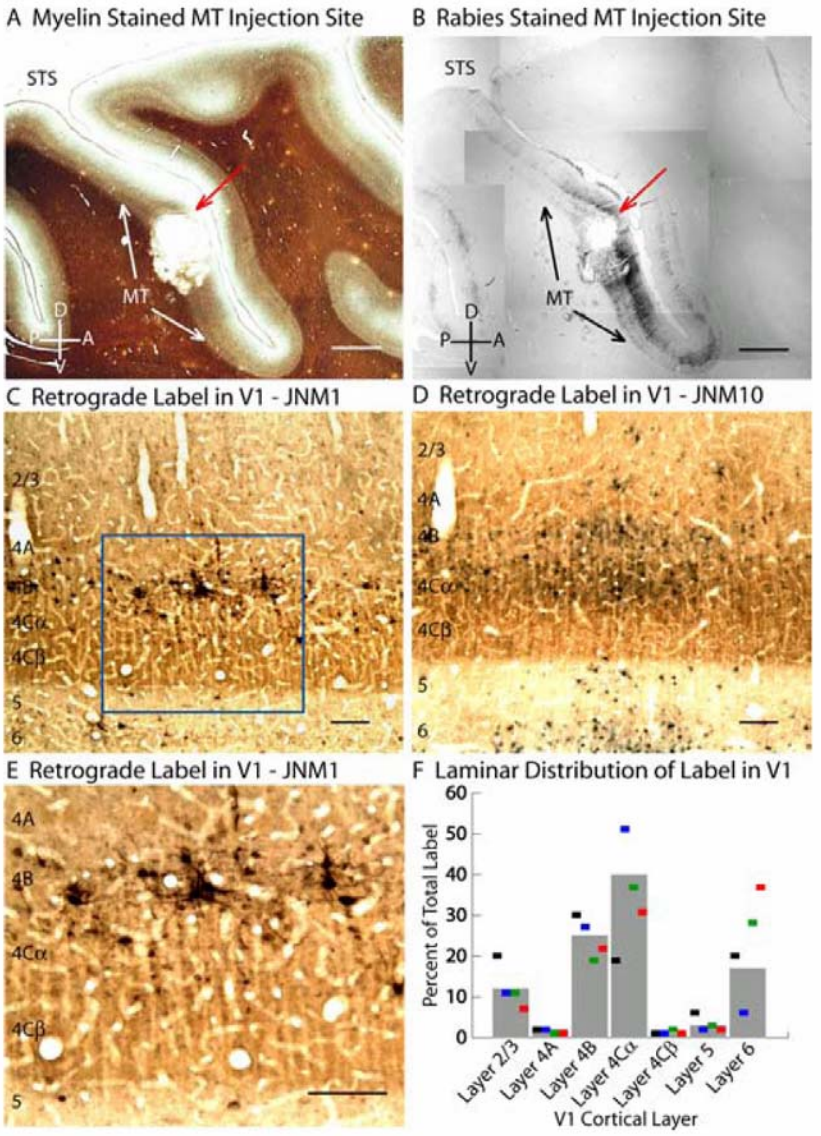

Figure 3.1: Retrogradely labeled neurons in V1 after a 3 d survival injection of rabies virus in cortical area MT.

A, A montage of digitally photographed images of a single parasagittally cut cortical section stained for myelin showing the location of the rabies-injected region (red arrow) in the uniformly dense myelination of area MT (white arrows) along the posterior bank of the STS. ***B***, A montage of digitally photographed images of an adjacent parasagittal cortical section to that in ***A*** stained for the nucleocapsid protein of the rabies virus (black). D, Dorsal; V, ventral; P, posterior; A, anterior. Scale bars: ***A***, ***B***, 2 mm. ***C***, ***D***, Parasagittally cut cortical sections of V1 from cases JNM1 (***C***) and JNM10R (***D***) stained for the nucleocapsid protein of the rabies virus (black) and for cytochrome oxidase (CO; brown). The bottom of the image in ***C*** is cropped at the layer 6/white matter border, and ~10% of layer 6 is cropped at the bottom of the image in ***D***. Cortical layers are indicated. ***E***, Higher magnification image of the location indicated by the blue rectangle in ***C*** of rabies-labeled cells in layers 4B and 4Cα of V1, but not 4Cβ. Scale bars: ***C–E***, 100 μm. ***F***, The percentages of rabies-labeled cells in each layer of V1 for a single region from JNM1 (blue squares) and three separate regions from JNM10R (black, green, red squares). The averaged values across all quantified regions and cases (gray bars) were derived from a total of 15,013 labeled cells.

obtained via structural magnetic resonance images. After a 3 d survival period the animals were perfused, and the brains were sectioned and stained for CO and an antibody against the rabies nucleocapsid protein (see Materials and Methods). The locations of the unilateral injections were confirmed histologically to be confined to MT (Fig. 3.1*A*,*B*) (see Materials and Methods). The needle penetration could be seen within the region of dense and uniform myelination along the posterior bank of the STS, and in an adjacent rabies-stained section the densest label was found in this same region (Fig. 3.1*A*,*B*). After the examination of histological sections, extensive label was found in all identified visual areas known to have monosynaptic connections with MT, including V1, V2, and V3 (Maunsell and van Essen, 1983). Within these areas substantial label was present in the layers known to connect monosynaptically with MT (Maunsell and van Essen, 1983) in addition to label outside of those layers that must consist of cells disynaptic to MT. Although extensive label was found in multiple visual areas, it is unlikely, based on the known cortical circuitry and our 3 d survival time, that rabies virus transported through one of these areas and into V1 (but see Discussion). Most importantly, any label in layer 4C of V1 absolutely must be disynaptic to MT-projecting V1 cells. This must be the case, because layer 4C neurons do not project axons out of V1 and could be labeled only by local connections to neurons within V1 that project to MT.

We found extensive label in V1 from both cases. In one case (JNM1) all of the label in V1 was confined to the calcarine sulcus (Fig. 3.1*C*), and in the other case (JNM10R) label was found primarily on the opercular surface (Fig. 3.1*D*). We counted cells in 12 sections from four separate regions of label, one from case JNM1

and three from case JNM10R. These were regions in which we found disynaptic label to be densest (see Materials and Methods). The laminar distribution of cell label was calculated for each region and subsequently averaged across regions and cases (Fig. 3.1*F*). As expected, labeled cells were found in large numbers in layers 4B (25%) and 6 (17%), layers of V1 known to project directly to MT (Fig. 3.1*C–F*). Labeled cells in these layers likely consisted of cells both monosynaptic and disynaptic to MT. We also observed label outside of these layers, which must be cells disynaptic to MT. Disynaptic label was found in layer 2/3 (12%), which likely connects to MT through both layers 4B and 6 (Fig. 3.1*C–F*). The label in layer 2/3 did not show any clear bias toward the blob or interblob regions, yet no quantitative analysis was used. Most interestingly, however, was the large number of cells disynaptic to MT found in layer 4C of V1. These cells were present almost exclusively in M-dominated layer 4Cα

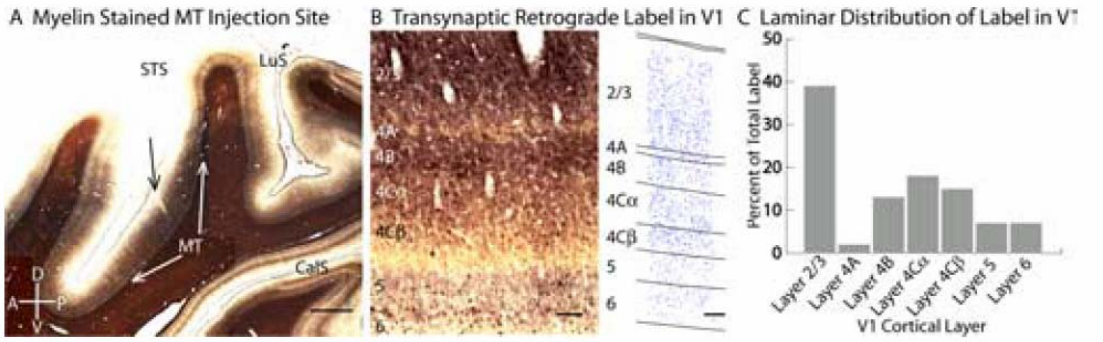

Figure 3.2: Retrogradely labeled neurons in V1 after a 6 d survival injection of rabies virus in cortical area MT.
A, A montage of digitally photographed images of a single parasagittally cut cortical section stained for myelin showing the location of the rabies-injected region (black arrow) in the uniformly dense myelination of area MT (white arrows) along the posterior bank of the STS. LuS, Lunate sulcus; CalS, calcarine sulcus. Scale bar, 2 mm. D, Dorsal; V, ventral; P, posterior; A, anterior. ***B***, Left, Parasagittally cut cortical section stained for the nucleocapsid protein of the rabies virus (black) and for CO (brown) through the central, densest region of label in V1 after a 6 d survival time. The bottom of the image is cropped at the layer 6/white matter border. ***B***, Right, Computer-assisted reconstruction of rabies-labeled cells (blue dots) in an adjacent parasagittally cut cortical section in the calcarine sulcus of V1. Cortical layers are indicated. Scale bars, ***A***, ***B***, 100 μm. ***C***, The percentages of rabies-labeled cells in each layer of V1 within the central, densest region of transsynaptic label in the calcarine sulcus. The values (gray bars) for this particular region were derived from a total of 2017 labeled cells.

(40%) and rarely in P-dominated layer 4Cβ (1%) (Fig. 3.1*C–F*). Averaged across cases, 97% of disynaptic label in layer 4C of V1 was found in layer 4Cα. Although there was clear variability across regions and cases in the percentages of labeled cells within each layer (Fig. 3.1*F*), the relative absence of labeled cells in layer 4Cβ as compared with layer 4Cα was clear and showed little variability. Furthermore, labeled cells within layer 4Cβ tended to be near the 4Cα/4Cβ border, raising the possibility that they could receive M LGN input via dendrites extending into 4Cα (Yabuta and Callaway, 1998). These results indicate that cells projecting directly from V1 to MT receive input almost exclusively from M-dominated layer 4Cα and rarely from P-dominated layer 4Cβ.

Although disynaptic input from layer 4C of V1 to MT originates almost exclusively in M-dominated layer 4Cα, MT nevertheless may receive substantial input from P-dominated layer 4Cβ. Such a pathway simply may require additional synaptic relays either within V1 or through areas V2 or V3 before reaching MT. To test whether MT indeed receives input from P-dominated layer 4Cβ, we made injections targeted to MT of one macaque monkey, in this case with a 6 d survival time, allowing rabies virus to transport up to four synapses past the cells that project directly to MT. The locations of the unilateral injections were confirmed histologically to be confined to MT (Fig. 3.2*A*). The needle penetration can be seen within the region of dense and uniform myelination along the posterior bank of the STS (Fig. 3.2*A*). The resulting transsynaptic label in V1 showed distinctive laminar patterns depending on the topographic location analyzed within V1 (Figs. 3.2, 3.3). In the densest, most central region of label, in this case extending ~2 cm mediolaterally and throughout the entire

anterior–posterior extent of the calcarine sulcus, label was found extensively throughout every layer of V1 (Fig. 3.2*B*,*C*). Particularly large numbers of rabies-labeled cells were found in layers 2/3 (39%), 4B (13%), 4Cα (18%), and 4Cβ (15%). Importantly, 46% of transsynaptic label in layer 4C of V1 was found in layer 4Cβ. Label in this region of V1 most likely corresponds to the locations of V1 cells projecting directly to the rabies-injected site in MT and transsynaptic spread predominantly across the local circuits of V1, but also through V2 and V3, up to four synapses past the directly infected cells.

As we analyzed areas of V1 outside of this central region of dense labeling, particularly 6 mm medial from center where the calcarine sulcus joins the opercular surface and extending onto the opercular surface as far as 10 mm laterally and just 10 mm posterior to the V1/V2 border, we noticed that the laminar patterns of label changed and that labeled cells quickly decreased in density. Along the opercular surface, ~16 mm from center, we found dense labeling in layers 4B (21%), 4Cα (29%), and 6 (22%) along with less but still substantial label in layers 2/3 (11%), 4Cβ (7%), and 5 (7%) (Fig. 3.3*A*,*B*). Just 2 mm anterior to this location, ~18 mm from center, the laminar distribution of cell label was similar to that after injections into MT with a 3 d survival, with the majority of cells in layers 4B (13%), 4Cα (24%) and 6 (42%) (Fig. 3.3*C*,*D*). Only 2% of the cell label was found in layer 4Cβ, with 94% of layer 4C cell label confined to layer 4Cα. Finally, farthest away from center, labeled cells were found only in layers known to connect monosynaptically with MT, layers 4B and 6. We suggest that these varying patterns of label likely reflect transsynaptic horizontal spread of rabies virus, primarily within layers 4B and 6 of V1, followed by

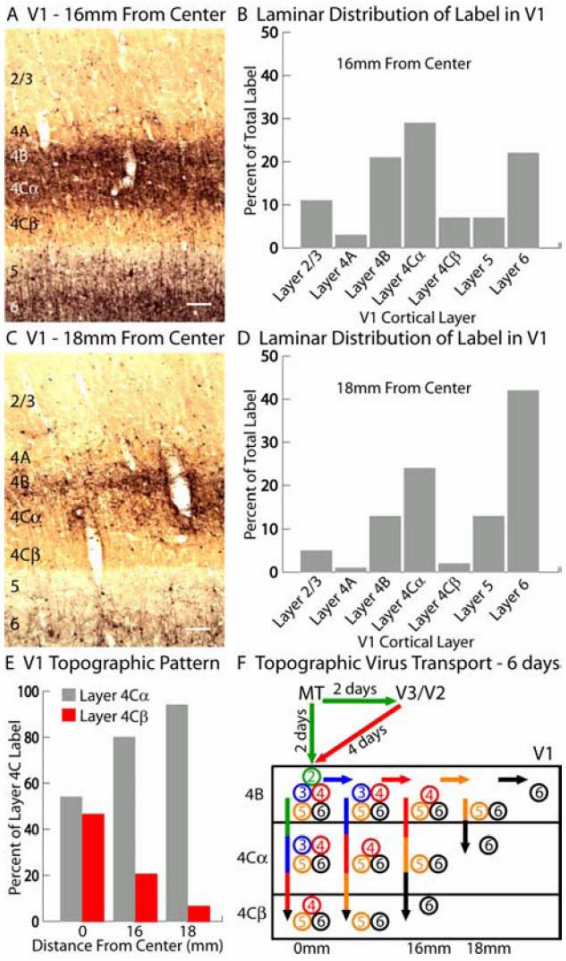

Figure 3.3: Transsynaptic spread of rabies-labeled cells in V1 after a 6 d survival injection of rabies virus in cortical area MT.
A, ***C***, Parasagittally cut cortical sections of V1 from case JNM11 stained for the nucleocapsid protein of the rabies virus (black) and for CO (brown). Outside of the central, densest regions of label in the calcarine sulcus of V1, the laminar profile of labeled cells changed considerably. A reduced density of label across layers and fewer numbers of cells located outside of layers 4B, 4Cα, and 6 were observed ~16 mm away from center (***A***). This reduction in cell density was even more prevalent 18 mm from center (***C***). Approximately 10% of layer 6 is cropped at the bottom of each image. Cortical layers are indicated. Scale bars: ***A***, ***C***, 100 μm. The percentages of rabies-labeled cells in each layer of V1 for regions ~16 mm (***B***) and 18 mm (***D***) away from the center of densest transsynaptic label are indicated. The values (gray bars) for these regions were derived from a total of 659 and 1804 labeled cells, respectively. ***E***, Percentages of rabies-labeled cells in layer 4Cα (gray bars) versus layer 4Cβ (red bars) of V1 within the central, densest region of label in the calcarine sulcus as well as regions ~16 and 18 mm from center. The proportion of transsynaptic label in layer 4Cβ gradually decreased at topographic regions farther away from the central region of label. ***F***, Schematic of potential transsynaptic retrograde viral transport from MT back to V1, based on a 6dsurvival time and the known cortical circuitry within and among V1, V2, V3, and MT. Colored, circled numbers indicate the minimum number of days required for retrograde transport to reach that topographic and laminar location. Within a 6 d survival time the rabies virus had time to spread four synapses past the cells in V1 that project directly to MT, most likely spreading along the long-distance horizontal connections within layers 4B and 6 of V1, followed by vertical spread within local columnar circuits to other layers. Rabies virus also had time to spread two synapses past the cells in V1 projecting indirectly to MT through V2 and V3.

vertical spread to other layers (Fig. 3.3*E*,*F*). Additionally, transsynaptic spread within MT and through V2 and V3 likely contributes to the pattern of label observed in V1. This suggests that, as one moves closer to the center of label, the laminar pattern reflects spread across progressively more synapses involving vertical connections. Most importantly, however, was that in the densest regions we found extensive label in layer 4Cβ (Figs. 3.2*B*,*C*, 3.3*E*). Within five synapses, MT received substantial input from P-dominated layer 4Cβ.

Although our 6 d survival MT injection provided clear evidence for a multisynaptic input from P-dominated layer 4Cβ to MT, the route by which this P pathway input arrives into MT remained unclear. The labeled cells observed in P-dominated layer 4Cβ could reach MT by many hypothesized pathways, the most plausible being via MT-projecting cells in V1, V2, and/or V3. Because V1 projects indirectly to MT through V3 and the CO thick stripes of V2 (Maunsell and van Essen, 1983; Shipp and Zeki, 1989b), we made injections of rabies virus into these two extrastriate cortical areas. Although it is known that V2 receives a strong input from the P pathway via layer 2/3 cells in V1, this pathway requires at least two synapses between layer 4Cβ and the layer 2/3 output cells (Sawatari and Callaway, 2000). Only layer 4B pyramidal cells in V1 both project to V2 and receive direct input from layer 4Cβ; thus we did not expect to observe any disynaptic label in layer 4Cβ unless our injections targeted the axons of large numbers of layer 4B cells. Because of the robust projection from layer 4B of V1 to V3 (Burkhalter et al., 1986), as well as the more balanced incidence of both color-selective and direction-selective neurons in V3 as compared with MT (Felleman and Van Essen, 1987; Gegenfurtner et al., 1997), a

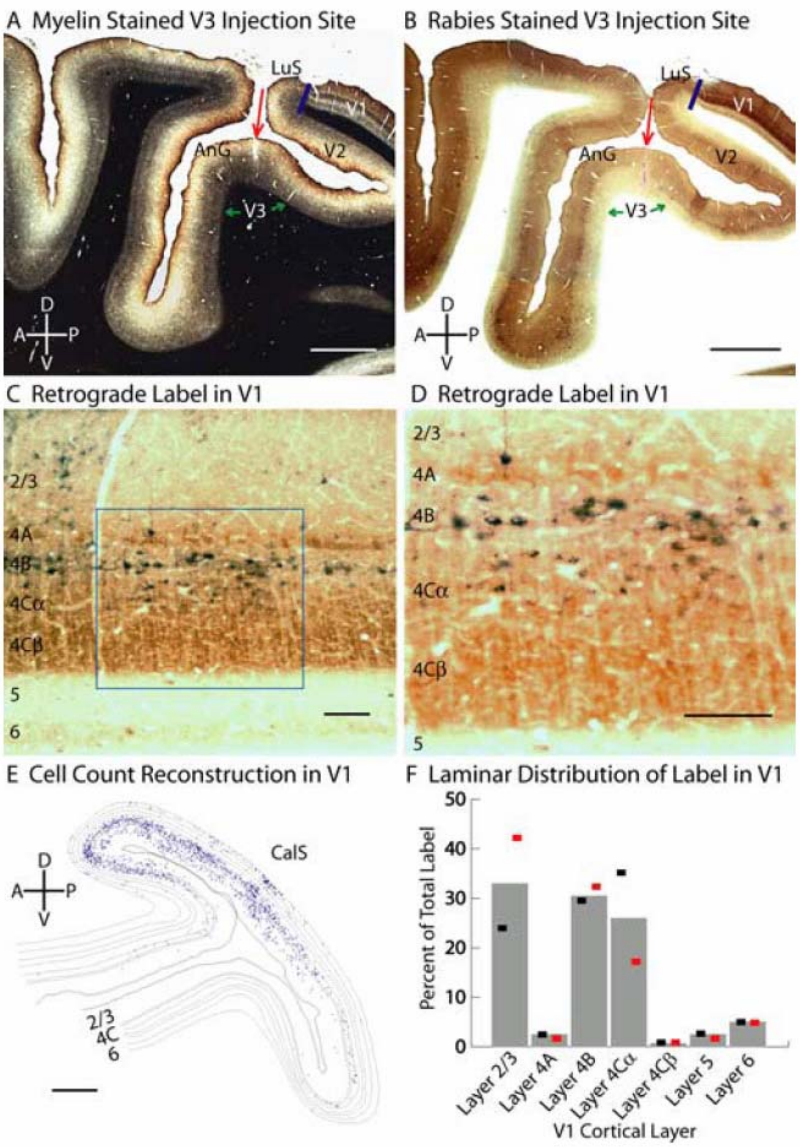

Figure 3.4: Retrogradely labeled neurons in V1 after injections of rabies virus in cortical area V3. ***A***, A montage of digitally photographed images of a single parasagittally cut cortical section stained for myelin showing the location of the rabies-injected region (red arrow) in the uniformly dense myelination of area V3 (green arrows) along the annectent gyrus (AnG), buried in the lunate sulcus (LuS) ~12 mm anterior to the V1/V2 border (blue line). ***B***, A montage of digitally photographed images of an adjacent parasagittal cortical section to that in ***A*** stained for the nucleocapsid protein of the rabies virus (black) and for CO (brown). D, Dorsal; V, ventral; P, posterior; A, anterior. Scale bars: ***A***, ***B***, 2 mm. ***C***, Parasagittally cut cortical section of V1 from case JNM4 stained for the nucleocapsid protein of the rabies virus (black) and for CO (brown). The bottom of the image is cropped at the layer 6/white matter border. Cortical layers are indicated. ***D***, Higher magnification image of the location indicated by the blue rectangle in ***C*** showing the presence of rabies-labeled cells in layers 4B and 4Cα of V1, but not 4Cβ. Scale bars: ***C***, ***D***, 100 μm. ***E***, Computer-assisted reconstruction of rabies-labeled cells (blue dots) in a single parasagittally cut cortical section through a dense region of label in the calcarine sulcus (CalS) of V1. Scale bar, 1 mm. ***F***, The percentages of rabies-labeled cells in each layer of V1 for JNM3 (black squares) and JNM4 (red squares). The averaged values across both cases (gray bars) were derived from a total of 8,515 labeled cells.

higher proportion of disynaptic label in P-dominated layer 4Cβ was expected.

Injections of rabies virus were targeted to dorsal V3 of two macaque monkeys with a 3 d survival time. The locations of the unilateral injections were confirmed histologically to be confined to V3 (Fig. 3.4*A*,*B*). The needle penetration can be seen within the region of dense and uniform myelination along the annectent gyrus, within the lunate sulcus, ~12 mm anterior to the V1/V2 border (Fig. 3.4*A*); in an adjacent CO and rabies-stained section the labeling is less dense at the injection site and more dense in the surrounding cortex (Fig. 3.4*B*). The absence of strong labeling in the immediate vicinity of the virus injection was typical in our studies and was expected because of mechanisms of rabies virus uptake and similar descriptions of injection site labeling from previous studies (Kelly and Strick, 2000). The resulting label in V1 of both cases was located mostly along the dorsal one-half of the calcarine sulcus, showing a very similar topographic pattern to that shown previously after injections of monosynaptic retrograde tracers into V3 (Fig. 3.4*E*) (Burkhalter et al., 1986). We counted cells in a total of six sections, three from each of two different cases, in regions in which we found disynaptic label to be densest (Fig. 3.4*E*) and calculated the resulting laminar distribution of cell label (Fig. 3.4*F*). As expected, label was found in large numbers in layer 4B (31%), the only layer of V1 known to project directly to V3 (but see Felleman et al., 1997) (Fig. 3.4*C–F*). Labeled cells in this layer probably consisted of cells both monosynaptic and disynaptic to V3. We also observed label outside of this layer, which includes cells disynaptic to V3. Label was found in large quantities in layer 2/3 (33%) (Fig. 3.4*C–F*) and did not show any clear bias toward the blob or interblob regions, yet no quantitative analysis was used. Large numbers of

cells disynaptic to V3 were found in layer 4C of V1. Surprisingly, these cells were present almost exclusively in M-dominated layer 4Cα (26%) and rarely in P-dominated layer 4Cβ (1%) (Fig. 3.4*C–F*). Averaged across cases, 98% of disynaptic label in layer 4C of V1 was found in layer 4Cα. Again, although there was clear variability across regions and cases in the percentages of labeled cells within each layer (Fig. 3.4*F*), the relative absence of label in layer 4Cβ as compared with layer 4Cα was clear and showed little variability. These results indicate that cells projecting directly from V1 to V3 receive input almost exclusively from M-dominated layer 4Cα and rarely from P-dominated layer 4Cβ.

Although we found little evidence for disynaptic input from P-dominated layer 4Cβ to MT or V3, the P pathway still could connect indirectly with MT through the CO thick stripes of V2 (Yabuta et al., 2001; Born and Bradley, 2005). It long had been thought that layer 2/3 blobs, layer 2/3 interblobs, and layer 4B of V1 connected specifically to V2 thin stripes, pale stripes, and thick stripes, respectively (Livingstone and Hubel, 1988). Recent evidence, however, suggests that there is not such a clean one-to-one correspondence between V1 and V2 compartments (Sincich and Horton, 2002; Xiao and Felleman, 2004), making it even less clear what the relative contributions of M and P pathways might be to any given V2 stripe type.

Injections of rabies virus were targeted to V2 of two macaque monkeys with a 3 d survival time, just posterior to the lunate sulcus along the opercular surface. Multiple injections were made unilaterally for each animal (additional details below), and their locations were confirmed histologically to be confined to V2 (Fig. 3.5*A*). The pipette penetration for one of the injections can be seen ~1 mm anterior to the

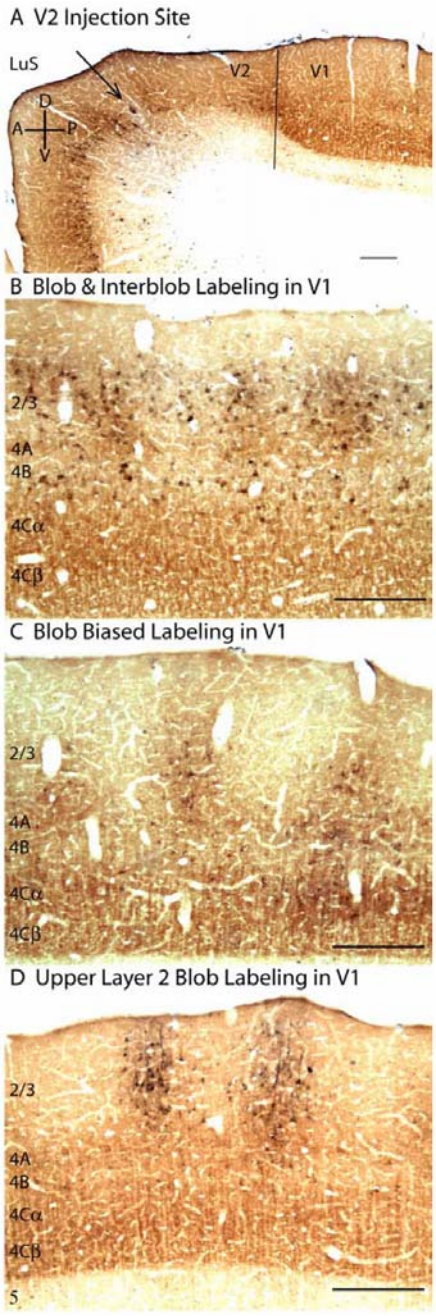

Figure 3.5: Retrogradely labeled neurons in V1 after injections of rabies virus in cortical area V2. ***A***, A single parasagittally cut cortical section stained for the nucleocapsid protein of the rabies virus (black) and for CO (brown) showing the location of the rabies-injected region (black arrow) ~1 mm anterior to the V1/V2 border (black line) just posterior to the lunate sulcus (LuS). D, Dorsal; V, ventral; P, posterior; A, anterior. ***B–D***, Parasagittally cut cortical sections of V1 from case JNM10L stained for the nucleocapsid protein of the rabies virus (black) and for CO (brown). Multiple patterns of retrograde label were observed in V1, including labeling with relatively unbiased scatter in both CO blobs and interblobs of layer 2/3 (***B***), labeling biased to the CO blobs in layer 2/3 (***C***), and labeling biased to the CO blobs of layer 2/3 and extending superficially to the top of layer 2 (***D***). Cortical layers are indicated. Scale bars, 250 μm.

V1/V2 border along the opercular surface and, importantly, an absence of label can be seen posterior to the injection site within close proximity to the V1/V2 border (Fig. 3.5*A*). The lack of label closely surrounding the V1/V2 border made us confident that the observed retrograde label in V1 was not the result of a large injection that spread across the V1/V2 border. We were not able to evaluate directly whether any of the V2 injections were confined to a particular CO stripe type, because we chose to section our tissue across layers to reveal clearly the laminar borders and depth in V1.

In case JNM13 10 injections were made in close proximity to each other, resulting in overlapping foci of retrograde label in V1. In case JNM10L, however, seven injections were made with greater separation between injection sites, resulting in foci of retrograde label in V1 that could be analyzed independently of one another. Although the resulting label in V1 after injections from the latter case could not be attributed with certainty to an individual thick, thin, or pale stripe, we did see systematic variation in the pattern of V1 label resulting from one injection site to another. Based on the known pattern of monosynaptic connections between V1 and particular stripe types in V2 (Livingstone and Hubel, 1987, 1988; Sincich and Horton, 2002; Sincich et al., 2006), as well as local V1 connections (Callaway, 1998, 2005), inferences as to the single stripe type or multiple stripe types involved in a particular injection site sometimes could be made and will be discussed additionally below. The resulting label in V1 was always found a certain distance posterior to the V1/V2 border that corresponded well retinotopically with the location of the injections into V2.

The overall laminar patterns of label in V1 varied between V2 injections, depending on the patterns of label in blobs versus interblobs of layer 2/3 as well as layer 4B. This suggested a dependence on injection location relative to V2 stripe compartments. First we describe foci with strong label in all three V1 compartments that project to V2 (blobs, interblobs, and layer 4B), likely the result of injections involving all three V2 stripe types (see below). We counted cells in 12 sections from four separate foci of label, two from case JNM10L and two from case JNM13, where

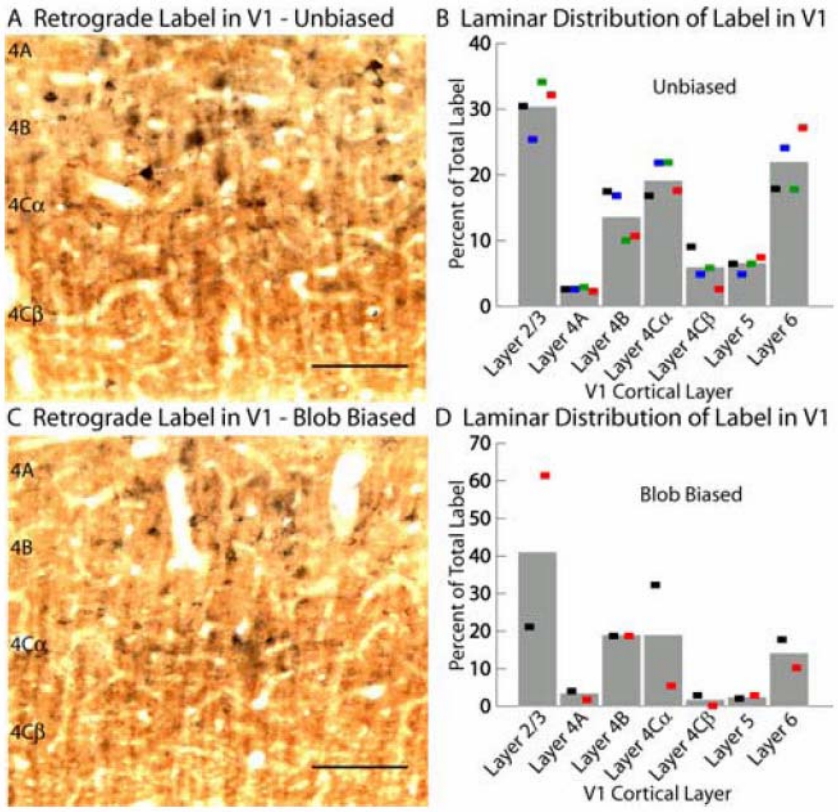

Figure 3.6: Laminar distribution of rabies-labeled cells in V1 after injections of rabies virus in cortical area V2.
A, ***C***, Parasagittally cut cortical sections of V1 (JNM10L) from a blob-unbiased (***A***) and blob-biased (***C***) pattern of label stained for the nucleocapsid protein of the rabies virus (black) and for CO (brown). Cortical layers are indicated. Scale bars: ***A***, ***C***, 100 μm. ***B***, The percentages of rabies-labeled cells in each layer of V1 for case JNM13 (green and red squares) and JNM10L (black and blue squares) from foci with blob-unbiased patterns of label. ***D***, The percentages of rabies-labeled cells in each layer of V1 for case JNM10L from two separate foci (black and red squares) with blob-biased patterns of label. The averaged values across all quantified foci and cases (gray bars) for blob-unbiased (***B***) and blob biased (***D***) patterns of label were derived from a total of 25,071 and 1,811 labeled cells, respectively.

we found disynaptic label to be densest. These four foci were distinguishable from the others based on the indiscriminate pattern of cells in layer 2/3 in relation to the blob and interblob regions (Fig. 3.5*B*). Overall, label was found in greatest proportion in layer 2/3 (30%) of V1, which is known to provide heavy, direct input primarily to the thin and pale stripes of V2 (Figs. 3.5*B*, 3.6*B*) (Livingstone and Hubel, 1988; Sincich and Horton, 2002; Sincich et al., 2006). The labeled cells in layer 2/3 did not show any clear bias toward the blob or interblob regions and presumably included cells both monosynaptic and disynaptic to V2. Substantial label, however, also was found in nearly every other layer. Earlier work has shown that all layers of V1 outside of layer 4C may connect monosynaptically with V2 (Kennedy and Bullier, 1985; Livingstone and Hubel, 1988; Rockland, 1992; Sincich and Horton, 2002) and that all of these layers also can provide local input to each other (Callaway, 1998). It is, therefore, unclear which label outside of layer 4C is monosynaptic versus disynaptic. Importantly, however, any label within layer 4C was certainly disynaptic to V2. Substantial label was found in layer 4B (14%) of V1, which is known to provide direct input primarily to the thick stripes of V2 (Figs. 3.5*B*, 3.6*A*,*B*). Additionally, label was found in layers 5 (7%) and 6 (22%) (Fig. 3.6*B*). Interestingly, however, in these selected foci of label we found disynaptic label in layer 4C of V1 to be much more balanced between 4Cα and 4Cβ as compared with injections into MT or V3. Labeled cells were found in both M-dominated layer 4Cα (19%) and P-dominated layer 4Cβ (6%) (Fig. 3.6*A*,*B*). Averaged across cases, 23% of disynaptic label in layer 4C of V1 was found in layer 4Cβ. Labeled cells in layer 4Cβ were found from the upper border with layer 4Cα to the lower border with layer 5, showing a strikingly different

distribution and prevalence than after injections into MT or V3. These results indicate that the group of cells projecting directly from V1 to the V2 compartments injected in these cases collectively receives mixed input from both M-dominated layer 4Cα and P-dominated layer 4Cβ.

As was noted earlier, however, some injections into V2 of case JNM10L resulted in differing patterns of label in V1. Two foci of label showed a pattern in which layer 2/3 cells were found primarily in the blob regions (Fig. 3.5*C*), likely the result of injections localized to a thin stripe (see below), and one focus of label showed a pattern in which cells extended more superficially within the blob regions of layer 2/3 than in other foci (Fig. 3.5*D*). We counted cells in six sections from two separate foci of label, both from case JNM10L, in which the pattern of label in layer 2/3 showed a clear bias toward the blob regions (Fig. 3.5*C*). In these foci labeling again was found in high proportion in layers 2/3 (41%), 4B (19%), and 6 (14%) (Figs. 3.5*C*, 3.6*D*). Although there was substantial variability in the proportion of cell label in these layers, disynaptic label was consistently absent from layer 4Cβ. Cells disynaptic to V2 in layer 4C of V1 were found almost exclusively in M-dominated layer 4Cα (19%) and rarely in P-dominated layer 4Cβ (2%) (Fig. 3.6*C*,*D*). Averaged across the two cases, 95% of disynaptic label in layer 4C of V1 was found in layer 4Cα. These results indicate that cells projecting directly from V1 to the V2 compartments injected in these cases receive direct input almost exclusively from M-dominated layer 4Cα and rarely from P-dominated layer 4Cβ.

Although we could not localize our V2 injections to any particular stripe type, we believe that any substantial disynaptic label in layer 4Cβ was likely the result of

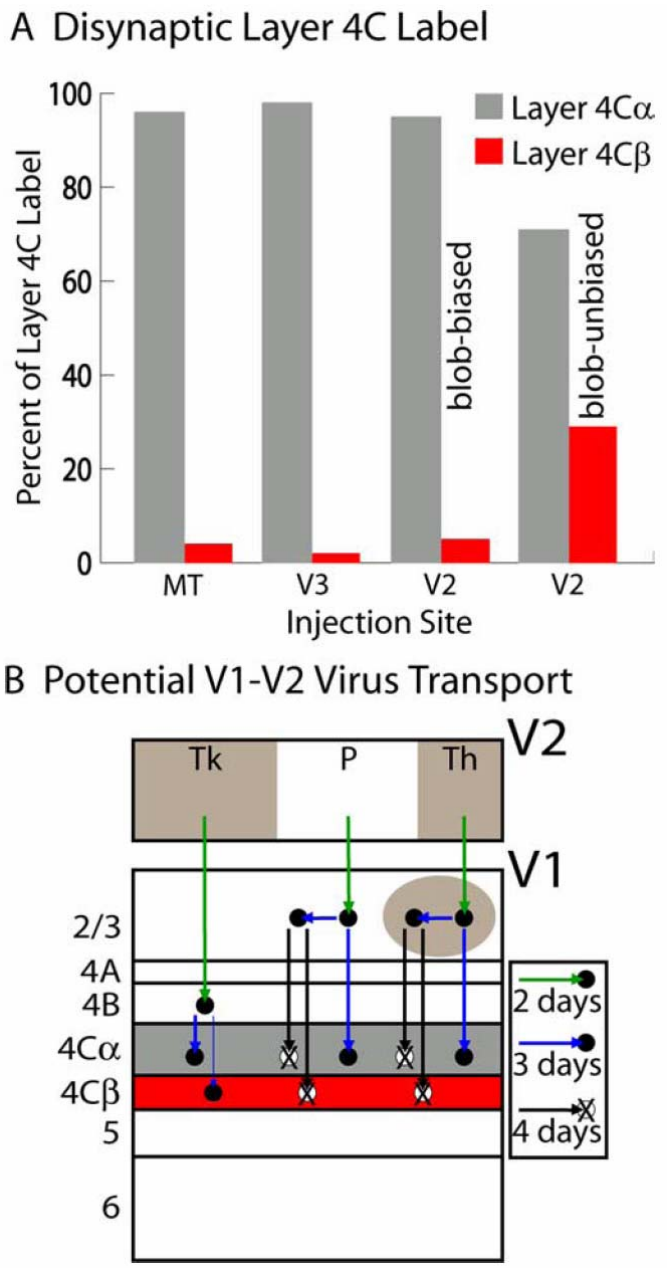

Figure 3.7: Cortical circuitry underlying varying patterns of retrograde label in layer 4C of V1. ***A***, Percentages of rabies-labeled cells in layer 4Cα (gray bars) versus layer 4Cβ (red bars) of V1 resulting from injections of rabies virus into MT, V3, or V2. Values were averaged across all quantified regions and cases for each cortical area that was injected. Only particular injections into V2, in which layer 2/3 label was relatively unbiased toward blobs versus interblobs, resulted in substantial disynaptic label in layer 4Cβ. ***B***, Schematic of potential retrograde viral transport from V2 back to V1 based on known cortical circuitry between the two visual areas, photostimulation data (Sawatari and Callaway, 2000), and the 3 d survival time in our experiments. Layer 3 projection neurons within V1 receive input from layer 4Cα, but not layer 4Cβ, making pale (P) and thin (Th) stripes of V2 unlikely sources of the observed disynaptic label in layer 4Cβ. Layer 4B projection neurons in V1, however, receive input from both layers 4Cα and 4Cβ, making thick (Tk) stripes the more likely source of the observed disynaptic label in layer 4Cβ.

injections involving a thick stripe (Fig. 3.7*B*). We recognize that this inference is likely to be contrary to the preconceived notions of many readers; however, it is supported strongly by the evidence we describe below. Previous studies that used photostimulation showed that layer 3 cells projecting outside of V1 receive input from layer 4Cα, but not layer 4Cβ; only layer 3 cells with exclusively local projections receive layer 4Cβ input (Sawatari and Callaway, 2000). Any layer 4Cβ contribution relayed from layer 3 to V2 must be trisynaptic (Lachica et al., 1992; Yabuta et al., 2001). Therefore, thin and pale stripes of V2, which receive the bulk of their input from layer 3 cells in the blob and interblob regions, respectively (Livingstone and Hubel, 1988; Rockland, 1992; Sincich and Horton, 2002; Sincich et al., 2006), are not likely to be the source of the observed disynaptic label in layer 4Cβ (Fig. 3.7*B*). Consistent with this interpretation, injections into V2 that resulted in retrograde V1 label primarily in the blobs of layer 2/3 (likely because of thin stripe injections) resulted in substantial disynaptic label in layer 4Cα, but not in layer 4Cβ (Fig. 3.7*A*). Only layer 4B pyramidal and deep layer neurons in V1 both project to V2 and receive layer 4Cβ input (Briggs and Callaway, 2001, 2005; Yabuta et al., 2001). These are the only cells that could mediate disynaptic connections from layer 4Cβ to V2. Therefore, thick stripes of V2, which receive the bulk of their input from layer 4B (Livingstone and Hubel, 1987) (but see Sincich and Horton, 2002), are the most likely source of the observed disynaptic label in layer 4Cβ (Fig. 3.7*B*). Consistent with this interpretation, only injections into V2 that resulted in retrograde label in both the blobs and interblobs of layer 2/3 and in layer 4B produced substantial disynaptic label in layer 4Cβ (Fig. 3.7*A*). These injections most likely involved V2 thick and/or pale stripes in

addition to a thin stripe. Interestingly, we found that, after these injections into V2, 23% of disynaptic label in layer 4C of V1 was confined to P-dominated layer 4Cβ. This corresponds well to previous photostimulation data showing that 30% of the layer 4C input to layer 4B pyramidal cells comes from layer 4Cβ (Yabuta et al., 2001). This additionally supports our contention that the observed label in layer 4Cβ reaches V2 through layer 4B pyramidal cells.

Discussion

Our observations demonstrate that the major ascending input through layer 4C of V1 to MT is dominated by the M pathway. The major input to V3 via layer 4C of V1 likewise is dominated by the M pathway. The P pathway nevertheless reaches MT indirectly, likely through the CO thick stripes of V2. After injections of rabies virus into MT (3 d survival) disynaptic label in layer 4C of V1 was found almost exclusively in M-dominated layer 4Cα. Our 6 d survival MT injections, however, resulted in substantial transsynaptic label throughout all layers of V1, including P-dominated layer 4Cβ. The design of this experiment did not allow us to identify the particular route by which layer 4Cβ was labeled, but it provided conclusive evidence for a substantial indirect input from P-dominated layer 4Cβ of V1 to MT. In an attempt to elucidate the route by which this P pathway input reaches MT, we made injections into areas V3 and V2. After injections of rabies virus into V3 (3 d survival), disynaptic label in layer 4C of V1 again was found almost exclusively in M-dominated layer 4Cα. Only after certain injections into V2, likely those that involved a thick

stripe (see Results), was substantial disynaptic label found in P-dominated layer 4Cβ, making the thick stripes of V2 the most likely relay for P pathway input to MT.

The pattern of monosynaptic and disynaptic label in V1 was different in important ways after injections into MT, V3, and V2. It is important to note that some label outside of layer 4C, instead of being disynaptic to projection cells within V1, could be disynaptic to projection cells outside of V1, possibly labeled via ascending V1 axons that terminate outside of layer 4 in extrastriate cortex. The following analysis, however, is made with the assumption that the majority of label within V1 is either monosynaptic to the injection site or disynaptic to those same V1 projection cells. The most salient difference between the laminar profiles after injections into V3 versus MT was the higher proportion of label in layer 2/3 and lower proportion of label in layer 6 after injections into V3 (Figs. 3.1*F*, 3.4*F*). There is some indication from earlier work that layer 2/3 of V1 may connect directly with V3 (Felleman et al., 1997), which would mean that the high proportion of label in layer 2/3 consists of cells both monosynaptic and disynaptic to V3. The lower proportion of label in layer 6 of V1 was expected because, unlike MT, V3 does not receive monosynaptic connections from this layer (Burkhalter et al., 1986). Most striking, however, was the disproportionate amount of label in layer 4Cα as compared with layer 4Cβ after injections into either of these two visual areas (Fig. 3.7*A*). The relative absence of label in layer 4Cβ after injections into V3 was somewhat surprising given the preponderance of color selectivity found in this area (Felleman and Van Essen, 1987; Gegenfurtner et al., 1997) and the prevalence of connections between V3 and both MT and V4 (Felleman and Van Essen, 1991). There is some indication, however, that

there is a modular organization to V3 similar to that of V2 (Lyon et al., 2002). Although unlikely, it remains possible that our injections into V3 involved only certain modules and that if all modules of V3 had been injected more substantial disynaptic label might have been observed in layer 4Cβ. Nevertheless, our injections into both MT and V3 resulted in disynaptic label almost exclusively within the M-dominated sub layer of 4C.

In contrast, after injections into V2, a more balanced proportion of label often was observed in layers 4Cα and 4Cβ (Fig. 3.7*A*), indicating mixed input from M and P pathways. Importantly, the prevalence of label in layer 4Cβ in these cases made it clear that the lack of label in layer 4Cβ after injections into MT and V3 was attributable to a weak or altogether nonexistent connection, eliminating the possibility that cells in layer 4Cβ are simply less vulnerable to rabies virus infection. Additionally, substantial amounts of label were found in every layer of V1 in these cases (Fig. 3.6*B*).

The laminar and columnar patterns of V1 label varied between V2 injections so that only some of our V2 injections resulted in substantial disynaptic label in P-dominated layer 4Cβ (Figs. 3.5, 3.6). Most of our injections into V2 resulted in retrograde label in V1 that was found indiscriminately in both blobs and interblobs of layer 2/3, as well as layer 4B (Fig. 3.5*B*). These injections most likely included all three stripe types in V2 and were the only injections that resulted in a substantial proportion of label in layer 4Cβ (Fig. 3.6*A*,*B*). Additionally, a few V2 injections resulted in retrograde label in V1 biased to the blobs of layer 2/3 (Fig. 3.5*C*). These injections most likely were isolated to a thin stripe in V2 and resulted in disynaptic

label almost exclusively in layer 4Cα as compared with layer 4Cβ (Fig. 3.6*C*,*D*). Finally, one injection into V2 resulted in retrograde label in V1 biased to the blobs of layer 2/3 and extending strikingly superficially to the top of layer 2 (Fig. 3.5*D*). In this particular case we did not observe any labeled cells in layer 4C. This pattern of label was similar to that described in the case of one retrograde tracer injection into V2 by Van Essen et al. (1986) and may be the result of an injection into a unique compartment in V2 that receives monosynaptic input specifically from upper layer 2 as opposed to lower layer 2 and layer 3. The absence of disynaptic rabies label in layer 4C then would be expected, because axons of layer 4C cells do not project above layer 3B (Lachica et al., 1992; Yabuta and Callaway, 1998).

Together, these results make it likely that the labeled cells we observe in layer 4Cβ provide disynaptic input to the CO thick stripes of V2 via pyramidal cells in layer 4B of V1 (Fig. 3.7*B*) (see Results). This is particularly significant because the thick stripes of V2 are known to project to MT (Shipp and Zeki, 1989b) and, thus, could provide input to MT from both M and P pathways. There is a chance, however, that the observed disynaptic label in P-dominated layer 4Cβ resulted from injections involving pale stripes and not thick stripes (Sincich and Horton, 2002) or even subpopulations of cells within the thick stripes that do not project to MT, allowing for the possibility that MT does not receive mixed input from both M and P pathways indirectly through V2. Although the compartmental organization of projections from V1 to V2 recently has been called into question (Sincich and Horton, 2002), it is nevertheless clear from our observations that MT receives a substantial indirect input

from P-dominated layer 4Cβ and that the thick stripes of V2 remain the most likely candidate to relay this information to MT.

Previous work from our lab has shown conclusive evidence for input from LGN P cells to MT that is only two synapses away (Nassi et al., 2006). This pathway bypasses layer 4Cβ and likely is mediated by layer 6 cells in V1. Although this disynaptic connection from LGN to MT is robust, it is nevertheless a minor connection compared with that through layers 4C and 4B of V1 (Shipp and Zeki, 1989a). The results described here provide additional evidence for a P input to MT

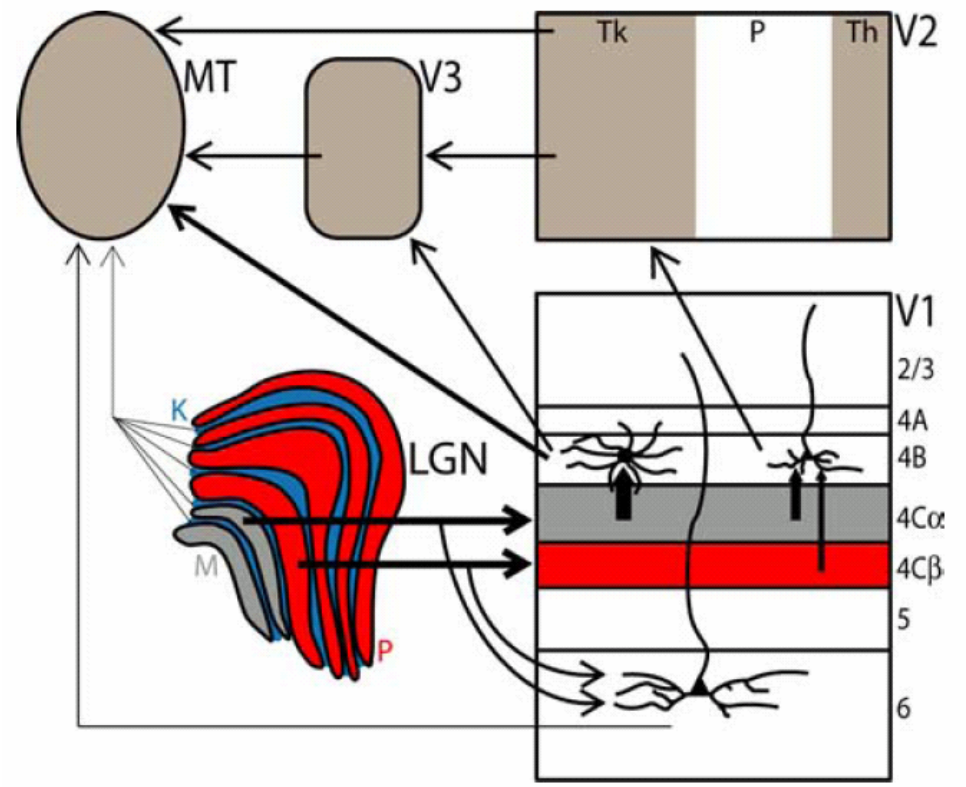

Figure 3.8: Multiple pathways from V1 to MT with varying degrees of M and P pathway convergence. Multiple pathways provide input to MT, with differing contributions from the M, P, and K pathways. A direct projection from LGN to MT is sparse and dominated by the K pathway (Sincich et al., 2004). A disynaptic connection from LGN to MT through layer 6 of V1 is more extensive and provides MT with convergent input from M and P pathways (Nassi et al., 2006). Trisynaptic input from LGN to MT via layer 4C of V1 is the most prominent and is dominated by the M pathway. Within a few more synapses, however, the P pathway contributes as well, likely via the CO thick stripes of V2. See Discussion for additional details. Tk, Thick stripe; P, pale stripe; Th, thin stripe.

that involves the more prominent pathway through layer 4C. The connection from P-dominated layer 4Cβ to MT likely involves between three and five synapses, including a potential relay through the CO thick stripes of V2.

It is clear from these studies and previous work that MT receives input from multiple pathways with varying amounts of convergence among the M, P, and koniocellular (K) processing streams (Fig. 3.8) (Sincich et al., 2004; Born and Bradley, 2005; Nassi et al., 2006). The pathways also differ in their number of synaptic relays and, thus, the speed with which they likely convey information to MT. Direct input from LGN to MT is sparse and dominated by the K pathway (Sincich et al., 2004). Disynaptic input from LGN to MT via layer 6 cells in V1 is more extensive and carries convergent input from M and P pathways (Nassi et al., 2006). Trisynaptic input from LGN to MT via layer 4C of V1 is the most prominent and is dominated by the M pathway, yet within a few more synapses the P pathway contributes as well, likely via the CO thick stripes of V2. We suggest that each of these pathways is suited uniquely to convey visual information with varying degrees of spatial and temporal resolution as well as contrast sensitivity and color selectivity. Additional studies will be necessary to elucidate the functional contributions of each of these unique input pathways to MT and to understand better the complex interactions among the M, P, and K pathways of the primate visual system.

Acknowledgements

This work was supported by National Institutes of Health Grants EY 010742 (E.M.C.) and 5 T32 AG00216 and 2 T32 MH20002 (J.J.N.).

We thank Dr. Roberta Kelly for crucial advice in the design and interpretation of these experiments and for participating in the execution and analysis of control experiments testing the rate of spread of rabies virus in the primate motor system. We also thank Dr. Donald Lodmell for providing the CVS-11 strain of rabies virus and antibodies to the rabies nucleocapsid; Cecelia Kemper for technical assistance with structural magnetic resonance imaging; Mauricio De La Parra for assistance with animal care and surgical procedures; and Drs. David Lyon, Greg Horwitz, and Vivien Casagrande for comments on this manuscript.

This chapter, in full, is a reprint of material as it appears in *J Neurosci* 2006; Nassi, JJ, and Callaway, EM; December 6, 26 (49): 12789-12798. The dissertation author was primary author on this paper. Secondary author was the thesis advisor.

References

Blasdel G.G., and Fitzpatrick, D. (1984). Physiological organization of layer 4 in macaque striate cortex. J. Neurosci. 4, 880–895.

Blasdel G.G., and Lund, J.S. (1983). Termination of afferent axons in macaque striate cortex. J. Neurosci. 3, 1389 –1413.

Born R.T., and Bradley, D.C. (2005). Structure and function of visual area MT. Annu. Rev. Neurosci. 28, 157–189.

Briggs, F., and Callaway, E.M. (2001). Layer-specific input to distinct cell types in layer 6 of monkey primary visual cortex. J. Neurosci. 21, 3600 –3608.

Briggs, F., and Callaway, E.M. (2005). Laminar patterns of local excitatory input to layer 5 neurons in macaque primary visual cortex. Cereb. Cortex 15, 479–488.

Burkhalter, A., Felleman, D.J., Newsome, W.T., and Van Essen, D.C. (1986). Anatomical and physiological asymmetries related to visual areas V3 and VP in macaque extrastriate cortex. Vision Res. 26, 63– 80.

Callaway, E.M. (1998). Local circuits in primary visual cortex of the macaque monkey. Annu. Rev. Neurosci. 21, 47–74.

Callaway, E.M. (2005). Neural substrates within primary visual cortex for interactions between parallel visual pathways. Prog. Brain Res. 149, 59–64.

DeYoe, E.A., and Van Essen, D.C. (1988). Concurrent processing streams in monkey visual cortex. Trends Neurosci. 11, 219 –226.

Felleman, D.J., and Van Essen, D.C. (1987). Receptive field properties of neurons in area V3 of macaque monkey extrastriate cortex. J. Neurophysiol. 57, 889 –920.

Felleman, D.J., and Van Essen, D.C. (1991). Distributed hierarchical processing in the primate cerebral cortex. Cereb. Cortex 1, 1– 47.

Felleman, D.J., Burkhalter, A., and Van Essen, D.C. (1997). Cortical connections of areas V3 and VP of macaque monkey extrastriate visual cortex. J. Comp. Neurol. 379, 21– 47.

Gegenfurtner, K.R., Kiper, D.C., and Levitt, J.B. (1997). Functional properties of neurons in macaque area V3. J. Neurophysiol. 77, 1906 –1923.

Kelly, R.M., and Strick, P.L. (2000). Rabies as a transneuronal tracer of circuits in the central nervous system. J. Neurosci. Methods 103, 63–71.

Kelly, R.M., and Strick, P.L. (2003). Cerebellar loops with motor cortex and prefrontal cortex of a nonhuman primate. J. Neurosci. 23, 8432– 8444.

Kennedy, H., and Bullier, J. (1985). A double-labeling investigation of the afferent connectivity to cortical areas V1 and V2 of the macaque monkey. J. Neurosci. 5, 2815–2830.

Lachica, E.A., Beck, P.D., and Casagrande, V.A. (1992). Parallel pathways in macaque monkey striate cortex: anatomically defined columns in layer III. Proc. Natl. Acad. Sci. USA 89, 3566 –3570.

Livingstone, M., and Hubel, D. (1988). Segregation of form, color, movement, and depth: anatomy, physiology, and perception. Science 240, 740 –749.

Livingstone, M.S., and Hubel, D.H. (1987). Connections between layer 4B of area 17 and the thick cytochrome oxidase stripes of area 18 in the squirrel monkey. J. Neurosci. 7, 3371–3377.

Lyon, D.C., Xu, X., Casagrande, V.A., Stefansic, J.D., Shima, D., and Kaas, J.H.

(2002). Optical imaging reveals retinotopic organization of dorsal V3 in New World owl monkeys. Proc. Natl. Acad. Sci. USA 99, 15735–15742.

Maunsell, J.H., and Van Essen, D.C. (1983). The connections of the middle temporal visual area (MT) and their relationship to a cortical hierarchy in the macaque monkey. J. Neurosci. 3, 2563–2586.

Merigan, W.H., and Maunsell, J.H. (1993). How parallel are the primate visual pathways? Annu. Rev. Neurosci. 16, 369–402.

Morimoto, K., Hooper, D.C., Carbaugh, H., Fu, Z.F., Koprowski, H., and Dietzschold, B. (1998). Rabies virus quasispecies: implications for pathogenesis. Proc. Natl. Acad. Sci. USA 95, 3152–3156.

Nassi, J.J., Lyon, D.C., and Callaway, E.M. (2006). The parvocellular LGN provides a robust disynaptic input to the visual motion area MT. Neuron 50, 319 –327.

Rockland, K.S. (1992). Laminar distribution of neurons projecting from area V1 to V2 in macaque and squirrel monkeys. Cereb. Cortex 2, 38–47.

Sawatari, A., and Callaway, E.M. (2000). Diversity and cell type specificity of local excitatory connections to neurons in layer 3B of monkey primary visual cortex. Neuron 25, 459–471.

Shipp, S., and Zeki, S. (1989a). The organization of connections between areas V5 and V1 in macaque monkey visual cortex. Eur. J. Neurosci. 1, 309 –332.

Shipp, S., and Zeki, S. (1989b). The organization of connections between areas V5 and V2 in macaque monkey visual cortex. Eur. J. Neurosci. 1, 333–354.

Sincich, L.C., and Horton, J.C. (2002). Divided by cytochrome oxidase: a map of the projections from V1 to V2 in macaques. Science 295, 1734 –1737.

Sincich, L.C., and Horton, J.C. (2003). Independent projection streams from macaque striate cortex to the second visual area and middle temporal area. J. Neurosci. 23, 5684 –5692.

Sincich, L.C., and Horton, J.C. (2005). The circuitry of V1 and V2: integration of color, form, and motion. Annu. Rev. Neurosci. 28, 303–326.

Sincich, L.C., Park, K.F., Wohlgemuth, M.J., and Horton, J.C. (2004). Bypassing V1: a direct geniculate input to area MT. Nat. Neurosci. 7, 1123–1128.

Sincich, L.C., Jocson, C.M., and Horton, J.C. (2006). Neurons in V1 patch columns project to V2 thin stripes. Cereb. Cortex, in press.

Tootell, R.B., Hamilton, S.L., and Silverman, M.S. (1985). Topography of cytochrome oxidase activity in owl monkey cortex. J. Neurosci. 5, 2786 –2800.

Ugolini, G. (1995). Specificity of rabies virus as a transneuronal tracer of motor networks: transfer from hypoglossal motoneurons to connected second-order and higher order central nervous system cell groups. J. Comp. Neurol. 356, 457– 480.

Van Essen, D.C., and Deyoe, E.A. (1994). Concurrent processing in the primate visual cortex. In: The Cognitive Neurosciences, M.S. Gazzuniga, ed. (Cambridge: MIT Press), pp. 383–400.

Van Essen, D.C., Maunsell, J.H., and Bixby, J.L. (1981). The middle temporal visual area in the macaque: myeloarchitecture, connections, functional properties and topographic organization. J. Comp. Neurol. 199, 293–326.

Van Essen, D.C., Newsome, W.T., Maunsell, J.H., and Bixby, J.L. (1986). The projections from striate cortex (V1) to areas V2 and V3 in the macaque monkey: asymmetries, areal boundaries, and patchy connections. J. Comp. Neurol. 244, 451– 480.

Xiao, Y., and Felleman, D.J. (2004). Projections from primary visual cortex to cytochrome oxidase thin stripes and interstripes of macaque visual area 2. Proc. Natl. Acad. Sci. USA 101, 7147–7151.

Yabuta, N.H., and Callaway, E.M. (1998). Functional streams and local connections of layer 4C neurons in primary visual cortex of the macaque monkey. J. Neurosci. 18, 9489 –9499.

Yabuta, N.H., Sawatari, A., and Callaway, E.M. (2001). Two functional channels from primary visual cortex to dorsal visual cortical areas. Science 292, 297–300.

Zeki, S., and Shipp, S. (1988). The functional logic of cortical connections. Nature 335, 311–317.

Chapter IV

Specialized Circuits from Primary Visual Cortex to V2 and Middle Temporal Area

Summary

Primary visual cortex (V1) integrates inputs from parallel magnocellular (M) and parvocellular (P) streams and recombines them to create functionally specialized outputs. Numerous studies have demonstrated the role of columnar or laminar compartments in this process. However, a clear understanding of the relationships between inputs and outputs is complicated by the fact that layer 4B, which provides outputs to dorsal visual areas, contains multiple cell types with the potential to be uniquely connected. Using a modified rabies virus that expresses green fluorescent protein, we show that layer 4B neurons projecting to MT are a majority spiny stellate, whereas those projecting to V2 are overwhelmingly pyramidal. Regardless of cell type, neurons projecting to MT have larger cell bodies, more total dendritic length, and are located deeper within layer 4B. Furthermore, pyramidal neurons projecting to MT are located preferentially underneath cytochrome oxidase blobs, where their apical dendrites extend into this M-recipient zone. We conclude that MT-projecting layer 4B cells are specialized for the fast transmission of information from the M pathway, while V2-projecting cells are likely to mediate slower computations involving mixed M and P signals.

Introduction

In the primate visual system, sensory input is parsed into magnocellular (M), parvocellular (P), and koniocellular (K) processing streams and relayed from the retina to primary visual cortex (V1) along routes which are anatomically separate and distinct (Blasdel and Lund, 1983; Dacey, 2000; Hendrickson et al., 1978; Hendry and

Reid, 2000; Hendry and Yoshioka, 1994; Michael, 1988). Within V1 the anatomical circuitry quickly becomes more complex, with substantial convergence of M, P, and K pathways (Lachica et al., 1992; Yabuta and Callaway, 1998; Yabuta et al., 2001; Yoshioka et al., 1994). The mixing of early parallel pathways within V1 and the apparent lack of compartmentalization in outputs from V1 to extrastriate cortical areas (Sincich and Horton, 2002; Xiao and Felleman, 2004), has been used as evidence for non-specificity within cortex and has led some to reject parallel processing models of the primate visual system. Nevertheless, the striking cell type specificity of local connection patterns within V1 (Callaway, 1998a) leaves open the possibility that outputs from V1 to extrastriate cortical areas relay specialized circuits with specific combinations of early parallel pathway input.

Beyond V1, visual information is processed in relatively independent dorsal and ventral streams (DeYoe and Van Essen, 1988; Livingstone and Hubel, 1988; Merigan and Maunsell, 1993; Zeki and Shipp, 1988). Dorsal stream cortical areas are specialized for analyses of object motion and spatial relationships, and ventral stream cortical areas are specialized for analyses of object attributes such as shape and color (Desimone and Ungerleider, 1989). Dorsal stream cortical areas receive their strongest input from layer 4B of V1, which connects directly with MT, V3, and the cytochrome oxidase (CO) thick stripes of V2 (Burkhalter et al., 1986; Livingstone and Hubel, 1987; Shipp and Zeki, 1989). It was long thought that layer 4B received input only from the M pathway through layer 4Cα, sending an M-dominated signal to dorsal stream cortical areas. However, in more recent years, photostimulation studies on monkey V1 slices showed that pyramidal cells in layer 4B of V1 receive functional

input from both M-dominated layer 4Cα and P-dominated layer 4Cβ (Yabuta et al., 2001). While pyramidal cells make up the majority cell type within layer 4B (Callaway and Wiser, 1996), a minority of cells have spiny stellate morphology and receive input only from M-dominated layer 4Cα, suggesting a possible means by which the dorsal stream could receive an M-dominated signal (Yabuta et al., 2001).

The projection from layer 4B of V1 to MT has been studied extensively in different primate species and using different methodological approaches (Boyd and Casagrande, 1999; Elston and Rosa, 1997; Shipp and Zeki, 1989; Tigges et al., 1981; vogt Weisenhorn et al., 1995). While available evidence suggests that MT in macaque monkey receives input from both spiny stellate and pyramidal cells in layer 4B of V1 (Shipp and Zeki, 1989; Sincich and Horton, 2003), attempts to definitively identify and quantify the proportions of each cell type have been limited due to technical considerations including partial cell fills and tangential sectioning. Although it is known that the neurons in layer 4B that project to MT are a separate population from those projecting to V2 (Sincich and Horton, 2003), it is unclear how these two populations differ morphologically. In the present study, we use a rabies virus that has been modified to serve as a powerful monosynaptic retrograde tracer by replacing the virus glycoprotein with green fluorescent protein (GFP) in its genome (Wickersham et al., 2007). By injecting this rabies virus into MT or V2 we obtained detailed dendritic morphology and were able to make quantitative comparisons between the cells projecting from layer 4B of V1 to these extrastriate cortical areas. We find that cells projecting to MT are a majority spiny stellate, whereas those projecting to V2 are overwhelmingly pyramidal. Morphological differences such as cell body size and

total dendritic length further differentiate the two cell populations regardless of cell type. Finally, differences exist in the tangential distribution of these populations relative to the overlying pattern of CO blobs and interblobs, with pyramidal cells projecting to MT biased toward blobs. These results provide evidence for specialized and distinct circuits in V1 that relay a fast M-dominated signal to MT and a mixed M and P signal to V2.

Results

We used a modified, GFP-expressing rabies virus as a monosynaptic retrograde tracer to study connections from V1 to areas MT and V2 of macaque monkey (Wickersham et al., 2007). In particular, we were interested in determining the proportion of pyramidal versus spiny stellate cells in layer 4B of V1 that project directly to MT or V2. Injections of rabies virus were targeted to cortical area MT of two macaque monkeys (three hemispheres) and V2 of two macaque monkeys (two hemispheres) (see Experimental Procedures). After a 7 day survival period (3 day survival period for JNM2) the animals were perfused, and the brains were sectioned and stained for CO and an antibody against GFP (see Experimental Procedures). The locations of the injections were confirmed histologically to be confined to either MT (Figures 4.1A-B) or V2 (Figure 4.1C) (see Experimental Procedures). The injected rabies virus infected glial cells at the injection site, allowing visualization of the needle track in sections stained for GFP. For MT cases, adjacent sections stained for myelin or Nissl were used to confirm that the needle penetration passed within the region of dense and uniform myelination along the posterior bank of the STS typical

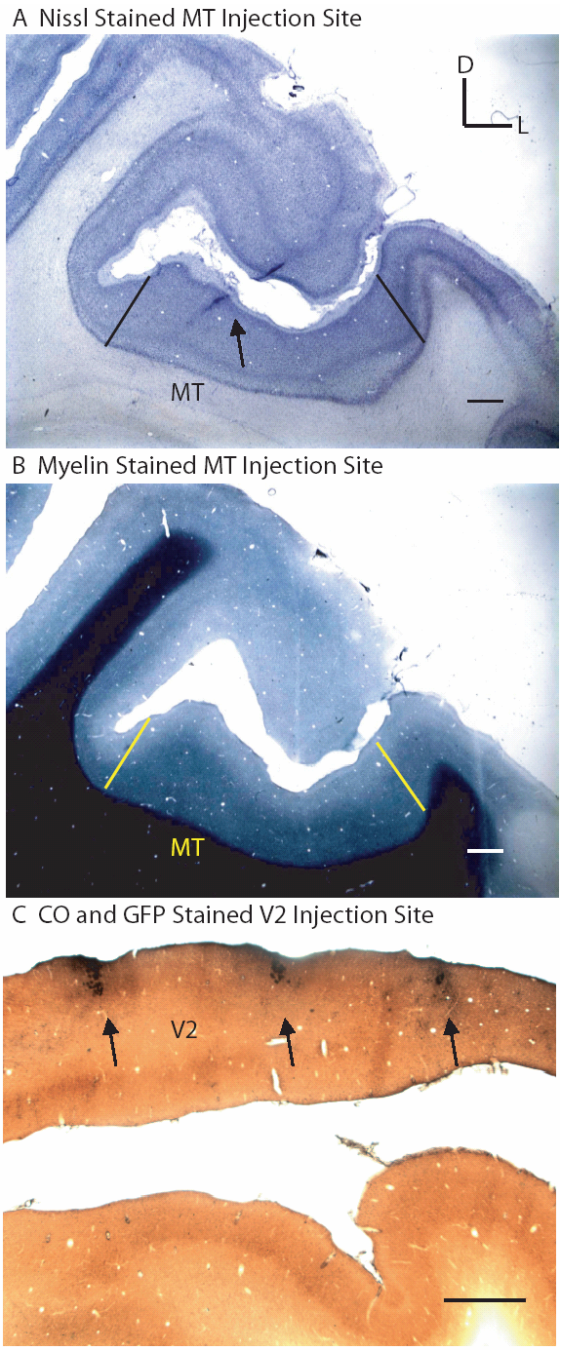

Figure 4.1: Rabies virus injections in MT or V2.
(**A**) A single coronally cut cortical section stained for Nissl showing the needle track location (black arrow) within the STS. Black lines denote the approximate lateral and medial borders of MT as determined by myelin. (**B**) A coronally cut cortical section, adjacent to that in (**A**), stained for myelin. Yellow lines denote the approximate lateral and medial borders of the uniformly dense myelination pattern typical of MT. D, dorsal; L, lateral. Scale bars in (**A**) and (**B**) equal 100 µm. (**C**) A single coronally cut cortical section stained for cytochrome oxidase (CO; brown) and GFP (black) showing the locations of rabies injected regions (black arrows) along the opercular surface in V2. Scale bar equals 1 mm.

of MT (Figures 4.1A-B). In V2 cases, the needle penetrations could be seen anterior to the distinctive CO pattern of V1 (Figure 4.1C). Upon examining histological sections, retrogradely labeled cells were found in visual areas known to have monosynaptic connections with the cortical area injected. As expected, extrastriate cortical areas that are known to provide feedforward input to MT had labeled cells confined to supragranular layers, and areas known to provide feedback input to MT or V2 had labeled cells confined to infragranular layers (Maunsell and van Essen, 1983).

Following MT injections, labeled cells within V1 were found in layers 4B and 6 as expected from previous reports (Figures 4.2A-B) (Shipp and Zeki, 1989). Labeled cells were scattered in the calcarine sulcus (JNM2, JNM14) and on the opercular surface (JNM14). The total number and density of rabies/GFP labeled cells, however, were lower than observed with standard tracers (Table 4.1), likely due to technical considerations such as rabies virus titer and efficiency of viral uptake at axons terminals. The number of layer 6 Meynert cells labeled in these cases was approximately 1 for every 10 layer 4B cells and was not numerous enough to analyze further (data not shown). The number of cells labeled in layer 4B, however, was substantial (Figures 4.2A-B). GFP was expressed throughout each cell's processes,

Table 4.1: Cell type proportions.

Injection Target	Case	Number of Stellates	Number of Pyramids	Number of Cells Total	Proportion Stellate	Average Proportion
MT	JNM2	14	1	15	0.93	0.76
	JNM14R	9	4	13	0.69	
	JNM14L	29	14	43	0.67	
	Combined	52	19	71	0.73	———
V2	JNM8	3	17	20	0.15	0.17
	JNM12	20	92	112	0.18	
	Combined	23	109	132	0.17	———

allowing for extensive morphological analysis (Figures 4.2A-B and 4.3A). In fact, classifying layer 4B cells as either pyramidal or spiny stellate was quite straightforward. Averaged across cases, 76% of layer 4B cells retrogradely labeled from MT injections were of spiny stellate morphology, with the remaining 24% pyramidal (Table 4.1; Figure 4.3C). There was some variation between cases, with as

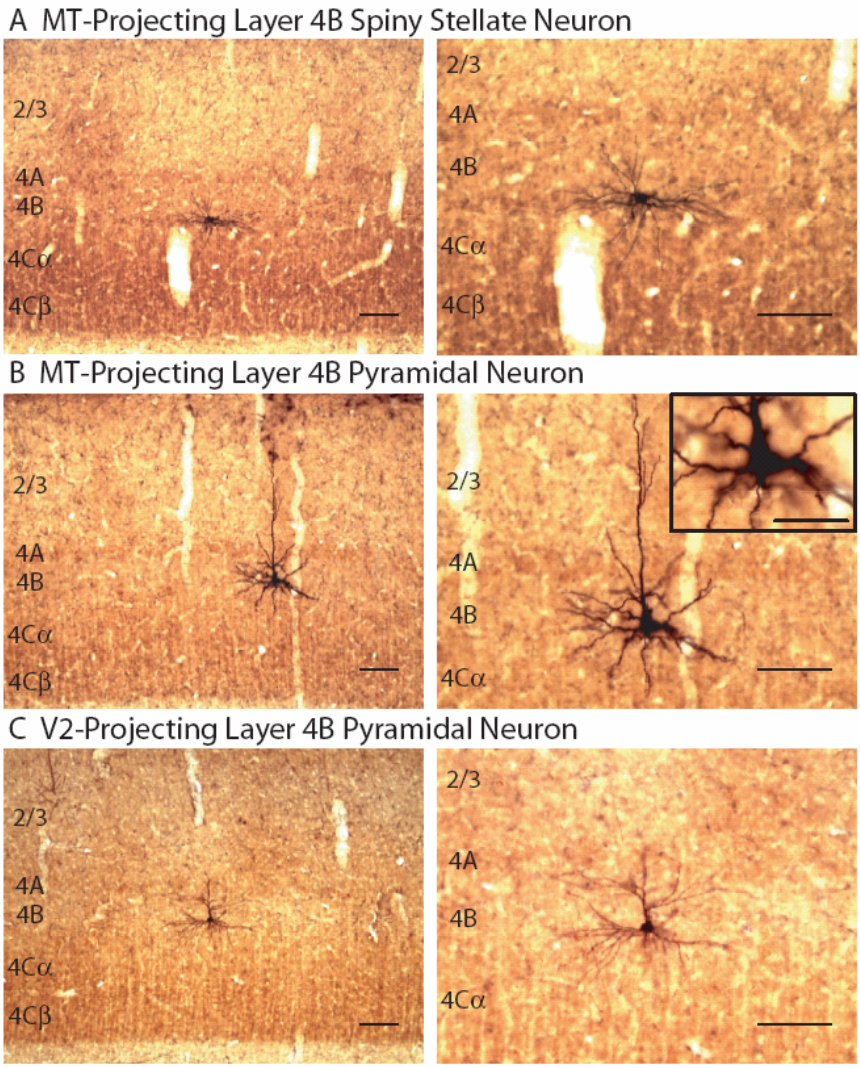

Figure 4.2: Retrogradely labeled neurons in layer 4B of V1 after injections in MT or V2. (**A** and **B**) Parasaggittal sections stained for CO and GFP showing a spiny stellate neuron (**A**) or pyramidal neuron (**B**) in layer 4B of V1 retrogradely labeled from MT. (**C**) A coronal section stained for CO and GFP showing a pyramidal neuron in layer 4B of V1 retrogradely labeled from V2. Low (left) and high (right) magnification images are shown with cortical layers indicated. A single higher magnification image is shown in the inset of (**B**). Scale bars in (**A**) and (**C**) equal 100 μm. Scale bar in inset of (**B**) equals 50 μm.

high as 93% spiny stellate cells in JNM2 and as low as 67% spiny stellate cells in JNM14L. This variation was not an obvious result of eccentricity, and may more likely be a result of variation at the MT injection site (i.e. different laminar depths). Nevertheless, in all cases the population of retrogradely labeled cells in layer 4B was at least two thirds spiny stellate (Figure 4.3C). It has been estimated previously by blind intracellular fills of layer 4B neurons in macaque V1 slice that pyramidal cells make up an approximate two thirds majority (Callaway and Wiser, 1996). The proportion of spiny stellates we observed after MT injections, therefore, was significantly higher than expected from a random sampling of layer 4B cells (Fisher's exact test, $p < 0.05$).

Following V2 injections, labeled cells within V1 were found in all layers outside of layer 4C. Particularly large numbers of labeled cells were found in layer 2/3 (data not shown), with substantial numbers of rabies/GFP labeled cells in layer 4B (Table 4.1; Figure 4.2C). We did not localize our V2 injections to particular stripe types and likely injected into multiple stripe types with each penetration. There is some indication that layer 4B projects to pale stripes in addition to thick stripes in V2

Table 4.2: Cell anatomical measurements.

Injection Target	Cell Type	Cell Body Area (µm2)	Cell Body Perimeter (µm)	Laminar Depth Index	Blob Distance Index	Apical Dendrite Thickness (µm)	Tufted Apical Dendrite Prop	Apical Dendrite Laminar Depth Index
MT	Stellate	**335.84** [46] (12.97)	**67.87** [46] (1.31)	**0.81** [36] (0.03)	**0.43** [30] (0.05)	———	———	———
	Pyramidal	**309.60** [17] (26.82)	**66.44** [17] (3.03)	**0.71** [18] (0.05)	**0.21** [16] (0.04)	**3.46** [18] (0.25)	**0.22** [18] (0.15)	**0.10** [18] (0.02)
	Combined	**328.76** [63] (11.89)	**67.49** [63] (1.25)	**0.78** [54] (0.02)	**0.35** [46] (0.04)	———	———	———
V2	Stellate	**121.23** [15] (10.03)	**41.83** [15] (2.05)	**0.90** [10] (0.03)	**0.63** [9] (0.08)	———	———	———
	Pyramidal	**153.22** [55] (6.98)	**46.80** [55] (1.09)	**0.63** [54] (0.03)	**0.60** [49] (0.05)	**3.50** [31] (0.15)	**0.22** [36] (0.12)	**0.18** [36] (0.02)
	Combined	**146.36** [70] (6.07)	**45.73** [70] (0.98)	**0.68** [64] (0.03)	**0.60** [58] (0.04)	———	———	———

Mean values are in bold. Values in square brackets to the right of the mean indicate numbers of cells. Values in parentheses below the mean indicate the standard errors.

(Sincich and Horton, 2002), however it remains likely that the majority of the layer 4B cells retrogradely labeled are the result of injections including a thick stripe in V2 (Sincich et al., 2007). Striking morphological detail was again obtained, allowing for rather straightforward classification of cells as either pyramidal or spiny stellate (Figures 4.2C and 4.3B). Averaged across cases, 83% of layer 4B cells retrogradely labeled from V2 injections were of pyramidal morphology, with the remaining 17% spiny stellate (Table 4.1; Figure 4.3C). There was little variation between the two cases, with 85% pyramidal cells in JNM8 and 82% pyramidal cells in JNM12. The proportion of pyramids we observed following V2 injections was not statistically different from that expected from a random sampling of layer 4B cells (Fisher's exact test, $p > 0.05$) (Callaway and Wiser, 1996). In striking contrast, the proportion of cell type projecting from layer 4B of V1 to MT is overwhelming spiny stellate and significantly different from the proportion of cell type projecting to V2 (Fisher's exact test, $p < 0.001$) (Figure 4.3C). These results suggest highly specialized circuits relaying different visual information to MT or V2.

While the populations of cells projecting from layer 4B of V1 to MT or V2 have very different cell type proportions, they nevertheless include both cell types in substantial number. We were, therefore, interested to investigate whether additional differences exist between the two cell populations. It has been reported previously that the two populations differ in cell body size (Sincich and Horton, 2003), and we indeed confirmed this finding (Table 4.2; Figure 4.4A). On average, cell bodies of MT-projecting cells were more than double the size of V2-projecting cells (MT: 329 μm^2, V2: 146 μm^2; t-test, $p < 0.001$). Cell body size did not depend on cell type, as

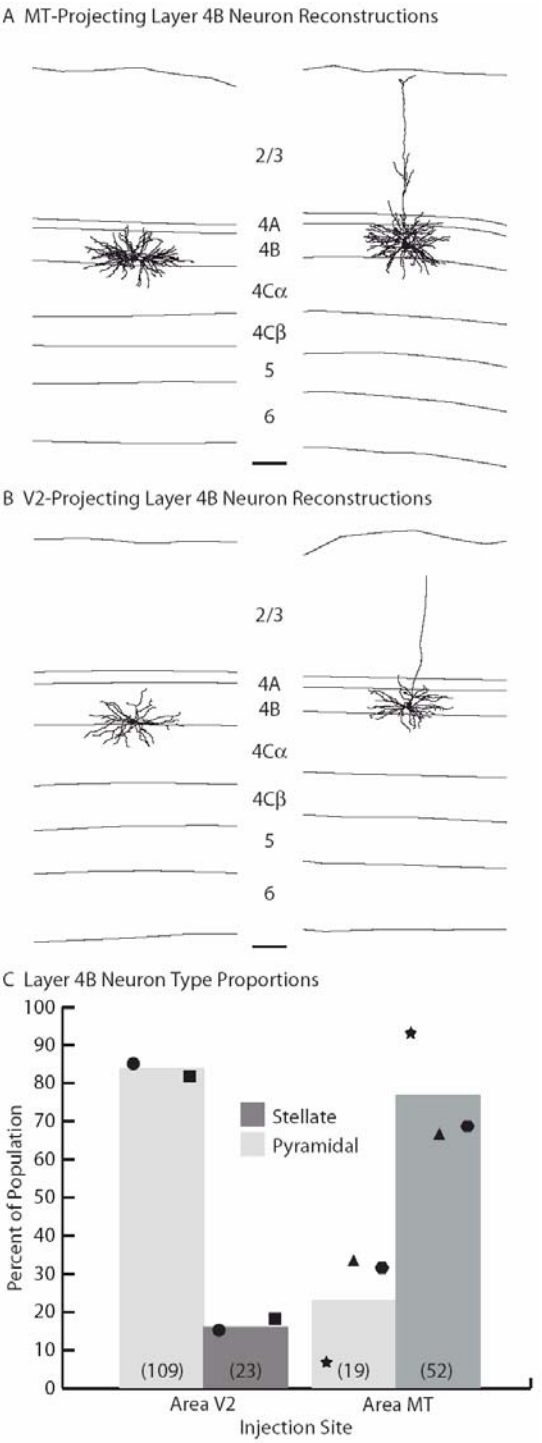

Figure 4.3: Cell types projecting from layer 4B of V1 to MT or V2.
(**A** and **B**) Computer-assisted dendritic reconstructions of spiny stellate (left) and pyramidal (right) neurons projecting to MT (**A**) or V2 (**B**). Layers are indicated. Scale bars equal 100 μm. (**C**) The average percentages of spiny stellate (dark gray) and pyramidal (light gray) neurons projecting to MT or V2. Cases JNM2 (star), JNM14L (triangle), and JNM14R (hexagon) for MT, and JNM8 (circle) and JNM12 (square) for V2 are shown. Total numbers of each cell type are indicated in parentheses.

there was no significant difference between pyramid and stellate for a given cortical injection target (Table 4.2). The distributions of cell body sizes do overlap substantially, however, with the largest V2-projecting cells having similar sizes to the smallest MT-projecting cells (Figure 4.4A). V2-projecting cells were also found to be located more superficially in layer 4B (laminar depth index = 0.68) than MT-projecting cells (laminar depth index = 0.78) (Mann-Whitney test, $p < 0.02$) (Figure 4.4B). While stellates projecting to V2 are consistently found toward the very bottom of layer 4B (laminar depth index = 0.90), pyramids projecting to V2 are found more superficially and throughout the layer (laminar depth index = 0.63) (Mann-Whitney test, $p < 0.001$). It is likely that the deeper location of the MT-projecting cells allows them to receive substantial input from within layer 4Cα.

In order to further assess more subtle differences in the two cell populations, we fully reconstructed the dendrites of a subset of cells projecting either to MT (5 stellate, 5 pyramidal) or V2 (3 stellate, 5 pyramidal) (Figures 4.3A-B). As expected, both pyramids and spiny stellates projecting to MT or V2 had the majority of their

Table 4.3: Dendritic length by layer.

Injection Target	Cell Type	Average Dendritic Lenth: Layer 2/3 µm	Layer 2/3 prop	Layer 4A µm	Layer 4A prop	Layer 4B µm	Layer 4B prop	Layer 4Cα µm	Layer 4Cα prop	Layer 4Cβ–6 µm	Layer 4Cβ–6 prop	Total µm
MT	Stellate (5)	**0** (0)	**0** (0)	**51.8** (17.8)	**0.01** (0)	**5,373.6** (677.7)	**0.79** (0.05)	**1,414.1** (173.8)	**0.21** (0.05)	**0** (0)	**0** (0)	**6,839.5** (530.7)
	Pyramidal (5)	**564.5** (95.2)	**0.08** (0.02)	**160.5** (43.5)	**0.02** (0.01)	**5,081.3** (265.1)	**0.73** (0.01)	**1,169.6** (286.3)	**0.17** (0.03)	**0** (0)	**0** (0)	**6,975.8** (430.2)
	Combined (10)	**282.2** (104.2)	**0.04** (0.02)	**106.2** (28.6)	**0.02** (0)	**5,227.5** (346.5)	**0.75** (0.03)	**1,291.8** (163.1)	**0.19** (0.03)	**0** (0)	**0** (0)	**6,907.7** (322.9)
V2	Stellate (3)	**0** (0)	**0** (0)	**4.1** (4.1)	**0.01** (0)	**1,997.7** (194.7)	**0.68** (0.01)	**867.6** (382.2)	**0.29** (0.02)	**0** (0)	**0** (0)	**2,869.3** (191.7)
	Pyramidal (5)	**384.6** (57.0)	**0.08** (0.01)	**182.7** (91.3)	**0.04** (0.01)	**3,248.9** (439.6)	**0.66** (0.05)	**1,122.5** (274.9)	**0.23** (0.07)	**0** (0)	**0** (0)	**4,938.7** (474.2)
	Combined (8)	**240.4** (78.2)	**0.05** (0.01)	**115.7** (63.6)	**0.02** (0.01)	**2,779.7** (354.2)	**0.66** (0.03)	**1,026.9** (211.7)	**0.26** (0.04)	**0** (0)	**0** (0)	**4,162.7** (477.1)

Mean values are in bold and indicate either the length of dendrites found in a layer (µm) or the proportion of total dendritic length found in a layer (prop). Values in parentheses below the means indicate the standard errors. Values in parentheses to the right of the cell type names indicate the numbers of cells reconstructed.

dendritic length in layer 4B (approximately 70%) (Table 4.3). Somewhat surprising, however, was the high percentage of dendritic length (approximately 20%) in layer 4Cα and the small percentage of dendritic length consistently present in layer 4A (approximately 2%). Dendrites were never found to extend below layer 4Cα and only the apical dendrites of pyramidal cells extended above layer 4A (Table 4.3). These apical dendrites were typically non-tufted (approximately 75%) and of similar thickness (approximately 3.5 μm) whether the cell projected to V2 or MT (Table 4.2). The only clear difference between the two populations was a higher total dendritic length among MT-projecting cells (MT: 6,908 μm, V2: 4,163 μm; t-test, $p < 0.01$) (Table 4.3). This was particularly the case in layer 4B, where both cell types projecting to MT had significantly more dendritic length than those projecting to V2 (t-test, $p < 0.01$). It was clear simply by eye that V2-projecting cells had much sparser dendritic fields (Figures 4.2 and 4.3). Additionally, pyramidal neurons projecting to MT had apical dendrites that terminated significantly closer to the top of layer 1 than the apical dendrites of pyramids projecting to V2 (t-test, $p < 0.01$) (Table 4.2).

The position of cells in layer 4B relative to the pattern of CO blobs in layer 2/3 was assessed for both pyramids and spiny stellates projecting to MT or V2. Since our sections were cut perpendicular to the cortical surface, we could not plot the locations of our cells relative to a full two dimensional map of CO blobs. Instead, we measured the distance of each cell body to the closest two CO blobs on either side and computed a blob distance index (Table 4.2; Figure 4.4C) (see Experimental Procedures). A blob distance index of zero indicates a cell body directly underneath a blob center, whereas a blob distance index of one indicates a cell body within an interblob, equidistant from

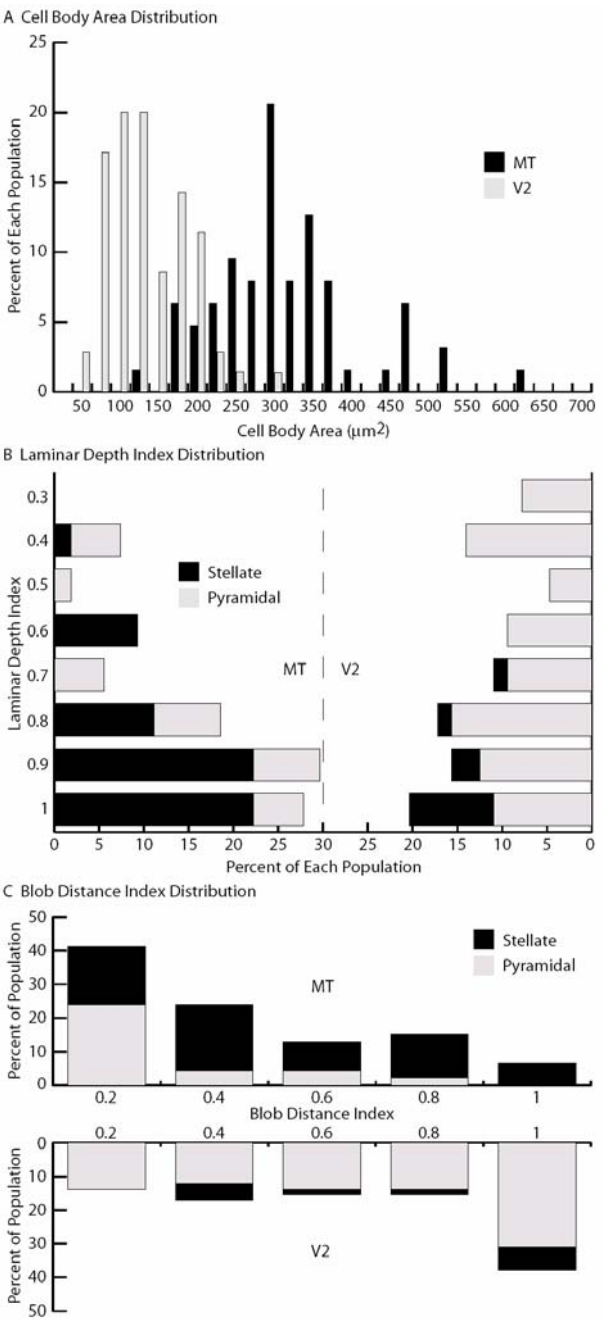

Figure 4.4: Anatomical differences between neurons projecting to MT or V2.
(**A**) Percentages of layer 4B neurons projecting to MT (black) or V2 (gray) according to their cell body area. (**B**) Percentages of layer 4B spiny stellate (black) and pyramidal (gray) neurons projecting to MT (left) or V2 (right) according to their laminar depth index. An index value of 1 indicates a neuron at the bottom of layer 4B and an index value of 0 indicates a neuron at the top of layer 4B. (**C**) Percentages of layer 4B spiny stellate (black) and pyramidal (gray) neurons projecting to MT (top) or V2 (bottom) according to their blob distance index. An index value of 1 indicates a neuron centered in an interblob equidistant from the two closest blobs and an index value of 0 indicates a neuron centered directly underneath a blob.

the blobs on either side. Given that our injections into V2 likely included all three CO stripe types, we expected our V2-projecting layer 4B cells to be located indiscriminately underneath both blobs and interblobs and this was indeed the case (blob distance index = 0.60) (Table 4.2; Figure 4.4C) (Sincich and Horton, 2002, 2003). Previous studies regarding the MT-projecting population are much less clear, with some evidence for no bias and other evidence for patchiness biased to the blobs (Boyd and Casagrande, 1999; Shipp and Zeki, 1989; Sincich and Horton, 2003). The overall population of MT-projecting cells which we labeled did not show a clear bias toward blobs or interblobs (blob distance index = 0.35). It is important to note that our total number of labeled cells is rather low and may have precluded us from observing a bias present in the population. However, when we analyzed the relationship of the individual cell types to the blob pattern, we were surprised to find that pyramidal cells were consistently located underneath blobs (Figures 4.2B and 4.4C). While spiny stellates showed no apparent bias for blobs or interblobs (blob distance index = 0.43), pyramidal cells showed a strong bias to the blobs (blob distance index = 0.21) (Table 4.2). Among MT-projecting cells, pyramids were found significantly closer to blob centers than stellates (Mann-Whitney test, $p < 0.01$). Furthermore, MT-projecting pyramids were found significantly closer to blob centers than V2-projecting pyramids (Mann-Whitney test, $p < 0.001$). This result might explain much of the previous discrepancy in the literature and has interesting circuit implications for connectivity with M versus P pathways (see Discussion).

Discussion

Our observations provide evidence for a highly specialized population of neurons projecting directly from V1 to MT which are distinct from neurons projecting to V2 along several anatomical dimensions. Neurons projecting from V1 to MT are mostly spiny stellate cells, whereas those projecting to V2 are mainly pyramidal. Regardless of cell type, neurons projecting to MT are much larger than those projecting to V2 and have more total dendritic length, particularly within layer 4B. Finally, pyramidal cells projecting to MT are located primarily underneath CO blobs, whereas stellates projecting to MT and neurons of both cell types projecting to V2 do not show any apparent bias toward blobs or interblobs.

We found that neurons projecting from layer 4B of V1 to MT are a majority spiny stellate. These neurons likely convey M-dominated input to MT as stellates have been shown to receive input only from M-dominated layer 4Cα (Yabuta et al., 2001). It is particularly striking that stellates make up the majority cell type that projects to MT, since they are only a small minority of the neurons within layer 4B (Callaway and Wiser, 1996). It is important to note, however, that small numbers of pyramids project to MT as well. Since disynaptic input to MT has previously been shown to originate almost exclusively from M-dominated layer 4Cα (Nassi and Callaway, 2006), it is possible that the small numbers of pyramidal cells that project to MT receive input only from M-dominated layer 4Cα and are, therefore, distinct from the majority of pyramids in layer 4B that receive mixed M and P input. This suggestion is further supported by the preferential location of MT-projecting pyramids under blobs (see further below). In contrast to the population projecting to MT, we

found pyramidal cells to be the majority cell type projecting to V2. These neurons likely convey mixed M and P input to V2 and possibly indirectly to MT (Yabuta et al., 2001; Nassi and Callaway, 2006). Taken together, these results suggest that the projection from V1 to MT is highly specialized and distinct from other V1 outputs.

Neurons projecting to MT could be distinguished from those projecting to V2 based on numerous parameters beyond cell type. Previous studies have reported that MT-projecting neurons are considerably larger than those projecting to V2 (Sincich and Horton, 2003). This was indeed the case, with the average neuron projecting to MT more than double the size of the average neuron projecting to V2. Importantly, this difference in cell body size could not be explained simply by stellates being larger than pyramids (Table 4.2), suggesting that even the pyramids projecting to MT are distinct from those projecting to V2. The larger cell body size of the MT-projecting cells is likely to correspond to a greater axon diameter, which would mediate relatively fast action potential conduction (Rockland, 1995).

Neurons projecting to MT were also located deeper within layer 4B, closer to the layer 4Cα border, than neurons projecting to V2. We believe that a more heterogeneous population of V2-projecting pyramidal cells scattered throughout the depth of layer 4B largely accounts for this difference; again, suggesting that the pyramids projecting to MT may be part of a specialized population distinct from pyramids projecting to V2 and other areas. Being located closer to layer 4Cα may allow MT-projecting neurons to receive more extensive input from M layers of the LGN or neurons in M-dominated layer 4Cα. Indeed, layer 4B neurons located more

superficially within layer 4B consistently had less dendritic length extending into layer 4Cα (data not shown).

In analyzing the laminar distribution of dendrites for neurons of each type projecting to MT or V2, it was apparent that there existed considerable similarities. Regardless of cell type or projection target, all layer 4B neurons had the vast majority of their dendrites in layers 4B and 4Cα, with small amounts of dendrite consistently present in layer 4A as well. None of the neurons ever had dendrites extending below layer 4Cα and only pyramidal neurons had dendrites extending above layer 4A. There were, however, a few important differences between the populations projecting to MT or V2. The most striking difference was that MT-projecting neurons had much more total dendritic length than V2-projecting neurons, particularly in layer 4B. This may be an indication that neurons projecting to MT receive more extensive input from other neurons in layer 4B or layer 4Cα. It was also the case that pyramids projecting to MT had more dendritic length in layer 2/3 than pyramids projecting to V2, with the apical dendrites of the former terminating significantly closer to the top of layer 1. Pyramids projecting to V2 often had apical dendrites that terminated well below layer 1, whereas those projecting to MT typically had apical dendrites that extended to the pia. Direct thalamic input from K layers in the LGN as well as feedback connections from MT and other areas may be received via the apical dendrite of MT-projecting pyramids within layer 1 (Blasdel and Lund, 1983; Ding and Casagrande, 1997; Shipp and Zeki, 1989).

Interestingly, pyramids projecting to MT were found consistently underneath CO blobs. Previous studies in macaque monkey have not observed a blob bias among

MT-projecting neurons (Shipp and Zeki, 1989; Sincich and Horton, 2003), likely due to the fact that the majority of these neurons are spiny stellates which were found indiscriminately underneath both blobs and interblobs in the present study. Only when analyzing MT-projecting pyramids separately from the total population of neurons did a blob bias become apparent among this cell type. Boyd and Casagrande (1999) reported a blob bias in bush baby and owl monkey which may be partly explained by the fact that pyramids constitute the majority of MT-projecting cells in these new world monkey species (Diamond et al., 1985; Shipp and Zeki, 1989). It may be that pyramids projecting to MT are preferentially located underneath CO blobs because, unlike interblobs, this is a location where apical dendrites are able to sample M input from layer 4Cα (Lachica et al., 1992; Yabuta and Callaway, 1998). This would be consistent with the fact that neurons projecting directly from V1 to MT have been shown previously to receive input almost exclusively from the M pathway (Nassi and Callaway, 2006). In contrast, pyramids projecting to the CO thick stripes in V2, which in turn project to MT, are preferentially located underneath CO interblobs (Sincich and Horton, 2002) where apical dendrites only have access to P input from layer 4Cβ (Lachica et al., 1992). This is consistent with the fact that neurons projecting from V1 to V2 have been shown previously to receive mixed input from both M and P pathways (Nassi and Callaway, 2006). We suggest that activity dependent developmental processes may underlie the selection of MT-projecting pyramids underneath the CO blobs due to the matching input pattern from the M pathway. MT-projecting pyramids underneath interblobs could receive P input, resulting in a mismatch between input and output. This mismatch could lead to the

retraction of the apical dendrite (Koester and O'Leary, 1992; Callaway, 1998b). Alternatively, pyramids under interblobs might initially project to multiple cortical areas and then retract projections to MT (Barone et al., 1995). These results serve as yet another indication that even the small numbers of pyramids that project to MT are specialized and distinct from those projecting to V2 and other areas.

Area MT receives its main ascending input from a highly specialized and distinct population of neurons in layer 4B of V1. This population of neurons allows M-dominated signals to be conducted quickly to MT despite the convergence of M and P pathways onto the majority of neurons within layer 4B. It is known that MT-projecting V1 neurons are highly direction selective (Movshon and Newsome, 1996), but more studies are necessary to fully characterize their response profiles. Neurons projecting from layer 4B of V1 to V2 receive convergent M and P inputs and likely relay different visual computations indirectly to MT. Future studies that can identify and record from each of the many input pathways to MT will be necessary to elucidate the functional contributions of each pathway to visual responses in MT and to the perception of motion and depth.

Experimental Procedures

Surgical procedures

Four adult macaque monkeys were used, following procedures approved by the Salk Institute Animal Care and Use Committee. In addition, all procedures using rabies virus were conducted using biosafety level 2 precautions as described previously (Kelly and Strick, 2000).

A 1.5 tesla Siemens (Erlangen, Germany) Symphony magnetic resonance scanner (University of California, San Diego Hillcrest Medical Center/Tenet Magnetic Resonance Institute, San Diego, CA) was used to obtain a full coronal series of 1-mm-thick images for each monkey used for injections into MT (JNM2, JNM14). Resulting structural images were used to calculate stereotaxic coordinates for our injections along the posterior bank of the superior temporal sulcus (STS). For V2 injections, we simply targeted the opercular surface just posterior to the lip of the lunate sulcus.

MT was targeted in two monkeys, JNM2 (right hemisphere) and JNM14 (both hemispheres). MT injections were made using Hamilton syringes with a 30 gauge needle. In monkey JNM2 two penetrations spaced 1 mm apart in the anterior-posterior plane were aimed at the posterior bank of the STS. Approximately 0.3 μl of the SAD ΔG-EGFP rabies virus (see below, Rabies virus strain) was injected at each of four depths spaced 1 mm apart. In monkey JNM14, two penetrations were made into the posterior STS of each hemisphere, and 0.3 μl of virus was injected at five different depths similarly as in JNM2.

V2 was targeted in two monkeys, JNM8 (right hemisphere) and JNM12 (right hemisphere). V2 injections were made by using glass micropipettes (tip diameter, ~30 μm), and pressure was applied by a Picospritzer. In monkey JNM8, four penetrations were made along the opercular surface, perpendicular to the cortical surface, just posterior to the lip of the lunate sulcus. Penetrations were each separated by 10 mm mediolaterally. Approximately 0.3 μl of virus with 10% rhodamine dextran (10,000 MW; Molecular Probes, Carlsbad, CA) was injected at each of three depths spaced 0.5 mm apart. In monkey JNM12 ten penetrations were made, each separated by 2 mm

mediolaterally. Approximately 0.3 μl of virus (without rhodamine) was injected similarly as in JNM8.

Rabies virus strain

To retrogradely label neurons that project directly from V1 to MT or V2, we injected the SAD ΔG-EGFP rabies virus and allowed a survival time of 7 days (except for a 3 day survival time for JNM2). This strain of rabies virus was obtained from Dr. Karl-Klaus Conzelmann, Max Von Pettenkofer Institute (Munich, GR). Studies have shown that rabies virus infects at axon terminals and travels only in the retrograde direction (Kelly and Strick, 2000; Ugolini, 1995). The rabies virus used in our study is derived from the SAD B19 vaccine strain of the rabies virus and has had its envelope glycoprotein gene replaced with the gene for GFP (Etessami et al., 2000). The glycoprotein of the rabies virus is essential for viral infection at axon terminals, so viral particles injected into the brain have glycoprotein on their membrane, infect cells at axon terminals, travel retrogradely within the cell, and express GFP. Importantly, though, new viral particles produced within the cell do not have glycoprotein on their membrane and are unable to infect further cells across synapses. The SAD ΔG-EGFP rabies virus has been shown to be a powerful monosynaptic retrograde tracer, expressing GFP at high levels up to 16 days post injection, with no evidence of cell lysis or virus spillage into the surrounding neuropil (Wickersham et al., 2007).

Histology

After 7 days survival time (except for a 3 day survival time for JNM2) the animals were killed by overdose with sodium pentobarbital and perfused with 4% paraformaldehyde (2% for JNM8), and their brains were removed. Sections were cut using a freezing microtome. In cases JNM2 and JNM14 sections were cut in two separate blocks. One block contained cortex including and posterior to the lunate sulcus (V1) and was cut parasagitally at 40 μm (JNM2) or 60 μm (JNM14). The other block contained cortex anterior to the lunate sulcus and was cut coronally at 40 μm. In case JNM8 sections were also cut in two separate blocks. V2 cortex was dissected away from V1, flattened, and cut tangentially at 50 μm. Remaining cortex was cut coronally at 60 μm. In case JNM12 a single block was cut coronally at 60 μm through V1 and V2.

First a series of every 12^{th} section was processed for both CO and GFP. We used this initially processed series to determine the extent of label in V1. Regions containing retrogradely labeled cells were processed in entirety. Each section was stained first for CO, followed by GFP immunostaining. Immunohistochemistry for GFP was performed by using the anti-GFP rabbit polyclonal antibody (Molecular Probes, Carlsbad, CA), the biotinylated goat anti-rabbit secondary antibody (Vector Laboratories, Burlingame, CA), and an ABC avidin-peroxidase kit (Vector Laboratories) and was revealed via a diaminobenzidine (DAB) reaction enhanced with nickel and cobalt (black reaction product).

For cases JNM2 and JNM14 a series of cortical sections that included the STS was processed for myelin, CO and GFP, or Nissl substance. Anatomical features of

MT (Tootell et al., 1985; Van Essen et al., 1981), such as heavy and uniform myelination (particularly in deep layers), dark and patchy CO staining, greater cortical thickness, and relative position on the posterior bank of the STS, were used to verify that injections were confined to area MT (see Figures 4.1A-B). Tangential (JNM8) and coronal (JNM12) sections through V2 were processed for CO and GFP to visualize the V1/V2 border and to verify that injections were confined to V2.

In the MT injections our needle penetrations likely involved some white matter directly underneath cortex. Previous studies have shown that rabies virus uptake along cut peripheral axons is inefficient compared with uptake at axon terminals, and rabies uptake along cut central axons has not been demonstrated (Kelly and Strick, 2000; Ugolini, 1995). In addition, in two other monkeys we injected directly into the white matter, missing cortex altogether. These cases resulted in a complete absence of labeled cells anywhere in the surrounding cortex (data not shown), suggesting that uptake and retrograde GFP labeling with the SAD ΔG-EGFP rabies virus and a 7 day survival time can only occur via axon terminals in cortex. We found no evidence of white matter uptake in JNM2 or JNM14, with retrogradely labeled cells localized to layers 4B and 6 in V1, exactly what we would expect from an injection in cortical MT (Shipp and Zeki, 1989).

Data analysis

Retrogradely labeled cells within V1 were classified as pyramidal or spiny stellate only when a sufficient number of adjacent sections were available to determine the presence or absence of an apical dendrite extending above layer 3. Those cells that

had an apical dendrite extending above layer 3 were classified as pyramidal, and those without such an apical dendrite were classified as spiny stellate. Labeled cells for which we could not conclusively determine the presence or absence of an apical dendrite were not included in the analysis. Dendritic reconstructions of labeled cells were carried out at 40x with Neurolucida software (MicroBrightField, Williston, VT). Reconstructions were subsequently analyzed using Matlab algorithms to calculate parameters such as dendritic length per cortical layer. Importantly, because cells extended through multiple adjacent sections, laminar borders were redrawn for each section and dendritic processes were assigned to a layer based on the laminar borders drawn for that same section.

Cell body sizes (area and perimeter) were determined by outlining the cell body at 20x. Cell bodies that were partially cut-off were not included in this analysis. Apical dendrite thickness was measured with 40x magnification at the first clear inflection points along the dendrite as it extended away from the cell body. Laminar depth was calculated by plotting the point where the main descending axon leaves the cell body. The distance between this point and the layer 4B/4A border was divided by the total thickness of layer 4B, resulting in a laminar depth index. An index of one indicates a cell body at the bottom of layer 4B and an index of zero indicates a cell body at the top of layer 4B. The apical dendritic laminar depth index was calculated by plotting the point at which the apical dendrite terminates. The distance between this point and the top of layer 1 was divided by the total thickness of layers 1-3. An index of zero indicates an apical dendrite that terminates at the top of layer 1.

The point where the main descending axon leaves the cell body was also plotted to calculate a CO blob distance index. Locations of CO blob centers were plotted for the two blobs to the immediate left and right of the cell body. The lateral distance (parallel to cortical layers) of the CO blob closest to the cell body was divided by the distance to the other blob, resulting in a blob distance index ranging from zero to one. An index of one indicates a cell body in an interblob and equidistant between two adjacent blob centers, while an index of zero indicates a cell body directly underneath a blob center. The angle of the plane of section relative to vertical was calculated by taking the sine of radial blood vessel length divided by the tissue thickness. When this angle was greater than 25°, CO blob centers were plotted in an adjacent section (aligned with the blood vessel pattern from original section) in which layer 3 was estimated to be directly vertical from the cell body.

Acknowledgements

We are grateful for support from the National Institutes of Health. We thank Dr. Karl-Klaus Conzelmann for providing the SAD ΔG-EGFP rabies virus, Cecelia Kemper for technical assistance with structural MRIs, and Mauricio De La Parra for assistance with animal care and surgical procedures.

This chapter, in full, has been submitted for publication; Nassi, JJ, and Callaway, EM. The dissertation author was primary author on this paper. Secondary author was the thesis advisor.

References

Barone, P., Dehay, C., Berland, M., Bullier, J., and Kennedy, H. (1995). Developmental remodeling of primate visual cortical pathways. Cereb. Cortex 5, 22-38.

Blasdel, G.G., and Lund, J.S. (1983). Termination of afferent axons in macaque striate cortex. J. Neurosci. 3, 1389-1413.

Boyd, J. D., and Casagrande, V. A. (1999). Relationships between cytochrome oxidase (CO) blobs in primate primary visual cortex (V1) and the distribution of neurons projecting to the middle temporal area (MT). J. Comp. Neurol. 409, 573-591.

Burkhalter, A., Felleman, D. J., Newsome, W. T., and Van Essen, D. C. (1986). Anatomical and physiological asymmetries related to visual areas V3 and VP in macaque extrastriate cortex. Vision Res. 26, 63-80.

Callaway, E. M. (1998a). Local circuits in primary visual cortex of the macaque monkey. Annu. Rev. Neurosci. 21, 47-74.

Callaway, E. M. (1998b). Prenatal development of layer-specific local circuits in primary visual cortex of the macaque monkey. J. Neurosci. 18, 1505-1527.

Callaway, E. M., and Wiser, A. K. (1996). Contributions of individual layer 2-5 spiny neurons to local circuits in macaque primary visual cortex. Vis. Neurosci. 13, 907-922.

Dacey, D. M. (2000). Parallel pathways for spectral coding in primate retina. Annu. Rev. Neurosci. 23, 743-775.

Desimone, R., and Ungerleider, L. G. (1989). Neural mechanisms of visual processing in monkeys. In: Handbook of Neuropsychology, F. Boller, and J. Grafman, eds. (Amsterdam: Elsevier), pp. 267-299.

DeYoe, E. A., and Van Essen, D. C. (1988). Concurrent processing streams in monkey visual cortex. Trends Neurosci. 11, 219-226.

Diamond, I. T., Conley, M., Itoh, K., and Fitzpatrick, D. (1985). Laminar organization of geniculocortical projections in Galago senegalensis and Aotus trivirgatus. J. Comp. Neurol. 242, 584-610.

Ding, Y., and Casagrande, V. A. (1997). The distribution and morphology of LGN K pathway axons within the layers and CO blobs of owl monkey V1. Vis. Neurosci. 14, 691-704.

Elston, G. N., and Rosa, M. G. (1997). The occipitoparietal pathway of the macaque monkey: comparison of pyramidal cell morphology in layer III of functionally related cortical visual areas. Cereb. Cortex 7, 432-452.

Etessami, R., Conzelmann, K. K., Fadai-Ghotbi, B., Natelson, B., Tsiang, H., and Ceccaldi, P. E. (2000). Spread and pathogenic characteristics of a G-deficient rabies virus recombinant: an in vitro and in vivo study. J. Gen. Virol. 81, 2147-2153.

Hendrickson, A. E., Wilson, J. R., and Ogren, M. P. (1978). The neuroanatomical organization of pathways between the dorsal lateral geniculate nucleus and visual cortex in Old World and New World primates. J. Comp. Neurol. 182, 123-136.

Hendry, S. H., and Reid, R. C. (2000). The koniocellular pathway in primate vision. Annu. Rev. Neurosci. 23, 127-153.

Hendry, S. H., and Yoshioka, T. (1994). A neurochemically distinct third channel in the macaque dorsal lateral geniculate nucleus. Science 264, 575-577.

Kelly, R. M., and Strick, P. L. (2000). Rabies as a transneuronal tracer of circuits in the central nervous system. J. Neurosci. Methods 103, 63-71.

Koester, S. E., and O'Leary, D. D. (1992). Functional classes of cortical projection neurons develop dendritic distinctions by class-specific sculpting of an early common pattern. J. Neurosci. 12, 1382-1393.

Lachica, E. A., Beck, P. D., and Casagrande, V. A. (1992). Parallel pathways in macaque monkey striate cortex: anatomically defined columns in layer III. Proc. Natl. Acad. Sci. U.S.A. 89, 3566-3570.

Livingstone, M., and Hubel, D. (1988). Segregation of form, color, movement, and depth: anatomy, physiology, and perception. Science 240, 740-749.

Livingstone, M. S., and Hubel, D. H. (1987). Connections between layer 4B of area 17 and the thick cytochrome oxidase stripes of area 18 in the squirrel monkey. J. Neurosci. 7, 3371-3377.

Maunsell, J. H., and van Essen, D. C. (1983). The connections of the middle temporal visual area (MT) and their relationship to a cortical hierarchy in the macaque monkey. J. Neurosci. 3, 2563-2586.

Merigan, W. H., and Maunsell, J. H. (1993). How parallel are the primate visual pathways? Annu. Rev. Neurosci. 16, 369-402.

Michael, C. R. (1988). Retinal afferent arborization patterns, dendritic field orientations, and the segregation of function in the lateral geniculate nucleus of the monkey. Proc. Natl. Acad. Sci. U.S.A. 85, 4914-4918.

Movshon, J. A., and Newsome, W. T. (1996). Visual response properties of striate cortical neurons projecting to area MT in macaque monkeys. J. Neurosci. 16, 7733-7741.

Nassi, J. J., and Callaway, E. M. (2006). Multiple circuits relaying primate parallel visual pathways to the middle temporal area. J. Neurosci. 26, 12789-12798.

Rockland, K. S. (1995). Morphology of individual axons projecting from area V2 to MT in the macaque. J. Comp. Neurol. 355, 15-26.

Shipp, S., and Zeki, S. (1989). The Organization of Connections between Areas V5 and V1 in Macaque Monkey Visual Cortex. Eur. J. Neurosci. 1, 309-332.

Sincich, L. C., and Horton, J. C. (2002). Divided by cytochrome oxidase: a map of the projections from V1 to V2 in macaques. Science 295, 1734-1737.

Sincich, L. C., and Horton, J. C. (2003). Independent projection streams from macaque striate cortex to the second visual area and middle temporal area. J. Neurosci. 23, 5684-5692.

Sincich, L. C., Jocson, C. M., and Horton, J. C. (2007). Neurons in v1 patch columns project to v2 thin stripes. Cereb. Cortex 17, 935-941.

Tigges, J., Tigges, M., Anschel, S., Cross, N. A., Letbetter, W. D., and McBride, R. L. (1981). Areal and laminar distribution of neurons interconnecting the central visual cortical areas 17, 18, 19, and MT in squirrel monkey (Saimiri). J. Comp. Neurol. 202, 539-560.

Tootell, R. B., Hamilton, S. L., and Silverman, M. S. (1985). Topography of cytochrome oxidase activity in owl monkey cortex. J. Neurosci. 5, 2786-2800.

Ugolini, G. (1995). Specificity of rabies virus as a transneuronal tracer of motor networks: transfer from hypoglossal motoneurons to connected second-order and higher order central nervous system cell groups. J. Comp. Neurol. 356, 457-480.

Van Essen, D. C., Maunsell, J. H., and Bixby, J. L. (1981). The middle temporal visual area in the macaque: myeloarchitecture, connections, functional properties and topographic organization. J. Comp. Neurol. 199, 293-326.

vogt Weisenhorn, D. M., Illing, R. B., and Spatz, W. B. (1995). Morphology and

connections of neurons in area 17 projecting to the extrastriate areas MT and 19DM and to the superior colliculus in the monkey Callithrix jacchus. J. Comp. Neurol. 362, 233-255.

Wickersham, I. R., Finke, S., Conzelmann, K. K., and Callaway, E. M. (2007). Retrograde neuronal tracing with a deletion-mutant rabies virus. Nat. Methods 4, 47-49.

Xiao, Y., and Felleman, D. J. (2004). Projections from primary visual cortex to cytochrome oxidase thin stripes and interstripes of macaque visual area 2. Proc. Natl. Acad. Sci. U.S.A. 101, 7147-7151.

Yabuta, N. H., and Callaway, E. M. (1998). Functional streams and local connections of layer 4C neurons in primary visual cortex of the macaque monkey. J. Neurosci. 18, 9489-9499.

Yabuta, N. H., Sawatari, A., and Callaway, E. M. (2001). Two functional channels from primary visual cortex to dorsal visual cortical areas. Science 292, 297-300.

Yoshioka, T., Levitt, J. B., and Lund, J. S. (1994). Independence and merger of thalamocortical channels within macaque monkey primary visual cortex: anatomy of interlaminar projections. Vis. Neurosci. 11, 467-489.

Zeki, S., and Shipp, S. (1988). The functional logic of cortical connections. Nature 335, 311-317.

Chapter V

Conclusions

Summary

The studies described in this dissertation were aimed at elucidating the contributions of early parallel pathways to processing streams in extrastriate visual cortex of macaque monkey. The magnocellular (M), parvocellular (P), and koniocellular (K) pathways originate in the retina and remain anatomically separate and distinct as they terminate within primary visual cortex (V1) (Blasdel and Lund, 1983; Dacey, 2000). Earlier studies relied on maintained segregation of early parallel pathways within V1 and compartmentalization of V1 outputs to infer the contributions of M, P, and K pathways to extrastriate cortex. However, once outside of the lateral geniculate nucleus (LGN)-recipient layers of V1, these pathways intermix significantly and converge to varying degrees onto the layers and compartments of V1 that feed dorsal and ventral stream cortical areas (Lachica et al., 1992; Yoshioka et al., 1994; Callaway and Wiser, 1996; Yabuta et al., 2001). Furthermore, the compartmentalization of these V1 outputs has recently been called into question (Sincich and Horton, 2002; Xiao and Felleman, 2004). This has made it difficult to assess the contributions of early parallel pathways to extrastriate visual cortex using standard anatomical and physiological techniques. We overcame many of these difficulties by using rabies virus as both a mono- and trans-synaptic retrograde tracer of neural circuits in the visual system of macaque monkey.

The transsynaptic form of the rabies virus allowed us to trace connections from identified extrastriate visual areas, through the output layers and compartments of V1, and back to either the LGN or the input layers of V1 where M and P pathways are well segregated. We first injected rabies virus into MT with a 3 day survival, allowing

virus to cross one synapse and infect cells disynaptic to the injection site. Surprisingly, we found large numbers of rabies-labeled cells in the M and P layers of the LGN. This was not expected because monosynaptic projections from the LGN to MT are sparse and dominated by K cells (Sincich et al., 2004) and a disynaptic route from LGN to MT was previously not known to exist. Our results, however, provide direct anatomical evidence that such a disynaptic pathway indeed exists and is most likely relayed via layer 6 Meynert cells in V1. The functional role of this pathway remains unclear as it bypasses the main ascending input to MT through layer 4C of V1. Nevertheless, a surprisingly direct P input to MT challenges previously held notions that MT and dorsal stream cortical areas receive M only inputs.

We next turned our attention to the main ascending input to MT through layer 4C of V1. After the very same injections into MT that resulted in labeled M and P cells in the LGN, disynaptic label in layer 4C of V1 was found almost exclusively in M-dominated layer 4Cα and rarely in P-dominated layer 4Cβ. Our 6 day survival injection into MT, however, showed that P-dominated layer 4Cβ eventually reaches MT and that it simply takes an additional few synapses. Only after certain injections into V2, but not V3, did we find more balanced disynaptic label in layers 4Cα and 4Cβ of V1, suggesting that the cytochrome oxidase (CO) thick stripes of V2 may be a relay of indirect P input to MT. These results provide evidence for yet another route by which the P pathway reaches MT. Despite this indirect P input, the most direct input through layer 4C of V1 to MT is dominated by the M pathway. Numerous pathways, therefore, exist between the LGN and MT with varying degrees of M and P convergence.

In a final set of experiments, we investigated the cell types and circuits within V1 that likely mediate the various pathways described above. To do this, we used a modified rabies virus that expresses GFP and doesn't cross synapses, to visualize the detailed morphology of neurons in layer 4B of V1 that project to either MT or V2. Of particular interest, was the proportion of spiny stellates and pyramids among each cell population, as it had been shown previously that stellates receive M only inputs and pyramids receive mixed M and P inputs (Yabuta et al., 2001). We found that cells projecting directly from layer 4B of V1 to MT are a majority spiny stellate, whereas those projecting to V2 are overwhelmingly pyramidal. Nevertheless, a small but substantial number of pyramids project to MT as well. Neurons projecting to MT were further differentiated from those projecting to V2 by their larger cell body size and higher total dendritic length. Furthermore, pyramids projecting to MT were found predominantly underneath CO blobs, whereas stellates projecting to MT and neurons projecting to V2 showed no such bias. These results suggest that the M-dominated signal that passes through layer 4C of V1 to MT is mediated by a specialized population of neurons in layer 4B of V1. This population is distinct from the population projecting to V2 which likely mediates a mixed M and P signal.

Discussion

All together, these studies provide strong evidence for multiple pathways between LGN and MT with varying degrees of M and P convergence. The most direct ascending input through layer 4C of V1 to MT is dominated by the M pathway. Less direct input through V3 appears similarly dominated by the M pathway. The thick

stripes of V2, however, receive mixed M and P inputs and may relay this signal indirectly to MT. Finally, a less prominent disynaptic pathway from LGN to MT bypasses layer 4C of V1 altogether and mediates mixed M and P inputs. Rather than maintain strict segregation or converge indiscriminately, the early parallel pathways appear to recombine in an orderly arrangement via specialized cell populations in V1. Each of these newly formed circuits can then provide specific combinations of M and P input to MT and other dorsal stream cortical areas.

The existence of multiple pathways indicates a level of circuit complexity not appreciated beforehand. Indeed, it is likely that many more pathways exist between the LGN and extrastriate cortex, each of which may serve specific functions and computational demands. A diverse group of retinal ganglion cells exists in the retina and we are just now beginning to learn about their visual response properties and anatomical connections (Dacey et al., 2003). The K pathway has proven rather inaccessible in macaque monkey, but the functional heterogeneity observed in the different K layers of various new world monkey species suggests many more pathways yet to be uncovered (Hendry and Reid, 2000). Even the M and P pathways are less homogeneous than typically described. In fact, two different connection patterns exist from M layers in the LGN to layer 4Cα in V1, with some M axons terminating throughout the depth of layer 4Cα and others confined just to the top (Blasdel and Lund, 1983). Likewise, two different connection patterns exist from P layers in the LGN to either layer 4A or 4Cβ in V1, with the former thought to mediate a blue-off color opponent signal and the latter a red-green signal (Chatterjee and Callaway, 2003). Two functional types of P layer cells have also been described, with

both types chromatically opponent but only one type spatially opponent as well (Wiesel and Hubel, 1966). Further studies are necessary to uncover the details of these pathways and how they recombine within V1 and contribute to dorsal and ventral processing streams.

One possible reason why visual cortex might require all of these pathways is that for any given combination of inputs, certain visual sensitivities must be sacrificed in order to maintain or build on others. For instance, the disynaptic route from LGN to MT may combine M and P inputs in a way that sacrifices temporal precision and color selectivity, but expands the range of sensitivities to luminance contrast and spatial and temporal frequency carried by M or P pathway alone. This may be particularly useful as a quick signal to MT (only two synapses) that helps in the initial detection and orienting toward a stimulus, which can then be processed in more detail by other circuits. The more prominent ascending input to MT through layer 4C of V1 may avoid P inputs in order to maintain high temporal precision, sacrificing a greater range of spatial and temporal sensitivity in the process. This may be the optimal strategy for detecting the direction and speed of low contrast, quickly moving stimuli. Meanwhile, the indirect route through the thick stripes of V2 to MT may combine M and P inputs in a way that maintains sensitivity to chromatic contrast and high spatial frequencies so that this information can serve as cues for segmenting and integrating local motion signals. These are just a few of the many possible strategies that these circuits might employ and future studies will be necessary to differentiate between them and elucidate their functions.

It is clear from our results that the recombination of early parallel pathways is a ubiquitous feature of visual cortex. Each cortical processing stream likely utilizes multiple strategies by which to combine the early parallel pathways in ways that can adequately serve specific computations and visual tasks. This is particularly relevant to the proposal that motion processing in MT and the dorsal stream depends on the M pathway alone and is essentially color blind due to a lack of P input. It is now clear that both P and K pathways provide input to MT and could contribute to computations that require detection of chromatic boundaries. Indeed, chromatic contrasts that are thought to poorly activate M cells can have a clear influence on direction selective responses in MT (Saito et al., 1989). Additionally, direction selectivity in V1 and motion perception itself have both been shown to survive M pathway lesions (Malpeli et al., 1981; Merigan et al., 1991). In fact, it has been suggested that the generation of direction selectivity in some V1 neurons may actually require the spatial and temporal quadrature of convergent M and P inputs (De Valois et al., 2000). Croner and Albright (1999) propose that motion and color stay separate for detection but not interpretation of image motion. It is tempting to postulate that the M-dominated pathway through layer 4C of V1 may underlie detection, whereas mixed M and P inputs through V2 may underlie some forms of interpretation. While more studies are necessary to understand how the early parallel pathways contribute to motion processing in MT, there is no longer any doubt that all three pathways play a role.

The studies described in this dissertation not only add to our understanding of how early parallel pathways contribute to cortical processing streams, but they also motivate the development of new techniques. In order to understand how the primate

visual cortex elaborates and integrates early parallel pathways into a unified and coherent percept, future studies will need to functionally characterize the specialized circuits we have described. This will require methods that can bridge anatomy and physiology in ways not possible before. For instance, single-cell electroporation of fluorescent dye or DNA can be used to anatomically identify specific cell types that have been functionally characterized in-vivo. Two-photon microscopy in combination with calcium sensitive dyes allows the activity of nearly all cells within a patch of cortex to be monitored simultaneously in-vivo. This powerful tool, in combination with standard or virally-based retrograde tracing methods, will make it possible to anatomically identify and physiologically characterize large numbers of a single cell type or circuit. Finally, genetic inactivation techniques will enable highly precise lesions of these specialized circuits with the power to uncover their functional contributions to perception and behavior.

References

Blasdel, G.G., and Lund, J.S. (1983). Termination of afferent axons in macaque striate cortex. J. Neurosci. 3, 1389-1413.

Callaway, E.M., and Wiser, K. (1996). Contributions of individual layer 2-5 spiny neurons to local circuits in macaque primary visual cortex. Vis. Neurosci. 13, 907-922.

Chatterjee, S., and Callaway, E.M. (2003). Parallel colour-opponent pathways to primary visual cortex. Nature 426, 668-671.

Croner, L.J., and Albright, T.D. (1999). Seeing the big picture: integration of image cues in the primate visual system. Neuron 24, 777-789.

Dacey, D.M. (2000). Parallel pathways for spectral coding in primate retina. Annu. Rev. Neurosci. 23, 743-775.

Dacey, D.M., Peterson, B.B., Robinson, F.R., and Gamlin, P.D. (2003). Fireworks in the primate retina: in vitro photodynamics reveals diverse LGN-projecting ganglion cell types. Neuron 37, 15-27.

De Valois, R.L., Cottaris, N.P., Mahon, L.E., Elfar, S.D., and Wilson, J.A. (2000). Spatial and temporal receptive fields of geniculate and cortical cells and directional selectivity. Vision Res. 40, 3685-3702.

Hendry, S.H., and Reid, R.C. (2000). The koniocellular pathway in primate vision. Annu. Rev. Neurosci. 23, 127-153.

Lachica, E.A., Beck, P.D., and Casagrande, V.A. (1992). Parallel pathways in macaque monkey striate cortex: anatomically defined columns in layer III. Proc. Natl. Acad. Sci. U.S.A. 89, 3566-3570.

Malpeli, J.G., Schiller, P.H., and Colby, C.L. (1981). Response properties of single cells in monkey striate cortex during reversible inactivation of individual lateral geniculate laminae. J. Neurophysiol. 46, 1102-1119.

Merigan, W.H., Byrne, C., and Maunsell, J.H.R. (1991a). Does primate motion perception depend on the magnocellular pathway? J. Neurosci. 11, 3422-3429.

Saito, H., Tanaka, K., Isono, H., Yasuda, M., and Mikami, A. (1989). Directionally selective responses of cells in the middle temporal area (MT) of the macaque monkey to the movement of equiluminous opponent color stimuli. Exp. Brain Res. 75, 1-14.

Sincich, L.C., and Horton, J.C. (2002). Divided by cytochrome oxidase: a map of the projections from V1 to V2 in macaques. Science 295, 1734-1737.

Sincich, L.C., Park, K.F., Wohlgemuth, M.J., and Horton, J.C. (2004). Bypassing V1: a direct geniculate input to area MT. Nat. Neurosci. 7, 1123-1128.

Wiesel, T.N., and Hubel, D.H. (1966). Spatial and chromatic interactions in the lateral geniculate body of the rhesus monkey. J. Neurophysiol. 29, 1115-1156.

Yabuta, N.H., Sawatari, A., and Callaway, E.M. (2001). Two functional channels from primary visual cortex to dorsal visual cortical areas. Science 292, 297-300.

Yoshioka, T., Levitt, J.B., and Lund, J.S. (1994). Independence and merger of thalamocortical channels within macaque monkey primary visual cortex: anatomy of interlaminar projections. Vis. Neurosci. 11, 467-489.

Xiao, Y., and Felleman, D.J. (2004). Projections from primary visual cortex to

cytochrome oxidase thin stripes and interstripes of macaque visual area 2. Proc. Natl. Acad. Sci. U.S.A. 101, 7147-7151.